A three amino acid sequence gates protein stability control of bHLH104 and iron uptake in *Arabidopsis thaliana*

Dibin Baby[1,2], Sarah Weldi[1], Marie Knopf[1], Vinitha Venkadasamy[1], Jessica Lee Erickson[3], Petra Bauer[1,2*]

[1]Institute of Botany, Heinrich Heine University, Düsseldorf 40225, Germany

[2]Cluster of Excellence on Plant Science (CEPLAS), Heinrich Heine University, Düsseldorf 40225, Germany

[3]Zentrum für Molekularbiologie der Pflanzen (ZMBP), Allgemeine Genetik, University of Tübingen, 72076 Tübingen, Germany.

***Corresponding author:** Petra Bauer, petra.bauer@hhu.de

Dibin Baby- https://orcid.org/0000-0003-0592-6067

Petra Bauer- https://orcid.org/0000-0002-0404-4532

Abstract

Iron (Fe) homeostasis is regulated to prevent iron imbalance, with the help of redundant basic helix-loop-helix (bHLH) IVc transcription factors that can be controlled by Fe-binding E3 ligases such as BRUTUS (BTS) in *Arabidopsis thaliana*. However, knowledge gaps remain to fully explain the mechanistic basis of this redundant protein interaction module. The C-terminus of bHLH104 interacts with BTS.Structural predictions suggest involvement of the three terminal amino acids, proline-alanine-alanine (PAA). However, the importance of the PAA short sequence for post-translational regulation of bHLH104 and resulting plant phenotypes has not been experimentally tested. Here, we demonstrate that transgenic plants expressing a bHLH104 variant lacking PAA (*b104^dPAA*) constitutively upregulated Fe acquisition and Fe transport genes and consequently accumulated Fe in contrast to wild-type bHLH104 protein-expressing plants. The extent of Fe accumulation in independent b104^dPAA lines correlated positively with b104^dPAA protein abundance. In contrast to the wild-type bHLH104 form, there was no indication that b104^dPAA interacted with BTS or was ubiquitinated by it. Together, these findings corroborated that the PAA sequence is required for post-translational control of bHLH104 by BTS. Hence,

targeted manipulation of bHLHIVc protein PAA sequence may represent a strategy for crop biofortification.

60-word Plain language summary

Plants tightly control iron levels. In *Arabidopsis thaliana*, transcription factor bHLH104 steers iron uptake. E3 ligases like BTS regulate bHLH104. We show that a three–amino acid terminal sequence of bHLH104 is needed for its targeting by the BTS pathway. bHLH104 lacking PAA leads to iron accumulation. Targeting this short sequence can be a strategy for crop biofortification.

Keywords: *Arabidopsis thaliana*, iron, bHLHIVc, transcription factor, ubiquitination, BTS

Introduction

Iron (Fe) is an essential micronutrient required for plant growth and development. It plays critical roles in photosynthesis, respiration, chlorophyll biosynthesis, and redox reactions (Briat et al., 2007; Jeong and Guerinot, 2009). Although Fe is abundant in the Earth's crust, it is mostly present in the ferric (Fe^{3+}) form, which is poorly soluble and difficult for plant roots to absorb—especially in alkaline or calcareous soils (Marschner, 2012). Excess Fe is toxic since it generates reactive oxygen species (ROS) (Panda and Yamamoto, 2019). Therefore, plants must tightly regulate Fe uptake, distribution, and storage to maintain internal balance.

In *Arabidopsis thaliana*, a group of basic helix–loop–helix (bHLH) IVc transcription factors—including bHLH34, bHLH104, ILR3 (bHLH105), and bHLH115—acts as an early regulatory module in the Fe deficiency (-Fe) response. These proteins activate the expression of internal Fe allocation and Fe deficiency response regulatory genes in roots and shoots (Schwarz and Bauer, 2020). Among their targets are also genes coding for bHLH Ib transcription factors that, together with the bHLH transcription factor FIT (FER-LIKE IRON DEFICIENCY-INDUCED TRANSCRIPTION FACTOR), induce root Fe uptake genes such as *IRT1* and *FRO2* (Long et al., 2010; Selote et al., 2015; Zhang et al., 2015; Li et al., 2016; Liang et al., 2017).

The regulation of the redundant bHLH IVc transcription factors is not fully understood. Notably, transcript levels of *BHLH IVc* genes do not change substantially under -Fe conditions (Zhang et al., 2015; Li et al., 2016; Liang et al., 2017), indicating that they are activated during the -Fe response primarily at protein level. It is proposed that bHLH IVc proteins are subject to post-translational regulation via the 26S proteasome, mediated by the E3 ubiquitin ligases, BRUTUS (BTS)/BTS-LIKE (BTSL) proteins (Zhao et al., 2026). However, this has not yet been demonstrated experimentally for all bHLH IVc proteins. It was shown that bHLH105/ILR3 and bHLH115 are recognized, ubiquitinated and degraded by BTS and BTSL proteins (Selote et al., 2015; Hindt et al., 2017; Zhao et al., 2026). Control by E3 ligases of the BTS/BTSL-type is particularly intriguing since stability of the BTS/BTSL E3 ligases is controlled by their N-terminus which contains hemerythrin domains for Fe and oxygen sensing (Selote et al., 2015; Pullin et al., 2025). Additionally, Fe and Zn binding to C-terminal zinc finger domains (CHY, CTCHY, RING) and rubredoxin-type folds of the BTS rice ortholog HEMERYTHRIN MOTIF-CONTAINING REALLY INTERESTING NEW GENE AND ZINC-FINGER PROTEIN (HRZ) may regulate its protein stability and activity, suggesting an additional mechanism for metal ion sensing (Shinkawa et al., 2025). Together, these findings support a model in which, under Fe deficiency, altered metal occupancy and redox state of BTS/BTSL domains attenuate E3 ligase activity toward bHLH IVc transcription factors, allowing accumulation of the transcription factors and subsequent activation of Fe uptake genes. This model is further supported by genetic studies demonstrating that loss of BTS (Selote et al., 2015; Long et al., 2010) or BTSL1/BTSL2 (Hindt et al., 2017; Rodríguez-Celma et al., 2019) results in activation of Fe deficiency responses. However, due to technical limitations and the redundancy among the involved proteins, there remain knowledge gaps.

One bHLH IVc group protein is bHLH104 (Zhang et al., 2015; Li et al., 2016). Phylogenetic analysis places bHLH104 together with bHLH34 in a distinct clade from bHLH105 and bHLH115, and individual bHLH IVc members show distinct expression patterns (Gao et al., 2019; Gao et al., 2024; Jiang et al., 2024), indicating that regulatory mechanisms cannot be directly extrapolated between members. T-DNA loss-of-function lines of *bHLH104* exhibit an Fe deficiency-sensitive phenotype (Li et al., 2016), which is expected for an upstream regulator of the Fe deficiency response. The protein-level regulatory mechanisms controlling bHLH104 function remain

incompletely characterized. The C-terminus of bHLH104 can interact with BTS/L proteins (Lichtblau et al., 2022). It possesses the sequence PAA at the very C-terminal end. In our previous study, we showed that deleting a 25-amino-acid-long stretch at the C terminus abolished bHLH104 interaction with BTS (Lichtblau et al., 2022). Other studies supported the implication of this C-terminal region in regulation of bHLH IVc proteins. (Li et al., 2021) demonstrated that substitution of the terminal alanine to valine in bHLH105 and bHLH115 abolished interaction with BTS in yeast two-hybrid assays and increased protein stability in transient expression assays. (Sharma and Yeh, 2020) identified an ethyl methanesulfonate (EMS)-induced C-terminal alanine-to-valine substitution in bHLH34 that conferred increased protein stability and metal accumulation in plants, but a connection to BTS was not established. A C-terminal sequence with terminal PAA is conserved in IRON MAN (IMA)/FE-UPTAKE-INDUCING PEPTIDE (FEP) signaling peptides. Interestingly, (Lichtblau et al., 2022) found that the C-terminal portion of IMA1 small proteins is needed for IMA1 to interact with the BTSL1 C-terminus. Moreover, they described that intact IMA1, but not IMA1 with a C-terminal deletion, disturbed interaction between C-terminal protein fragments of BTSL1 and either bHLH34, bHLH104, or bHLH115, but not ILR3. (Li et al., 2021) showed that substitution of the terminal alanine to valine in IMA3 abolished BTS interaction, further demonstrating the importance of this terminal residue for protein recognition by BTS. Structural predictions suggested that the conserved three–amino acid short sequence—proline–alanine–alanine (PAA)—of a bHLH transcription factor may bind at the BTS-binding interface (Lichtblau et al., 2022). In all, the BTS and BTSL recognition may thus be narrowed down to PAA/PVA. Hereafter, we refer to this as the "PAA short sequence".

Although BTS-mediated ubiquitination has been demonstrated for *A. thaliana* bHLH105 and bHLH115 (Li et al., 2021; Zhao et al., 2026), direct ubiquitination of bHLH104 by BTS has not been shown, nor has the requirement of PAA for this interaction been established. Genetic evidence supports that bHLH104 acts downstream of BTS, as loss of bHLH104 partially suppresses the Fe deficiency tolerance of the *bts-2* mutant (Zhang et al., 2015). Yet, the biochemical basis of this regulation remained unresolved.

The key open questions and knowledge gaps of this study were to examine whether targeting the bHLH104 PAA short sequence in a deletion study would cause any Fe-

127 related plant growth phenotypes. Further, if so, we intended to study whether the
128 underlying mechanism could be explained by disturbed protein abundance. Moreover,
129 we aimed to examine the relevance of PAA for protein interaction with BTS and BTS-
130 mediated ubiquitination. Our work provides evidence that the PAA short sequence is
131 indeed critical for regulating bHLH104 stability and Fe homeostasis across plant
132 development, and our data highlight a potential new strategy for Fe biofortification.

133

134 **Results**

135 **Plants with bHLH104 lacking PAA (*b104^dPAA*) have distinct growth**
136 **phenotypes**

137 We hypothesized that the PAA short sequence plays a role in the functionality of
138 bHLH104 in plants (Figure 1). To test this, we studied transgenic *Arabidopsis thaliana*
139 lines in the wild-type Col-0 background expressing either regular full-length
140 mTurquoise2 fluorophore-tagged bHLH104 (hereafter *pb104::b104*) or a mutant
141 deletion variant lacking the conserved PAA short sequence (hereafter
142 *pb104::b104^dPAA*), both driven by the native *BHLH104* promoter (Figure 2A). The N-
143 terminal mTurquoise2-tagged *-b104^dPAA* complemented the *bhlh104-1* seedling -Fe
144 sensitivity phenotype indicating functionality of the fusion protein (Supplementary
145 Figure S1).

146 Interestingly, phenotypic variation was visible in the T1 population of the
147 *pb104::b104^dPAA* transgenics, indicating a dominant transgene effect: While the
148 majority of plants displayed severely reduced growth with brown necrotic spots on
149 leaves, some plants appeared indistinguishable from wild type (WT) (Supplementary
150 Figure S2). To capture these contrasting phenotypes, we selected and propagated
151 four *pb104::b104^dPAA* lines, two with severe phenotypes (#1, #2) and two with no
152 obvious macroscopic phenotype (#3, #4), in addition to *pb104::b104 #1* and *#2*
153 controls.

154 To quantify phenotypic variation across the life cycle, detailed morphological and
155 physiological assessments were made with T3 plants selected for transgene presence
156 by genotyping PCR and grown on agar plates or soil. In 12-day-old seedlings of
157 *pb104::b104^dPAA* lines *#1* and *#2*, we found significantly shorter primary roots than

158 in seedlings of #3, #4 or in *pb104::b104* control lines (Figure 2B, 2C). Root Fe(III)
159 reductase activity is necessary for reduction-based Strategy I Fe uptake (Yi and
160 Guerinot, 1996). Ferric reductase activity measurements revealed that
161 *pb104::b104^dPAA* lines *#1* and *#2* had higher Fe reductase activity compared to #3,
162 #4 and the controls (Figure 2D). The machine-aided Phenospex PlantEye phenotyping
163 platform can reliably depict minor variation in leaf color and rosette size in *A. thaliana*
164 (Knopf and Bauer, 2025). By four weeks, *pb104::b104^dPAA* lines *#1* and *#2* displayed
165 smaller rosette area (Figures 2E, 2F) and low normalized difference vegetation index
166 (NDVI) values (Figure 2G), which indicate lower chlorophyll content, lower
167 photosynthetic efficiency, and reduced growth performance compared with other lines.
168 Flowering was delayed compared to the other lines (Figure 2H) and seed yield was
169 significantly lower for *pb104::b104^dPAA* lines *#1* and *#2* compared to the other lines
170 (Figure 2I).

171 Reduced root and shoot growth, as observed in plants of *pb104::b104^dPAA* line #2,
172 can be a consequence of Fe toxicity (Naranjo-Arcos et al., 2017). Thus, we tested
173 whether the growth defects observed in *pb104::b104^dPAA* #2 plants were alleviated
174 in conditions of Fe deficiency. We grew the representative lines on alkaline calcareous
175 soil (ACS; pH 8.1), which provides Fe-limiting conditions (Supplementary Figure S3;
176 Knopf and Bauer, 2025). Notably, *pb104::b104^dPAA line #2*, which exhibited
177 pronounced growth defects in control soil (pH 5.9), showed increased 3D leaf area in
178 ACS, indicating partial recovery under Fe-limited ACS conditions (Supplementary
179 Figure S3C). NDVI values, which were low in control soil, were restored to near-WT
180 levels in ACS, suggesting improved leaf health (Supplementary Figure S2D). While
181 flowering remained delayed relative to WT, it occurred earlier in ACS than in control
182 soil (Supplementary Figure S3E). These findings show that the growth defects
183 observed in control soil are largely alleviated when Fe availability is limited, linking the
184 b104^dPAA-associated phenotypes to Fe status.

185 Together, these results show that removal of the PAA short sequence in bHLH104 can
186 lead to drastic dominant growth phenotypes across the life cycle. To explore whether
187 these phenotypes reflect altered Fe homeostasis, we next examined tissue Fe content
188 and expression of Fe-responsive genes in both seedlings and plants at the
189 reproductive stage. For further detailed experiments, we focused on two

representative *pb104::b104^dPAA* lines, namely a strong line, #2, and a weak phenotype line, #3.

b104^dPAA Can Cause Constitutive Iron Uptake and Transcriptional Misregulation of Fe Deficiency Response genes in Seedlings

After a few days of germination, *A. thaliana* seedlings rely on external Fe supply. To assess whether b104^dPAA affects Fe homeostasis during early development, we measured total Fe content via ICP-MS and analyzed gene expression profiles in 10-day-old seedlings of WT, control and contrasting *pb104::b104^dPAA* lines #2 and #3 in both +Fe and -Fe conditions (Figure 3A, B). As an additional control, we used *pUBQ10::b104* lines expressing full-length bHLH104 constitutively from the strong *UBIQUITIN10* promoter, allowing us to assess whether transcript levels alone affect Fe homeostasis. Morphologically, *pUBQ10::b104* lines #1 and #2 are indistinguishable from WT, except for slightly shorter roots (Supplementary Figure S4).

Elemental profiling revealed that *pb104::b104^dPAA* line #2 accumulated substantially more Fe than all other genotypes under both +Fe and –Fe conditions (Figure 3C). This increase was observed in both roots and shoots, with roots showing higher Fe levels than shoots. In contrast, *pb104::b104^dPAA* line #3 and the *pb104::bHLH104* and *pUBQ10::b104* lines had Fe contents similar to WT. All lines exhibited reduced Fe contents under –Fe, confirming the effectiveness of the -Fe treatment (Figure 3C).

Differences were also detected for manganese (Mn), zinc (Zn), and copper (Cu) levels (Supplementary Figure S5). Uptake of these metal ions is closely connected with Fe homeostasis (Connolly et al., 2002). In *pb104::b104^dPAA* line #2, Zn and Cu were elevated in roots under –Fe, and Cu was increased in shoots. Notably, Zn levels were elevated even under +Fe in *pb104::b104^dPAA* roots compared to WT. Roots of *pUBQ10::b104* lines also showed increased Mn under –Fe compared to WT. Metal concentrations in the other lines were similar to WT. Hence, these findings suggest that *pb104::b104^dPAA* line #2 has increased Fe accumulation and affects the uptake of other micronutrients like Zn and Cu. This highlights the importance of proper regulation of bHLH104 function in maintaining metal homeostasis under varying Fe conditions.

To elucidate the transcriptional response, we analyzed gene expression patterns via RNA-seq following -Fe treatment at the seedling stage in both root and shoot tissues. The highest number of differentially expressed genes (DEGs) was observed in shoot tissue of *pb104:b104^dPAA #2* line, with 4,645 DEGs under +Fe conditions and 2,857 DEGs under -Fe conditions after 10 days of treatment, compared to WT. There was also substantial differential expression in roots, with 1,210 DEGs under +Fe conditions and 111 DEGs under -Fe conditions (Supplementary Figure S6A).

Gene Ontology (GO) analysis revealed that the upregulated genes in shoot tissue of the *pb104:b104^dPAA* #2 plants were enriched in terms related to hypoxia and oxidative stress, while genes associated with photosynthesis were downregulated. In *pb104:b104^dPAA* root tissue, upregulated gene categories were additionally enriched for terms related to metal ion transport, while downregulated categories showed enrichment for cell wall modification-related GO terms (Supplementary Figure S6B). Hence, the *pb104:b104^dPAA* #2 plants indeed show symptoms of Fe overload with associated oxidative stress.

Gene expression profiles can inform on misregulation in mutants and transgenic lines (Schwarz and Bauer, 2020).We examined the expression patterns of selected genes involved in Fe uptake and homeostasis regulation to characterize their specific regulatory expression profiles. Interestingly, Fe acquisition and mobilization genes were constitutively upregulated in pb104::b104^dPAA#2 line regardless of Fe availability at the seedling stage (Supplementary Figure S7). *BHLHIVc* genes, *BHLH104, ILR3*, and *BHLH115*, were upregulated in the roots of the *pb104::b104^dPAA line #2* under +Fe compared to other lines (Figure 3D). Their target genes, such as *BHLH39, BHLH100, IMA1, BTS, BTSL1, BTSL2* and *PYE*, were also upregulated, indicating activation of the Fe deficiency response signaling which includes a negative feedback loop via *BTS, BTSL1, BTSL2* and *PYE* genes. Likewise, the further downstream targets in roots, like Fe acquisition genes *IRT1, FRO2, FIT,* were up-regulated (Figure 3D), consistent with the elevated Fe uptake and Fe content. Interestingly, expression of negative regulators of the Fe deficiency response and of Fe sufficiency markers, such as *BHLH11* and *FER1* were also increased, suggesting a proper response to elevated Fe (Figure 3D). In the shoot tissue, the Fe storage related gene *FER1* was strongly upregulated in *pb104::b104^dPAA line #2* compared to controls, regardless of Fe availability, in agreement with the elevated Fe content in

254 this line (Figure 3D). Targeted expression profiling using reverse transcription
255 quantitative PCR (RT-qPCR) in seedling-stage samples confirmed expression
256 patterns to those observed in the transcriptome analysis (Supplementary Figure S8).

257 To summarize, the misregulation of Fe response genes indicates that bHLH104 with
258 deleted PAA disrupts normal Fe homeostasis by constitutively activating Fe acquisition
259 while preventing proper feedback inhibition of Fe uptake during seedling development.
260 This results in excessive Fe acquisition and resulting toxicity.

261 **b104^dPAA Causes Constitutive Fe Uptake and Transcriptional Misregulation at**
262 **a Reproductive Growth Stage**

263 Plants redistribute nutrients during reproduction to support flowering and seed
264 development (Waters and Grusak, 2008; Pottier et al., 2018). To assess whether
265 b104^dPAA affects Fe homeostasis during later developmental stages, we analyzed
266 30-day-old flowering Arabidopsis plants grown hydroponically, subjected at 27 days to
267 a 3-day ±Fe treatment (Figure 4A). However, the strong-phenotype plants of
268 *pb104::b104^dPAA #2* were severely growth-compromised in hydroponic culture and
269 had to be excluded from this analysis. Instead, we focused on the weak-phenotype
270 line *pb104::b104^dPAA #3*. Old leaves, young leaves, and roots were collected for
271 gene expression analysis, as described in (Ngigi et al., 2025) (Figure 4C-D).

272 Elemental profiling showed that *p104::b104^dPAA line #3* accumulated more Fe than
273 control lines at the late developmental stage (Figure 4E). Under +Fe, roots of
274 *pb104::b104^dPAA* #3 had increased Mn and Zn levels compared to WT
275 (Supplementary Figure S9). Cu levels were similar as WT.

276 In transcriptome analysis, *pb104:b104^dPAA* #3 plants had the highest DEG counts
277 in young leaves (3,877 DEGs) and old leaves (1,895 DEGs) under +Fe conditions
278 compared with controls, while root tissue exhibited minimal differential expression
279 differences (71 DEGs) (Supplementary Figure S10A). GO term enrichment analysis
280 revealed that genes associated with immune response were significantly upregulated
281 in both old and young leaves of *pb104:b104^dPAA* #3 plants under +Fe conditions. In
282 contrast, 3-day -Fe treatment resulted in young leaves in the upregulation of terms
283 related to Fe homeostasis (Supplementary Figure S10B). This indicates a tissue-
284 specific transcriptional response to Fe availability at the reproductive stage.

285 Specifically, expression analysis showed that in roots of *pb104::b104^dPAA line #3*
286 genes were upregulated under +Fe, similar as we reported above for the #2 line at the
287 seedling stage, namely upregulation of *BHLHIVc* genes, Fe deficiency response, Fe
288 sufficiency marker and negative regulator genes (Figure 4F). Interestingly, Fe
289 deficiency response genes such as *BTS*, *IMA1*, *BHLH100*, and *PYE* were upregulated
290 under –Fe in young leaves of pb104::b104 #1 compared to pb104::b104^dPAA line #3
291 (Figure 4F). *FER1* was upregulated in young and old leaves of *pb104::b104^dPAA* line
292 #3 compared to pb104::b104 #1 and WT under +Fe. Targeted expression profiling by
293 RT-qPCR confirmed again the transcriptome data (Supplementary Figure S11).
294 Hence, even though at the seedling stage *pb104::b104^dPAA* line #3 did not display
295 iron accumulation phenotypes, this was clearly the case at the flowering stage,
296 indicating that proper bHLH104 function may be more important at later than early
297 growth stages.

298 Finally, as *pb104::b104^dPAA* line #2 did not grow in +Fe hydroponic conditions, we
299 modified the hydroponic growth system and changed to a Fe resupply assay.
300 Seedlings were transferred at an early stage to -Fe (instead of the usual +Fe) medium
301 for 27 days, followed by a 3-day +/- Fe resupply. Here, we found interesting
302 phenotypes. While WT plants remained chlorotic and accumulated Fe mostly in the
303 roots following the Fe resupply, *pb104::b104^dPAA* line #2 showed substantial Fe
304 accumulation in root and leaves despite persistent leaf chlorosis, suggesting high root-
305 to-shoot Fe translocation. Interestingly, *pb104::b104^dPAA* line #2 accumulated
306 significantly less Mn, Zn, Cu compared to control plants in old and young leaves
307 (Supplementary Figure S12). This shows that at the reproductive stage, there is a
308 particularly elevated Fe uptake and translocation towards shoots in
309 *pb104::b104^dPAA* #2 compared to the WT, while that of Mn, Zn and Cu is
310 suppressed.

311 Since 30-day-old *pb104::b104^dPAA* #3 plants accumulated not only Fe but also Mn
312 and Zn under + Fe in roots, we examined the possibility that this might have been
313 caused by altered expression of metal transporter genes. We found elevated
314 expression of metal transporter genes, including NRAMP1, COPT2, MTP8, and ZIP
315 family members, in *pb104::b104^dPAA* roots under both +Fe and -Fe at the seedling
316 stage, and under +Fe at the reproductive stage, consistent with the observed metal
317 accumulation patterns (Supplementary Figure S13).

318 To summarize, *pb104::b104^dPAA* lines accumulated Fe throughout the tested
319 reproductive stage. Metal accumulation and associated phenotypes due to
320 b104^dPAA expression remained consistent from seedling to advanced
321 developmental stages.
322

323 **The PAA short sequence is required for 26S Proteasome-mediated degradation**
324 **of bHLH104**

325 The severity of phenotypes in *pb104::b104^dPAA* lines was not explained by
326 differences in transgene transcript levels (Supplementary Figures S8). Additionally,
327 *pUBQ10::b104* lines showed no significant phenotype compared to WT apart from
328 shorter roots despite elevated *bHLH104* transgene expression (Supplementary Figure
329 S4, Supplementary Figure S8C). Therefore, we suspected that variation in bHLH104
330 protein accumulation underlies the observed phenotypic differences.

331 We thus examined *in vivo* accumulation of mTurquoise2-tagged bHLH104 and
332 b104^dPAA protein, expressed under either the *UBQ10* or *BHLH104* promoter (Figure
333 5A, B). Immunoblotting of root tissue proteins detected mTurquoise2-b104^dPAA
334 protein in *pb104::b104^dPAA* lines #1 and #2 (Figure 5B, Supplementary Figure S14).
335 In contrast, mTurquoise2-tagged protein was barely detectable in *pb104::b104^dPAA*
336 lines *#3* and *#4*, *pb104::bHLH104*, and *pUBQ10::b104* lines. Hence, mTurquoise2-
337 b104^dPAA protein levels coincided with the strength of Fe accumulation phenotypes,
338 while the wild type mTurquoise2-b104 was not detected.

339 To check whether the low abundance of mTurquoise2-bHLH104 is due to proteasomal
340 degradation, we treated samples with proteasome inhibitor MG132. MG132 treatment
341 stabilized full-length mTurquoise2-bHLH104 in *pUBQ10::b104* lines by more than two-
342 fold. However, MG132 treatment did not affect the abundance of mTurquoise2-
343 bHLH104 in any native promoter lines (Figure 5B-C). To confirm that bHLH104 is
344 subject to proteasomal degradation, a cell-free degradation assay was performed.
345 When recombinant His-bHLH104 protein, purified from *Escherichia coli*, was
346 incubated with whole protein extracts from WT seedlings, it was rapidly degraded. This
347 degradation was inhibited by the proteasome inhibitor MG132, supporting the
348 involvement of the 26S proteasome (Figure 5D).

349 Confocal imaging of root tips further confirmed the increased abundance of
350 mTurquoise2-b104^dPAA, as indicated by fluorescence signals in nuclei of root tip
351 cells in *pb104::b104^dPAA* lines, whereas fluorescence was undetectable in lines
352 expressing full-length mTurquoise2-bHLH104 (Figure 5E).

353 Altogether, these findings show that the PAA short sequence is required for
354 degradation of bHLH104 by the 26S proteasome. Removing this short sequence
355 seems to prevent normal turnover of the protein.

356 **The C-terminal PAA sequence of bHLH104 mediates interaction with BTS E3**
357 **ligases and enables ubiquitination**

358 To understand how the PAA sequence contributes to bHLH104 degradation, we
359 examined its role in mediating interaction with BTS.

360 AlphaFold2 multimer modeling (Evans et al., 2021; Jumper et al., 2021) and
361 electrostatic surface analysis (Pettersen et al., 2004) revealed a charge-based
362 interface with high predicted Local Distance Difference Test (pLDDT) scores,
363 indicating strong confidence in the predicted structure (Figure 6A-B). These models
364 suggest that the PAA sequence forms a stable and specific docking surface for BTS,
365 likely critical for E3-substrate recognition.

366 To further study protein interaction in the presence and absence of PAA experimentally,
367 we made use of established protein expression systems. Due to the difficulties of
368 detecting bHLH104 and BTS in plant cell assays, we opted for the yeast two hybrid
369 (Y2H) assay (Lichtblau et al., 2022). BTS interacts non-reciprocally with the C-terminal
370 part of bHLH104 (bHLH104-C) in yeast, and bHLH104-C does not auto-activate in the
371 yeast-two-hybrid (Y2H) system (Figure 6C), as previously shown (Lichtblau et al.,
372 2022). We now tested whether interaction is different with bHLH104-C^dPAA. Indeed,
373 deletion of the PAA sequence abolished the interaction with BTS (Figure 6D).
374 bHLH104 is known to homodimerize (Zhang et al., 2015; Li et al., 2016; Lichtblau et
375 al., 2022). bHLH104-C^dPAA still dimerized with bHLH104-C, confirming that
376 bHLH104-C^dPAA is present and properly folded in yeast cells. A similar loss of
377 interaction ability was found between bHLH104-C-dPAA and BTSL1 and BTSL2
378 (Supplementary Figure S15), indicating that the PAA sequence is broadly required for
379 recognition by BTS/ BTSL E3 ligases.

380 To test whether bHLH104 is ubiquitinated by BTS with requirement of the PAA short
381 sequence, we established the bacterial UbiGate system (Kowarschik et al., 2018;
382 Ortmann et al., 2023) to reconstitute a BTS-dependent ubiquitin-conjugation cascade
383 for bHLH104 (Figure 7A). The UbiGate system co-expresses all ubiquitination and
384 target components within living bacterial cells, providing a cellular context for a direct
385 ubiquitination reaction while enabling unambiguous assignment of E3-substrate
386 specificity through distinct epitope tags on each component (Figure 7B, C). Differences
387 in banding patterns between controls lacking individual cascade components and cells
388 containing the complete cascade are indicative of ubiquitination. Since full-length BTS
389 was not stably expressed in *E. coli*, we used a truncated version (BTS-HC) lacking the
390 first two hemerythrin domains. The relevant assay consists of comparing the Strep-
391 tagged bHLH104-C protein patterns in the presence (lanes 1, 2, and 5 of Figure 7B,C)
392 and absence of E2 (UBC8) (lanes 3 and 6 of Figure 7B,C), and E3 (BTS-HC) lanes 4
393 and 7 of Figure 7B,C). Immunodetection with the anti-Strep antibody confirmed that
394 bHLH104-C was expressed in all sample cultures, with a band at the expected size of
395 the unmodified protein (~40 kDa), as indicated by brown arrows in Figure 7B. Some
396 higher molecular weight bands occur independently of the E3 ligase and are therefore
397 not specific to BTS-HC activity, as indicated by grey arrows in Figure 7B. However, in
398 the presence of all cascade components, one band (~70 kDa),as indicated by a green
399 arrow in Figure 7B, appears that is absent from b104-C^dPAA under identical
400 conditions and absent from the substrate-negative control (Figure 7B, Supplementary
401 Figure S16). The size of this band is consistent with polyubiquitination of bHLH104-C,
402 as its molecular weight shift of approximately 30 kDa corresponds to the addition of
403 three to four ubiquitin moieties, resembling a characteristic ubiquitination pattern
404 (Kowarschik et al., 2018). This meets the minimum chain length of four ubiquitins
405 required for efficient 26S proteasome recognition (Thrower, 2000). These data suggest
406 that the PAA short sequence is required for BTS-mediated ubiquitination of bHLH104.
407 BTS autoubiquitination, reported previously (Kobayashi et al., 2013; Selote et al.,
408 2015), served as a positive control for the ubiquitination reaction in the UbiGate system
409 (Figure 7C). bHLH115 has been previously indicated as a target of BTS-dependent
410 degradation (Selote et al., 2015; Xing et al., 2021). Consistent with these reports, we
411 found that bHLH115 is also likely ubiquitinated by BTS-HC in the UbiGate system,
412 indicating that this assay is suited (Supplementary Figure S17).

413 These results suggest that bHLH104 can act as a substrate of BTS in a cellular
414 environment and that the PAA short sequence is required for both physical interaction
415 and ubiquitination. The specificity of this finding is supported by the bHLH104-C^dPAA
416 control, which differs from bHLH104-C by only three amino acids yet does not show
417 the specific band, indicating that the presence of the PAA short sequence is required
418 for interaction and ubiquitination by BTS.

419

420 **Discussion**

421 This study demonstrates functional relevance of the terminal PAA short sequence of
422 bHLH104 by studying a PAA deletion variant. Our data showed and are interpreted as
423 follows, in agreement with recent literature on other bHLHIVc transcription factors:
424 bHLH104 is degraded via the proteasome. Lack of PAA prevents binding of
425 bHLH104^dPAA to BTS E3 ligase. Hence, bHLH104^dPAA is not ubiquitinated nor
426 targeted by the proteasome. This leads to protein stabilization and the observed higher
427 abundance of bHLH104^dPAA. bHLH104^dPAA is functionally active. Its enhanced
428 abundance causes target genes of the Fe deficiency response pathway to be
429 constitutively up-regulated throughout plant development. Resulting excessive uptake
430 of Fe and misregulation of Fe homeostasis lead to accumulation of Fe and other
431 metals. This causes oxidative stress and perturbs plant performance, resulting in small
432 plants exhibiting Fe toxicity in leaves. Yet, the level of bHLH104^dPAA protein can vary
433 in transgenic lines, so that some lines can accumulate Fe over their life span but their
434 growth is not compromised.

435 **bHLH104 abundance is controlled via the proteasome**

436 Our results show that wild-type bHLH104 protein is susceptible to degradation in a
437 plant cell environment, and inhibition of the proteasome pathway increases bHLH104
438 abundance. The post-translational regulation of bHLH IVc proteins has been
439 previously reported, with transcript levels remaining largely unchanged under Fe
440 deficiency, suggesting that regulation occurs primarily at the protein level (Zhang et
441 al., 2015; Li et al., 2016; Liang et al., 2017; Selote et al., 2015). Selote et al. (2015)
442 showed in a cell-free degradation assay that bHLH105/ILR3 and bHLH115 were
443 degraded when mixed with wild-type seedling whole protein extracts, whereas
444 bHLH104 remained stable even after 8 hours of incubation. In contrast, our

445 recombinant bHLH104 purified from *E. coli* was degraded within 1 hour in a
446 proteasome-dependent manner (Figure 5D). This difference may be attributed to the
447 protein expression system, as Selote et al. (2015) used in vitro translated protein from
448 wheat germ extract, which may differ from bacterially expressed protein in folding or
449 modifications that affect susceptibility to degradation. Proteasomal degradation of
450 bHLH104 is further supported by our in planta observations: mTurquoise2-bHLH104
451 protein was barely detectable by immunoblotting in transgenic lines, including
452 *pUBQ10::b104* lines despite their high transcript levels, and MG132 treatment resulted
453 in increased protein detection (Figure 5B, C). Consistently, mTurquoise2 fluorescence
454 was undetectable by confocal imaging in lines expressing full-length bHLH104,
455 whereas b104^dPAA lines showed clear nuclear signals (Figure 5E). Our data are
456 consistent with the overall model of proteasomal regulation of bHLH IVc proteins and
457 extend it to bHLH104 specifically, as our UbiGate data indicate that BTS can
458 ubiquitinate bHLH104 in a PAA-dependent manner. In line with this, a recent study
459 showed that BTSL1 and BTSL2 also target bHLH105 and bHLH115 for degradation in
460 roots (Zhao et al., 2026), indicating that multiple BTS-type E3 ligases act redundantly
461 on bHLH IVc proteins in root tissue, where Fe acquisition takes place. Interestingly,
462 MG132 treatment also resulted in higher b104^dPAA abundance (Figure 5B, C), even
463 though b104^dPAA escapes BTS-mediated ubiquitination. This indicates that PAA-
464 independent proteasomal degradation mechanisms also contribute to bHLH104
465 turnover. Such alternative degradation could involve additional E3 ligase systems, as
466 demonstrated for the apple orthologue MdbHLH104, which is targeted by the CUL3-
467 BTB/TAZ complex MdBT2-MdCUL3 independently of HRZ/BTS (Zhao et al., 2016), or
468 could involve selective autophagy, which has been shown to degrade transcription
469 factors in plants (Wang et al., 2021; Raffeiner et al., 2023). This would explain why
470 complete protein stabilization is not achieved by PAA deletion alone.
471 Interestingly, despite elevated *mTurq2-bHLH104* transcript levels in shoots,
472 *pUBQ10::b104* lines showed no phenotype, in contrast to previously reported
473 *p35S::bHLH104-GFP* lines that displayed enhanced Fe deficiency tolerance,
474 increased ferric-chelate reductase activity, and Fe overaccumulation (Zhang et al.,
475 2015). Several factors may account for this discrepancy. The 35S promoter typically
476 drives stronger expression than the *UBQ10* promoter, potentially saturating BTS-
477 mediated degradation capacity. Additionally, the C-terminal GFP tag in *35S::bHLH104-*
478 *GFP* lines may affect BTS accessibility to the adjacent PAA short sequence, whereas

479 an N-terminal mTurquoise2 tag leaves the C-terminus unobstructed. The
480 *pb104::b104*^dPAA line #2 exhibited upregulation of *ILR3/BHLH105, BHLH115,*
481 *BHLH39* and *BHLH100* in roots under both +Fe and -Fe conditions. This indicates that
482 functional output of bHLH104 depends on protein accumulation rather than transcript
483 abundance. Whether the observed upregulation of *BHLHIVC* genes reflects direct
484 transcriptional autoregulation or indirect effects through altered Fe status remains to
485 be determined; however, these findings suggest a potential positive feedback loop
486 within the bHLH IVc network that is gated by BTS-mediated degradation. The direct
487 interaction of bHLH104 with the BTS E3 ligase has been reported previously (Long et
488 al., 2010; Selote et al., 2015; Lichtblau et al., 2022), and genetic evidence supported
489 a regulatory upstream relationship of BTS towards bHLH104 (Zhang et al., 2015). We
490 tested this regulatory relationship and identified that the PAA short sequence is needed
491 for BTS interaction with bHLH104. We propose a model (Figure 8) in which bHLH104
492 protein is maintained at low abundance through proteasome-mediated degradation.
493 A limitation of this study is the difficulty in visualizing mTurquoise2-tagged full-length
494 bHLH104 in planta due to rapid degradation, whereas b104^dPAA was detectable in
495 early developing seedlings (Figure 5E). Future studies should investigate additional
496 post-translational modifications and identify environmental and physiological
497 conditions that promote bHLH104 stabilization.

498 **b104^dPAA stimulates Fe and metal ion accumulation and potential for**
499 **biofortification**

500 Multiple metals accumulated in *pb104::b104*^dPAA plants. The multi-metal
501 accumulation can be explained by persistent activation of a broad array of metal
502 transporters in root cells, like Fe-, Zn and Mn-transporting IRT1, Fe- and Mn-
503 transporting NRAMP1, Cu-transporting COPT2, Mn-transporting MTP8 (Connolly et
504 al., 2002; Vert et al., 2002; Cailliatte et al., 2010; Eroglu et al., 2016). The genes
505 encoding these transporters are under control of the FIT transcription factor (Schwarz
506 and Bauer, 2020), and the FIT pathway was found active downstream of bHLH104 in
507 our study. Since b104^dPAA plants accumulate excess metals including Zn, this could
508 further amplify the Fe deficiency signal. This is consistent with reports that heavy
509 metals like Zn can induce Fe deficiency responses at the level of Fe sensing rather
510 than by directly inhibiting Fe transport (Lešková et al., 2017), and with the
511 demonstration that Zn or Fe binding to multiple domains of HRZ E3 ligases modulates

512 their stability and function in response to Fe nutritional status (Shinkawa et al., 2025).
513 Thus, the accumulated metals in *pb104::b104^dPAA* plants may reinforce Fe
514 deficiency signalling, creating a positive feedback loop that sustains constitutive Fe
515 uptake. Similar phenotypes where Fe accumulation disrupts plant growth have been
516 reported in *BTS* loss-of-function mutants and in overexpression lines of *BHLH39* or
517 *BHLH105* (Zhang et al., 2015; Li et al., 2016; Hindt et al., 2017; Naranjo-Arcos et al.,
518 2017). A still unresolved question is why the known negative post-translational
519 regulation mechanisms, e.g. IRT1 ubiquitination and degradation under low Fe and
520 excessive Zn and Mn, are not in place here (Dubeaux et al., 2018; Abuzeineh et al.,
521 2022). Perhaps this type of regulation requires that Zn and Mn are supplied in the
522 rhizosphere rather than inside the root. In our experimental settings, excessive Zn and
523 Mn were not supplied and Zn and Mn accumulated due to plant internal imbalance.

524 We observed that b104^dPAA protein abundance in seedling roots correlated with
525 phenotype severity among *pb104::b104^dPAA* lines. A plausible explanation is that
526 this variation in protein abundance across lines results from differences in transgene
527 copy number arising from the floral dip transformation method (Gelvin, 2003; Nagaya
528 et al., 2005; Meiser et al., 2011; Li et al., 2016). Notably, *pb104::b104^dPAA line #3*,
529 which showed negligible b104^dPAA protein in seedling roots, grew normally during
530 early development but accumulated Fe in leaves at the reproductive stage. This
531 suggests that minimal b104^dPAA activity can increase Fe content without causing
532 severe growth defects, highlighting potential for Fe biofortification strategies. We
533 acknowledge that our transgenic lines have b104^dPAA along with endogenous
534 bHLH104 protein activity, so that b104^dPAA alone or together with endogenous
535 bHLH104 could contribute to the observed phenotypes. Additional investigations will
536 be required to define the precise threshold at which bHLH104^dPAA protein levels
537 enhance Fe accumulation without compromising plant growth. As demonstrated by the
538 growth defects in strong b104^dPAA -expressing lines, careful optimization of protein
539 levels would be required to achieve Fe biofortification without compromising plant
540 health. The milder phenotype of *pb104::b104^dPAA line #3*, which showed elevated
541 leaf Fe content at reproductive stage without severe growth defects, suggests that
542 fine-tuning of this system may be achievable through careful selection of lines with
543 appropriate expression levels. More broadly, the findings integrate with emerging work
544 on BTS/BTSL hemerythrin-based Fe/oxygen sensing (Selote et al., 2015; Pullin et al.,

545 2025) and clarify how post-translational control translates Fe status into transcriptional
546 outputs.

547 **Pleiotropic and tissue-specific effects of b104^dPAA**

548 The phenotypes observed in *pb104::b104^dPAA* plants extend beyond simple Fe
549 accumulation, suggesting that constitutive Fe deficiency signaling has broader
550 physiological consequences. Several phenotypes observed in these lines may reflect
551 activation of multiple stress regulatory pathways. First, the delayed flowering
552 phenotype may result from -Fe response signaling interfering with flowering time
553 control through epigenetic, circadian, and hormone pathways (Cheng et al., 2004;
554 Salomé et al., 2012; Chen et al., 2013; Hong et al., 2013; Wild et al., 2016; Dutta et
555 al., 2017; Maruoka et al., 2022). Second, gene ontology analysis of
556 *pb104::b104^dPAA* leaves showed enrichment of immune signaling and salicylic acid
557 signaling terms. Fe deficiency treatment is known to elevate salicylic acid levels and
558 induce salicylic acid-responsive genes (Shen et al., 2016), and bHLH105 can integrate
559 Fe homeostasis with plant immune responses against pathogens (Rampey et al.,
560 2006; Aparicio and Pallás, 2017; Samira et al., 2018). This suggests that the Fe
561 deficiency response is interconnected with immune signaling pathways.

562 Expression of b104^dPAA in *pb104::b104^dPAA* lines results in distinct tissue-specific
563 consequences. The lack of upregulation of internal Fe allocation genes such as *BTS,*
564 *PYE, IMA1*, *BHLH100, BHLH39* under -Fe condition in the leaves of mature
565 *pb104::b104^dPAA* lines suggests that elevated local Fe levels in the leaves suppress
566 the Fe deficiency response downstream of bHLH104, consistent with recent evidence
567 that leaf Fe responses are determined mainly by local Fe status rather than root-
568 derived systemic signals (Nguyen et al., 2022; Ngigi et al., 2025). In contrast, in roots
569 of *pb104::b104^dPAA* lines, -Fe acquisition genes such as *FIT*, *IRT1* and *FRO2* were
570 upregulated. This indicates that, rather than systemic signaling, an active and
571 constitutive Fe acquisition response is maintained in the roots. In wild-type plants,
572 bHLH104 is expected to be stabilized only under Fe deficiency, enabling transient
573 activation of uptake genes. Lack of PAA prevents this regulation, resulting in
574 constitutive bHLH104 activity and continuous Fe uptake regardless of Fe status.
575 Interestingly, we observed enhanced Fe mobilization to young leaves in
576 *pb104::b104^dPAA line #2* after 3 days of Fe supply following growth in –Fe. In

577 contrast, wild-type plants retained most Fe in roots The enhanced root-to-shoot Fe
578 mobilization in pb104::b104^dPAA line #2 may be partly explained by the elevated
579 IRT1 expression in these lines. (Quintana et al., 2022) showed that IRT1 protein,
580 independent of its Fe(II) transport activity, is necessary for effective root-to-shoot Fe
581 partitioning, suggesting that constitutive IRT1 upregulation driven by b104^dPAA could
582 promote Fe translocation to shoots.. This shows that bHLH104 protein stability serves
583 as a critical control point linking Fe sensing to transcriptional responses in roots,
584 whereas leaves respond primarily to local Fe availability through regulatory
585 mechanisms independent of bHLH104 protein stability. Grafting experiments would
586 help determine whether the effects of stabilized bHLH104 are root- and leaf-
587 autonomous or involve systemic signaling.

588 **The PAA short sequence is critical for protein regulation**

589 The present study found that the terminal PAA sequence of bHLH104 mediates critical
590 interactions. Additionally, small proteins IMA1 and IMA3, which interact with BTS and
591 BTSL1, also contain a conserved C-terminal PAA sequence, indicating that this
592 sequence is broadly conserved for E3 ligase recognition (Li et al., 2021; Lichtblau et
593 al., 2022). Other members of the bHLH IVc family have instead a PVA terminal
594 sequence. It has not yet been examined which role PVA plays and whether it is similar
595 to PAA. One possible explanation is that the middle alanine in the PAA sequence of
596 bHLH104 may not be essential. Previous studies have shown the significance of
597 terminal alanine residue in bHLH IVc protein regulation. The terminal alanine in
598 bHLH115 and bHLH105 is essential for BTS interaction (Li et al., 2021), while
599 overexpression of bHLH34 with its terminal alanine substituted to valine resulted in a
600 metal accumulation phenotype similar to our observations (Sharma and Yeh, 2020).
601 Taken together, these observations support the conclusion that the PAA sequence is
602 required for the recognition of bHLH104 by the proteasomal degradation system. Our
603 findings refine the BTS recognition requirement from the larger bHLH104 C-terminal
604 deletions previously used to map this interaction to a three-residue sequence. The
605 conservation of this sequence in bHLH104 orthologues, and its presence with minor
606 variations in other bHLH IVc members, corrobates the evidences on the conserved
607 BTS(L) recognition interface within the family. In future studies, the specificity and
608 position effects of each amino acid in the PAA and PVA short sequences can be further
609 examined. It will also be interesting to test whether artificial addition of PAA to

610 transcription factors can target them for degradation by BTS/L proteins under Fe
611 deficiency, which would establish PAA as both necessary and sufficient for BTS
612 recognition. If so, this can be exploited in future synthetic and plant biotechnological
613 approaches.

614 **Concluding remarks and perspectives**

615 This study provides evidence that a short three–amino acid PAA sequence in
616 bHLH104 is required for post-translational regulation of protein abundance and
617 activity.

618 The conserved PAA sequence provides opportunities for biotechnological
619 applications. As bHLH IVc proteins are conserved across plant species (Jiang et al.,
620 2024), genome editing of this sequence in crop orthologues may enhance Fe
621 accumulation for biofortification. In contrast to whole-gene overexpression, precise
622 PAA editing offers potential to increase Fe content while minimizing pleiotropic effects.
623 However, because the PAA sequence is also present in IMA proteins, which positively
624 regulate Fe uptake, editing approaches must specifically target bHLH IVc genes
625 without affecting *IMA* genes. Testing whether PAA addition to other transcription
626 factors targets them for BTS/BTSL-mediated degradation could enable Fe-responsive
627 protein degradation systems for synthetic biology applications.

628 Overall, our findings provide comprehensive evidence which shows that post-
629 translational regulation of bHLH104 is necessary to maintain a balance between Fe
630 acquisition and normal growth and development, and that disrupting this control can
631 lead to wide-ranging physiological effects. This research has direct impact for
632 improving crop productivity on alkaline/calcareous soils and under climate stress.
633 Identifying sequence motifs that control master regulators of Fe uptake such as
634 bHLH104 provides paths for crop improvement and biofortification. Our finding is that
635 a three–residue PAA short sequence in bHLH104 can be a precise target for tuning
636 Fe acquisition in plants. Given current efforts to enhance micronutrient use efficiency
637 and nutritional quality, these insights are both mechanistically fundamental and directly
638 translatable.

639 **Materials and methods**

640 **Gene Accession numbers**

641 The following *Arabidopsis thaliana* genes were the focus of this study: bHLH104
642 (AT4G14410), BTS/BRUTUS (AT3G18290), BTSL1 (AT1G74770), and BTSL2
643 (AT1G18910).

644 **Plant Material and Growth Conditions**

645 *Arabidopsis thaliana* Columbia-0 (Col-0) was used as the wild type in this study. The
646 transgenic lines were generated using the floral dip method using Rhizobium
647 radiobacter strain GV3103 (*Agrobacterium tumifaciens)* (Clough and Bent, 1998).
648 Constructs for generating transgenic lines were assembled using the GreenGate
649 cloning system (Lampropoulos et al., 2013). The following modules were assembled
650 into pGGZ003 destination vector: Promoter sequence (pUBQ10/ pbHLH104 (1636-bp
651 sequence upstream of *BHLH104* gene)), an N-terminal mTurquoise2 fluorescent tag,
652 Coding sequence (*BHLH104/BHLH104^dPAA*), bHLH104 terminator sequence (975
653 bp), Hygromycin selection marker. Primers used are listed in Supplementary Table 1.

654 For plate-based experiments, plants were grown as described in (Lingam et al., 2011;
655 Lichtblau et al., 2022) in modified half-strength Hougland medium. Fe was supplied as
656 50 µM Fe(III)-EDTA for +Fe or omitted for -Fe conditions. The efficacy of Fe deficiency
657 treatment was validated by confirming upregulation of canonical Fe deficiency marker
658 genes (*IRT1, FRO2, bHLH39, bHLH100*) in WT plants (Supplementary Figure S18).

659 All plants for the phenotyping experiments were genotyped for the presence of
660 transgene. For hydroponic experiments, seedlings were initially grown on modified
661 half-strength Hoagland agar plates for 12 days before being transferred to a
662 hydroponic setup as described in (Ngigi et al., 2025).

663 For soil-based phenotyping experiments, seedlings were transferred to soil on the
664 eighth day after germination. Phenotypic measurements were taken after three weeks
665 of soil growth.

666 **Phenotyping and Image Acquisition**

667 Automated phenotyping was performed using the MicroScan system equipped with a
668 PlantEye F600 sensor (Phenospex, Heerlen, The Netherlands) and controlled by the
669 implemented software HortControl (Phena version 2.0, HortControl version 3.85) as
670 previously described (Arend et al., 2016; Hüther et al., 2020; Knopf and Bauer, 2025).
671 The PlantEye system recorded three-dimensional and spectral parameters. Spectral

672 data included, the normalized difference vegetation index (NDVI), calculated as (near-
673 infrared reflectance [NIR] − red reflectance [RED])/(NIR + RED).

674 Manual morphological phenotyping like flowering time, root length was performed as
675 described in (Knopf and Bauer, 2025).

676 Fe reductase activity was measured using a protocol described in (Gratz et al., 2019).
677 Each assay included at least three biological replicates.

678 Seed number was estimated based on seed weight. For each biological replicate, 100
679 seeds were manually counted and weighed to determine the mean weight per 100
680 seeds. The total seed number was calculated as (total seed weight/ weight of 100
681 seeds) × 100. Three biological replicates were analyzed for each genotype.

682 **Plant Protein Extraction and Immunoblotting**

683 Total proteins were extracted from roots of Arabidopsis thaliana seedlings grown in
684 modified half-strength Hougland media plates. Proteins were solubilized in 2× SDG
685 buffer (125 mM Tris-HCl, pH 6.8, 5% SDS, 4% DTT, 20% glycerol, 0.02% bromophenol
686 blue) at a ratio of 10 µl buffer per 5 mg homogenized root tissue. After rotation for 10
687 minutes and centrifugation (13,000 rpm, 10 minutes, 4°C), supernatants were
688 collected and boiled at 60°C for 10 minutes.

689 Proteins were separated by SDS-PAGE using 4–20% Mini-PROTEAN TGX Stain-Free
690 gels (Bio-Rad) and transferred to 0.45 µm nitrocellulose membranes (Bio-Rad) with
691 the Trans-Blot Turbo Transfer System (Bio-Rad).

692 Membranes were blocked for 5 minutes in EveryBlot Blocking Buffer (Bio-Rad) and
693 incubated for 1 hour at room temperature with primary antibodies against mTurquoise2
694 (Biozol, NBS-ASJ-L9MMEL-60; 1:1000 dilution) in 2.5% TBST with blocking buffer.
695 After three washes in 1× TBST, membranes were incubated with HRP-conjugated
696 secondary antibody - mouse anti-goat for mTurquoise2 [Invitrogen, G-21040; 1:1000
697 dilution] in TBST with 5% milk] for 1 hour. Chemiluminescent signals were developed
698 with ECL substrate (Amersham ECL Select or SuperSignal West Femto) and imaged
699 using the ChemiDoc MP Imaging System.

700 To assess the effect of proteasome inhibition on bHLH104 protein stability, 10-day-old
701 Arabidopsis seedlings were transferred to liquid Hoagland medium and incubated for

702 18 hours in a plant growth chamber under the same growth conditions described
703 above. Seedlings were treated with either 50 μM MG132 or an equal volume of DMSO
704 (control). After treatment, total protein from roots was extracted and analyzed by
705 immunoblotting. Band intensities were quantified using Biorad-Image Lab™ Software,
706 and normalized to total protein staining. For each genotype, three independent
707 biological replicates were used.

708 **Cell-Free Protein Degradation Assay**

709 The coding sequence of bHLH104 was cloned into an expression vector containing an
710 N-terminal His tag and transformed into *Escherichia coli Rosetta (DE3)* cells. Single
711 colonies were cultured overnight in LB medium with ampicillin, and secondary cultures
712 were inoculated at 1% volume, grown at 37°C to OD_{600} = 0.6–0.8, and induced with 1
713 mM IPTG at 28°C for 10–12 hours. Cells were harvested by centrifugation and stored
714 at –70°C.

715 For purification, frozen cell pellets were thawed on ice, resuspended in lysis buffer (30
716 mM Tris-HCl, pH 8.0, 150 mM NaCl) supplemented with protease inhibitors (Roche),
717 and sonicated. Lysates were clarified by centrifugation (14,000 rpm, 30 minutes, 4°C),
718 and His-tagged bHLH104 protein was purified using a Ni-NTA column (Cytiva) on a
719 Bio-Rad NGC chromatography system. Bound proteins were batch-eluted with 250
720 mM imidazole in lysis buffer, and fractions containing the target protein were pooled,
721 concentrated using Amicon centrifugal filters, and quantified using absorbance at 280
722 nm with a NanoQuant plate (Tecan). Protein concentrations were calculated using the
723 molar extinction coefficient predicted by ExPASy ProtParam, and proteins were
724 aliquoted and stored at –70°C.

725 We followed protocol from Wang et al., 2009, for cell-free degradation assay.
726 Degradation reactions were initiated by incubating 50 μl of plant extract with purified
727 His-bHLH104 protein at 22°C. Protein extracts were treated with either 160 μM MG132
728 or an equal volume of DMSO (control). Reactions were stopped at indicated time
729 points by adding SDS loading buffer and boiling at 95°C for 10 minutes. Proteins were
730 separated by SDS-PAGE, transferred to nitrocellulose membranes, and detected by
731 immunoblotting using an HRP-conjugated anti-His antibody (Thermo Fisher Scientific,
732 MA1-21315-HRP).

733 **Confocal Microscopy**

734 Confocal imaging was performed using a Zeiss LSM 880 laser-scanning confocal
735 microscope equipped with a 40× C-Apochromat water immersion objective. Two-day-
736 old Arabidopsis thaliana seedlings grown under +Fe conditions were used for imaging.
737 Excitation of mTurquoise2 fluorescence was carried out using a 458 nm laser line, and
738 emitted fluorescence was collected between 493 nm and 613 nm. Images were
739 processed and analyzed using the manufacturer's software ZEN lite (Zeiss).

740 **ICP-MS Analysis**

741 Tissues were harvested, washed sequentially in Tris-EDTA buffer and deionized water,
742 dried on tissue paper, transferred into pre-weighed 5-ml Falcon tubes, and oven-dried
743 at 65°C for up to two weeks. Tissue digestion was performed with 67% nitric acid (ICP-
744 MS grade) at volumes adjusted to sample mass (1 ml for 20–35 mg, 500 µl for 10–20
745 mg, 350 µl for <10 mg). Samples were incubated at room temperature overnight and
746 then heated at 95°C until clear. After centrifugation (4000 rpm, 30 minutes, 4°C),
747 supernatants were diluted with deionized water to maintain a final acid concentration
748 below 5% (v/v). Elemental analysis was performed using inductively coupled plasma-
749 mass spectroscopy (ICP-MS, Agilent 7700). ICP-MS measurements were corrected
750 for background signal and normalized by sample dilution factors.

751 **RNA Isolation and RT-qPCR Analysis**

752 Total RNA was extracted using the RNeasy Plant Mini Kit (Qiagen) with on-column
753 DNase digestion. First-strand cDNA synthesis was performed with the RevertAid
754 Reverse Transcriptase kit (Thermo Fisher Scientific) using 300–500 ng RNA per
755 reaction. RNA was treated with DNase I, followed by heat inactivation with EDTA and
756 oligo(dT) primer annealing. Reverse transcription was carried out at 42°C for 1 hour.
757 cDNA was diluted 1:10 and 1:100 for downstream applications and stored at –20°C.

758 Quantitative PCR (qPCR) was performed according to protocol in (Ngigi and Bauer,
759 2023). Each sample was measured in technical duplicates alongside a six-point
760 standard curve (10^7–10^2 copies) for each gene. The PCR program included an initial
761 denaturation (95°C, 3 min) followed by 40 cycles of 95°C denaturation (10 sec),
762 annealing at gene-specific temperature (15 sec), and extension (5 sec). Melt curve
763 analysis was conducted from 65°C to 95°C.

764 Starting quantities were calculated from the standard curves and normalized as
765 described in (Ngigi and Bauer, 2023; Ngigi et al., 2025). Normalized expression values
766 were visualized as z-score heatmaps using R.

767 **RNA Sequencing and analysis**

768 RNA sequencing (RNA-seq) was performed by BMKGENE (Biomarker Technologies).
769 Library preparation and sequencing were conducted according to the service
770 provider's standard protocols. Data was processed following protocol in (Mai, 2024).

771 For DEG analysis, RNA-seq matrices were analyzed in R (v4.3+) with limma (v3.58+)
772 using the limma-trend workflow appropriate for TPM data. Expression values were
773 log2-transformed as log2(x + 0.5), where x is TPM value. For each comparison (line
774 vs WT), linear models were fit with empirical Bayes moderation, and contrasts were
775 estimated to obtain log2 fold-changes (log2FC) and Benjamini–Hochberg (BH)-
776 adjusted P values. Genes were called differentially expressed if FDR ≤ 0.05 and
777 |log2FC| ≥ 0.58 (~1.5-fold).

778 **Gene Ontology enrichment**

779 GO Biological Process enrichment was performed with clusterProfiler (v4.10+) against
780 the appropriate org.*.eg.db annotation. Up- and down-regulated DEG sets were tested
781 separately. The gene universe for each test comprised all genes assessed in the
782 corresponding comparison. Over-representation p values were computed by the
783 hypergeometric test and adjusted by Benjamini–Hochberg; terms with FDR ≤ 0.05
784 were considered significant. When indicated, redundant terms were condensed with
785 simplify() (Wang similarity measure (Wang et al., 2007); cutoff = 0.7), retaining the
786 most significant representative.

787 **Bioinformatic analyses**

788 Protein domain architecture of bHLH104 was analyzed using the MyHits Motif Scan
789 server (https://myhits.sib.swiss/cgi-bin/motif_scan)(Pagni et al., 2007). bHLH domain
790 was identified at residues 121-181. The leucine zipper (LZ) domain was identified at
791 residues 181-202. Protein structures for bHLH104, BTS and its interaction interfaces
792 were predicted using AlphaFold Multimer (Evans et al., 2021; Jumper et al., 2021). For
793 each protein-protein complex, 25 models were generated (5 models × 5 random
794 seeds) to ensure comprehensive conformational sampling. Model quality was

795 assessed using pLDDT (predicted Local Distance Difference Test) scores for per-
796 residue confidence and ipTM (interface predicted Template Modeling) scores for
797 interface accuracy.

798 The resulting structures were visualized and analyzed using UCSF ChimeraX
799 (Pettersen et al., 2004).

800 **Yeast Two-Hybrid Assay**

801 Yeast two-hybrid assays were performed as described by (Gietz and Schiestl, 2007;
802 Lichtblau et al., 2022). C-terminal fragments of bHLH104 and b104^dPAA were cloned
803 into the Gateway-compatible yeast vectors pACT2-GW and pGBKT7-GW. Primers
804 used are listed in Supplementary Table 1. Full-length BTS, BTSL1, and BTSL2
805 constructs were described in (Lichtblau et al., 2022).

806 Yeast strain AH109 was co-transformed with plasmid pairs using the lithium acetate
807 (LiAc) method and selected on synthetic dropout (SD) medium lacking leucine and
808 tryptophan (SD–Leu–Trp). Colonies were cultured overnight in liquid SD–Leu–Trp
809 medium, adjusted to an OD_{600} of 1.0, and spotted (10 µl) in tenfold dilution series onto
810 SD medium lacking leucine, tryptophan, and histidine (SD–Leu–Trp–His). To suppress
811 autoactivation, SD–Leu–Trp–His plates supplemented with 15 mM 3-amino-1,2,4-
812 triazole (3-AT) were used specifically for assays involving BTSL2. Plates were
813 incubated at 30°C, and growth was monitored for up to 14 days.

814 **UbiGate Assay**

815 Ubiquitination assays were performed using the UbiGate system as described
816 previously (Kowarschik et al., 2018). Constructs for generating transgenic lines were
817 assembled using the Golden Gate assembly. The following modules were assembled
818 into pGG-pET28 destination vector: 6×His-tagged ubiquitin, E1 ligase (*Arabidopsis*
819 *thaliana* UBA1), E2 ligase (Arabidopsis thaliana UBC8), E3 ligase (BTS-HC), substrate
820 (*BHLH105* and *BHLH104* coding sequences were codon-optimized for E. coli
821 expression using GeneArt Gene Optimizer software and synthesized by GeneArt
822 Gene Synthesis, Thermo Fisher Scientific). Primers used are listed in Supplementary
823 Table 1. Assembled vectors were transformed into *Escherichia coli Rosetta (DE3)* and
824 expressed by induction with 1 mM IPTG and 3% ethanol at 28°C for 3 hours. Cells

825 were harvested by centrifugation and stored at –80°C. Protein extraction and sample
826 preparation was performed as previously described in (Ortmann et al., 2023).

827 Proteins were separated by SDS-PAGE using TGX precast gels (Bio-Rad) and
828 transferred to 0.2 µm nitrocellulose membranes with the Trans-Blot Turbo system (Bio-
829 Rad). Membranes were blocked with 5% (w/v) non-fat dry milk in TBST and probed
830 with the following primary antibodies: HRP-conjugated anti-Myc (Thermo Fisher
831 Scientific, R951-25-HRP), anti-GST (clone 8-326, Thermo Fisher Scientific) followed
832 by HRP-conjugated secondary antibody (Jackson ImmunoResearch), HRP-
833 conjugated Strep-Tactin (Fisher Scientific), and HRP-conjugated anti-6×His (Thermo
834 Fisher Scientific, MA1-21315-HRP). Signals were detected using the Amersham ECL
835 Prime kit (Cytiva) and visualized with the ChemiDoc MP Imaging System (Bio-Rad).

836 **Statistical Analysis and Data Visualization**

837 All statistical analyses and data visualization were performed using RStudio (version
838 2025.04.1). Phenotyping data were visualized using ggplot2. Gene expression data
839 were Z-score normalized using the scale() function in R, and gene expression
840 heatmaps were created using the pheatmap package to visualize normalized
841 expression levels across tissues and experimental conditions. For ICP-MS data
842 visualization, the ggPlantMap package (Jo and Kajala, 2024) was used.

843 Statistical comparisons were performed using two-way ANOVA followed by Tukey's
844 Honest Significant Difference (HSD) test for multiple comparisons. A p-value threshold
845 of 0.05 was considered significant.

846 **Acknowledgements**

847 We thank Elke Wieneke for excellent technical assistance. The authors thank the
848 Biocenter-MS Platform, Sabine Ambrosius and Sabine Metzger, University of Cologne,
849 for conducting and providing support in the ICP-MS measurements. The authors thank
850 Center for Advanced Imaging (CAi) at Heinrich Heine University for providing
851 advanced imaging facility. DB and VV were members of the international graduate
852 school iGRAD-Plant, Düsseldorf (the DFG International Research Training group
853 2466). Chat GPT 4.0 has been used to edit and shorten text, and correct and improve
854 language.

855 **Author contributions**

DB, PB planned and designed the research. DB, SW, MK, VLVS performed experiments and analysed data. JLE provided materials and protocol. DB wrote the manuscript. All authors read, corrected and approved the manuscript.

Funding

This project was funded by the Deutsche Forschungsgemeinschaft (DFG, German Research Foundation) under Germany´s Excellence Strategy – EXC-2048/1 – project ID 390686111. This project received funding through the DFG International Research Training group 2466 (GRK F020512056 (NextPlant)). Funded by the Deutsche Forschungsgemeinschaft (DFG) – TRR 341/1 – 456082119.

Data Availability

The RNA-seq data generated in this study have been deposited in ArrayExpress at EMBL-EBI under accession number E-MTAB-16555. Confocal microscopy images have been deposited in the BioImage Archive under accession number S-BIAD2765.

Figure 1. Conceptual model of bHLH104 regulation by its conserved PAA sequence.

In the full-length bHLH104 protein, the PAA sequence forms the interaction interface with an E3 ligase, likely enabling ubiquitination and proteasomal degradation of bHLH104.

Figure 2. Transgenic expression of bHLH104 lacking the PAA sequence leads to growth alterations and physiological changes in Arabidopsis.
(A) Schematic representation of constructs used to generate transgenic lines expressing either full-length bHLH104 (pb104::b104) or a C-terminal deletion variant lacking the conserved three–amino acid PAA sequence (pb104::b104^dPAA). Both constructs are driven by the native bHLH104 promoter (2,069 bp) and fused at the N-terminus to an mTurquoise2 fluorescent tag. The deleted PAA sequence in b104^dPAA is indicated by a red cross at the C-terminus. Scale bar = 200 bp.

(B) Representative images of 10-day-old seedlings grown on +Fe medium (scale bar = 2 cm).

(C) Primary root length of 12-day-old seedlings grown vertically on Hoagland medium supplemented with Fe.

885 (D) Fe reductase activity in roots of 10-day-old seedlings grown under +Fe. Activity
886 was quantified spectrophotometrically as Fe(II)–ferrozine complex formation and
887 normalized to total root length.

888 (E) Representative images of four-week-old soil-grown plants (scale bar = 2 cm).
889 Shown are Col-0 (WT), two independent pb104::b104 lines (#1, #2), and four
890 independent pb104::b104^dPAA lines (#1–4).

891 (F–G) Quantitative analysis of aboveground phenotypes using the Phenospex
892 PlantEye system: (F) 3D leaf area (mm²); (G) NDVI (Normalized Difference Vegetation
893 Index)

894 (H) Flowering time, recorded as days to bolting.

895 (I) Seed number per plant, estimated from total seed weight based on mean weight
896 per 100 seeds.

897 Data represent means ± SD (n = 7–12 biological replicates per line). Statistical
898 analysis was performed using two-way ANOVA followed by Tukey's post hoc test.
899 Different letters indicate statistically significant differences at $p < 0.05$.

900 **Figure 3.** Transgenic lines expressing bHLH104^dPAA exhibit increased iron
901 accumulation and altered iron homeostasis gene expression in seedling stage.

902 (A) Schematic representation of the experimental design. Arabidopsis seedlings were
903 grown for 10 days after sowing (DAS) under either iron-sufficient (+Fe) or iron-deficient
904 (–Fe) conditions. Shoot and root tissues were collected separately for ICP-MS and
905 gene expression analyses. (B) Genotypes used in this study. Abbreviations of lines
906 used: L1, wild-type Col-0; L2, pb104::mTurquoise2-bHLH104 line #1; L3,
907 pb104::mTurquoise2-bHLH104 line #2; L4, pb104::mTurquoise2-b104^dPAA line #2;
908 L5, pb104::mTurquoise2-b104^dPAA line #3; L6, pUBQ10::mTurquoise2-bHLH104
909 line #1; L7, pUBQ10::mTurquoise2-bHLH104 line #2.(C) Iron content in shoot and root
910 tissues of seedlings grown under +Fe and –Fe conditions, measured by ICP-MS. Data
911 represent the mean of three biological replicates (n = 3). Heat map intensity reflects
912 iron concentration (μg/g dry weight). Color shading was rendered using the R package
913 ggplantmap, with darker blue indicating higher Fe accumulation. Notably,
914 pb104::b104^dPAA lines show increased Fe accumulation in roots and shoots under
915 +Fe conditions. Asterisks indicate genotypes that differ significantly from WT within the
916 same tissue and treatment condition ($p < 0.05$), as determined by two-way ANOVA

917 and Tukey's post hoc test (n = 3 for each group). (D) Clustered heatmaps showing the
918 expression profiles (RNA sequencing) of selected Fe homeostasis genes. Heatmaps
919 were generated in RStudio version 4.4.1 using calculated Z-scores of normalized gene
920 expression values across tissues for both +Fe and –Fe conditions. Purple indicates
921 low expression and yellow indicates high expression.

922 **Figure 4.** Elevated shoot iron accumulation and altered Fe deficiency responses in
923 reproductive-stage bHLH104^dPAA transgenic lines.

924 (A) Plant lines used In this experiment. Abbreviations of lines used: L1, wild-type Col-
925 0; L2, pb104::mTurquoise2-bHLH104 line #1; L3, pb104::mTurquoise2-bHLH104 line
926 #2; L4, pb104::mTurquoise2-b104^dPAA line #2; L5, pb104::mTurquoise2-b104^dPAA
927 line #3; L6, pUBQ10::mTurquoise2-bHLH104 line #1; L7, pUBQ10::mTurquoise2-
928 bHLH104 line #2.

929 (B) Representative images of 30-days-old Arabidopsis plants grown in hydroponic
930 system (scale bar = 5 cm). Among grown plant lines, pb104::b104^dPAA #2 (L4) grew
931 poorly and was not used in ICPMS and gene expression analysis.

932 (C) Experimental design for the dataset shown. Arabidopsis plants were grown
933 hydroponically under iron-sufficient (+Fe) conditions for 27 days, followed by a 3-day
934 treatment with either +Fe or –Fe media.

935 (D) Schematic representation of tissue separation used for both ICP-MS and RT-qPCR
936 analysis. Young and old leaves were separated from the roots to examine tissue-
937 specific iron accumulation and gene expression. The same tissue layout is used to
938 represent heatmaps in the ICP-MS dataset.

939 (E) Iron content in young leaves, old leaves, and roots under +Fe and –Fe conditions,
940 measured by ICP-MS. Data represent mean values from three biological replicates (n
941 = 3). Heat map intensity reflects iron concentration (μg/g dry weight). Color shading
942 was generated using the R package ggplantmap, with deeper blue indicating higher
943 Fe content. Asterisks indicate genotypes that differ significantly from WT within the
944 same tissue and treatment condition ($p < 0.05$), as determined by two-way ANOVA
945 and Tukey's post hoc test (n = 3 for each group).

946 (F) Clustered heatmaps showing the expression profiles (RNA sequencing) of selected
947 Fe homeostasis genes in young leaves, old leaves, and roots under both +Fe and –
948 Fe conditions. Data represent the mean of three biological replicates (n = 3). Z-scores

949 were calculated from normalized RNA expression values and visualized in RStudio
950 version 4.4.1. Yellow indicates high expression; purple indicates low expression.

951 **Figure 5.** The PAA short sequence mediates bHLH104 protein stability and affects its
952 abundance in Arabidopsis.

953 (A) Genotypes and transgenic lines used in this experiment.
954 (B) Immunoblot analysis of mTurquoise2-tagged bHLH104 and b104^dPAA in
955 different transgenic lines treated with either DMSO (control) or 50 μM MG132.
956 Total protein and anti-mTurquoise2 blots are shown. Samples are labeled from
957 #L1 to #L9. The transgenic lines exhibiting increased protein abundance
958 correspond to those that displayed altered growth phenotypes in Figure 1,
959 suggesting a link between protein stability and the observed developmental
960 responses. Red arrows indicate the expected band position for mTurquoise2-
961 bHLH104 fusion protein. Additional blots for replicate studies are provided in
962 Supplementary Figure S14. Original uncropped blot is shown in Supplementary
963 Figure S19.
964 (C) Relative protein levels of mTurquoise-tagged bHLH104 were determined by
965 Western blot. Band intensities were normalized to total protein, and fold-change
966 was calculated as the ratio of MG132-treated to DMSO-treated samples. Bars
967 represent mean ± SEM; individual data points are shown.
968 (D) Cell-free degradation assay showing in vitro degradation of His-tagged
969 bHLH104 protein when incubated with protein extracts from 10-day-old Col-0
970 (WT) Arabidopsis thaliana seedlings. His-bHLH104 was expressed in E. coli and
971 remained stable on its own, but degraded upon incubation with the plant
972 extracts, indicating proteasome-mediated degradation. Total protein from whole
973 seedlings was extracted using standard protein extraction procedures. Samples
974 were collected at the indicated time points and analyzed by immunoblotting with
975 anti-His and anti-Actin antibodies. MG132 treatment stabilizes bHLH104,
976 indicating proteasome-dependent degradation.
977 (E) Confocal microscopy of mTurquoise2 fluorescence in roots of transgenic
978 Arabidopsis seedlings expressing full-length bHLH104 (left) or b104^dPAA
979 (right). Images show two representative seedlings (S1 and S2) per genotype.
980 Arabidopsis thaliana seedlings were at the germination stage, 5 days old,
981 corresponding to 2 days after stratification, and grown on +Fe medium. TM,

982 transmitted light; Overlay, merged mTurq2 and TM channels. Scale bar = 25 µm;
983 excitation at 458 nm; emission collected from 493–613 nm.
984

985 **Figure 6.** The PAA short sequence is required for bHLH104 interaction with BTS.
986 (A) Structural prediction of the bHLH104–BTS complex using AlphaFold2 Multimer
987 (Evans et al., 2021; Jumper et al., 2021). Left: Chain-colored model showing BTS
988 (rose color) and bHLH104 (bronze color). Right: Per-residue confidence model with
989 pLDDT scores color-coded as very high (pLDDT > 90), confident (90 > pLDDT > 70),
990 low (70 > pLDDT > 50), and very low (pLDDT < 50). Dashed circle marks the
991 interaction interface formed by BTS and bHLH104.
992 (B) Electrostatic surface potential modeling (Pettersen et al., 2004) reveals a
993 negatively charged region near the proline–alanine–alanine (PAA) sequence in
994 bHLH104 that complements a positively charged surface in the leucine–cysteine–
995 arginine (LCR) domain of BTS. The electrostatic scale ranges from –10 (purple) to +10
996 (cyan) kT/e.

997 (C) Schematic representation of full-length bHLH104, bHLH104-C and bHLH104-C-
998 dPAA used for Y2H and UbiGate assays. C-terminal parts lack the N-terminus and the
999 DNA-binding basic Helix Loop Helix (bHLH) domain. LZ is Leuzine zipper domain.
1000 Numbers indicate amino acid positions.

1001 (D) Yeast two-hybrid assays testing protein–protein interactions between bHLH104-
1002 C^dPAA and BTS. bHLH104-C and BTS heterodimerization and bHLH104-C
1003 homodimerization serve as positive controls. Note that C-terminal bHLH104 fragments
1004 were used since full length bHLH104 shows autoactivation in Y2H (Lichtblau et al.
1005 2022). Black arrows indicate positive interaction due to colony growth in the selective
1006 condition.

1007 **Figure 7.** The PAA short sequence leads to a specific bHLH104-C band in the UbiGate
1008 system testing for BTS-mediated ubiquitination of bHLH104 in E. coli cells.

1009 (A) Schematic overview of the ubiquitin/26S proteasome pathway. Each component
1010 was expressed in E. coli using the UbiGate system (Kowarschik et al., 2018).
1011 Recombinant bHLH104-C or bHLH104-C^dPAA proteins (Strep-tagged) were used as
1012 substrates. BTS-HC served as the E3 ligase (Myc-tagged), in combination with UBC8
1013 as E2 ligase (GST-tagged), an E1 activating enzyme, and ubiquitin (His-tagged).

1014 (B) The relevant immunoblot for assessing substrate ubiquitination is the anti-Strep
1015 blot. The anti-Strep antibody detects predominantly the Strep-tagged substrate protein
1016 in as an expected band corresponding to a non-ubiquitinated form (~40 kDa; brown
1017 arrows). Only in the presence of all components, there are multiple higher than 40 kDa
1018 protein bands, indicative of a protein ubiquitination ladder (Kowarschik et al., 2018),
1019 with one particular unique form (~70 kDa) potentially corresponding to
1020 polyubiquitinated bHLH104-C (green arrow corresponding to ~70 kDa plus molecular
1021 weight shift of approximately 30 kDa corresponding to the addition of three to four
1022 ubiquitin moieties of ~8.6 kDa each; grey arrows indicating additional higher molecular
1023 weight bands indicating a ubiquitination ladder pattern). The 70 kDa band is absent in
1024 the relevant controls, either bHLH104-C^dPAA lane under identical conditions or in
1025 control samples lacking individual components. Strep bands are also detectable in
1026 control lanes, these are not considered ubiquitination signals. The assay has been
1027 performed three times with similar outcome of the unique 70 kDa band which might
1028 point to the polyubiquitinated bHLH104-C target (additional replicates in
1029 Supplementary Figure S16).

1030 (C) Shown are three types of control immunoblots confirming expression of all proteins
1031 for ubiquitination activity of the E3 ligase in the UbiGate assay. All panels are from the
1032 same membrane, sequentially probed with different antibodies after stripping. Anti-
1033 GST detects E2 ligase (GST-UBC8); anti-Myc detects E3 ligase (Myc-BTS-HC); anti-
1034 His-UBQ detects total ubiquitin conjugates (His-Ub). Violet bracket indicates
1035 autoubiquitinated E2 ligase; blue bracket indicates autoubiquitinated E3 ligase. Bands
1036 in control lanes of the anti-ubiquitin blot represent E2 and E3 autoubiquitination, which
1037 is independent of substrate ubiquitination.

1038 **Figure 8.** Working model of bHLH104 regulation through the C-terminal PAA sequence
1039 and its impact on Fe homeostasis.

1040 The C-terminal PAA sequence in bHLH104 mediates interaction with BTS-type E3
1041 ligases, targeting the protein for proteasomal degradation. Deletion of the PAA motif
1042 (b104^dPAA) disrupts this interaction, leading to protein stabilization. The increased
1043 abundance of stabilized b104^dPAA enhances Fe acquisition responses in
1044 Arabidopsis.

1045 **Supplementary Figure S1.** mTurquoise2-tagged bHLH104^dPAA complements the
1046 bhlh104-1 phenotype under Fe deficiency.

1047 Representative images of 12-day-old seedlings grown on iron-deficient (–Fe) medium.
1048 Left panel: wild-type Col-0 and bhlh104-1. Right panel: pb104::mTurq2-
1049 b104^dPAA/bhlh104-1 and pUBQ10::mTurq2-b104^dPAA/bhlh104-1
1050 complementation lines. The bhlh104-1 displays chlorotic leaves compared to Col-0
1051 under iron deficiency. Expression of mTurquoise2-tagged bHLH104^dPAA under
1052 either the native bHLH104 promoter or the UBQ10 promoter restores leaf health in the
1053 bhlh104-1 background, demonstrating that the mTurquoise2-tagged protein is
1054 biologically functional. Scale bars: 2 cm.

1055 **Supplementary Figure S2.** Preliminary phenotypic screen of independent transgenic
1056 Arabidopsis lines expressing bHLH104 or bHLH104^dPAA.

1057 26 days old plants of Col-0 wild type (WT), pb104::b104 (4 independent lines),
1058 pb104::b104^dPAA (8 independent lines), and pUBQ10::b104 lines (4 independent
1059 lines), were grown under same conditions. Each tray contained eight plants derived
1060 from an independent T1 transgenic line. Lines selected for further analysis in the main
1061 study are indicated: pb104::b104 lines #1 and #2, and pb104::b104^dPAA lines #1–#4
1062 and pUBQ10::b104 lines #1 and #2, scale bar = 2 cm.

1063 **Supplementary Figure S3.** Response of bHLH104^dPAA transgenic lines to iron-
1064 limiting conditions in alkaline calcareous soil (ACS).

1065 Arabidopsis thaliana transgenic lines were grown in either control soil (pH 5.9) or
1066 alkaline calcareous soil (ACS, pH 8.1). (A) Photos of four-week-old plants grown in
1067 control and ACS soil conditions.(B) List of plant lines used in this experiment,
1068 numbered from L1 to L7. scale bar = 2 cm (C) 3D leaf area measurements: Plants
1069 were evaluated for leaf expansion and overall growth in both conditions. (D) NDVI
1070 (Normalized Difference Vegetation Index): NDVI values were measured to assess
1071 photosynthetic activity in response to ACS conditions.(E) Flowering time: Flowering
1072 time was compared between control and ACS conditions, with letters indicating
1073 statistical differences. Statistical significance was assessed by two-way ANOVA
1074 followed by Tukey's HSD test ($p < 0.05$). N = 8 plants per line.

1075 **Supplementary Figure S4.** Constitutive expression of bHLH104 did not alter growth
1076 and physiological traits in Arabidopsis.

1077 (A) Schematic representation of the construct used to generate transgenic lines
1078 expressing full-length bHLH104 (pUBQ10::bHLH104). The construct is driven by the
1079 ubiquitin 10 (UBQ10) promoter and is fused at the N-terminus to the mTurquoise2
1080 fluorescent tag. Scale bar = 200 bp.
1081 (B-C) Photos and root length quantification data of 12-day-old seedlings grown
1082 vertically on Hoagland medium supplemented with iron (+Fe). Scale bar =2 cm
1083 (D) Representative images of 4-week-old Arabidopsis plants grown in soil. Shown are
1084 Col-0 (WT) and two independent pUBQ10::b104 lines (#1, #2). Scale bar = 2 cm
1085 (E–F) Quantitative analysis of aboveground phenotypes acquired using the
1086 Phenospex PlantEye system: (E) 3D leaf area (mm^2); (F) NDVI (Normalized Difference
1087 Vegetation Index).
1088 (G) Flowering time, measured manually as the number of days to bolting.
1089 Data represent means ± SD (n = 7–12 biological replicates per line). Statistical
1090 analysis was performed using two-way ANOVA followed by Tukey's post hoc test.
1091 Different letters indicate statistically significant differences at $p < 0.05$.

1092 **Supplementary Figure S5.** Elemental content analysis of Mn, Zn, and Cu in 10-day
1093 old Arabidopsis seedlings.

1094 Heatmap showing the distribution of Mn, Zn, and Cu content (in µg/g dry weight)
1095 across different Arabidopsis seedlings, including wild-type (WT), pb104::b104 (lines
1096 #1, #2), pb104::b104^dPAA (lines #2, #3), pUBQ10::b104 (lines #1, #2). The color
1097 scale indicates the range of elemental concentrations from low (light blue) to high (dark
1098 blue). Seedlings were grown in Hoagland media with or without 50 mM Fe
1099 supplementation. Data were collected from 10-day-old seedlings, with elemental
1100 content measurements obtained via ICP-MS analysis. Three biological replicates per
1101 line were used. The plot was generated using the ggPlantMap package in RStudio.
1102 Asterisks indicate genotypes that differ significantly from WT within the same tissue
1103 and treatment condition ($p < 0.05$), as determined by two-way ANOVA and Tukey's
1104 post hoc test (n = 3 for each group).

1105 **Supplementary Figure S6.** Differential expression and GO enrichment across
1106 seedling tissues.

1107 (A) Counts of differentially expressed genes (DEGs) for each line vs WT in root and
1108 shoot under Fe(+) and Fe(−). Orange = up-regulated; blue = down-regulated; numbers

above/below bars indicate counts for each category. Total DEGs for each condition are the sum of up-regulated and down-regulated counts. DEGs were defined at FDR ≤ 0.05 and |log2FC| ≥ 0.58. X-axis labels show the abbreviated line IDs.

(B) GO Biological Process enrichment for the up-regulated (left panel) and down-regulated (right panel) DEG sets. Columns correspond to tissue/Fe combinations (Root Fe(+), Root Fe(−), Shoot Fe(+), Shoot Fe(−)). Each dot represents a significant term (BH FDR ≤ 0.05); dot size = number of genes in the term, fill = −log10(FDR), and ring color = GeneRatio. Terms plotted are the top-ranked per panel; the gene universe was all genes tested in the corresponding comparison.

Supplementary Figure S7. Expression profiles of 23 selected Fe homeostasis genes involved in Fe acquisition and mobilization

(A)Plant lines used In this experiment

(B)Clustered heatmap showing expression profiles of 23 Fe homeostasis genes (gene selection based on Ngigi et al., 2025; Schwarz et al., 2020) obtained using RNA sequencing in root and shoot tissues under +Fe and –Fe conditions. Arabidopsis seedlings were grown for 10 days after sowing (DAS) under either iron-sufficient (+Fe) or iron-deficient (–Fe) conditions.

(C) Clustered heatmap showing expression profiles of 23 Fe homeostasis genes (gene selection based on Ngigi et al., 2025; Schwarz et al., 2020) obtained using RNA sequencing in young leaves, old leaves, and roots under both +Fe and –Fe conditions. Arabidopsis plants were grown hydroponically under iron-sufficient (+Fe) conditions for 27 days, followed by a 3-day treatment with either +Fe or –Fe media.

Heatmap was generated in RStudio version 4.4.1 using calculated Z-scores of normalized gene expression values. Purple indicates low expression and yellow indicates high expression.

Supplementary Figure S8. Targeted gene expression profiling in seedlings.

(A) Schematic representation of the experimental design. Arabidopsis seedlings were grown for 10 days after sowing (DAS) under either iron-sufficient (+Fe) or iron-deficient (–Fe) conditions. Shoot and root tissues were collected separately for RT-qPCR analyses. (B) Genotypes used in this study. Abbreviations of lines used: L1, wild-type Col-0; L2, pb104::mTurquoise2-bHLH104 line #1; L3, pb104::mTurquoise2-bHLH104

1140 line #2; L4, pb104::mTurquoise2-b104^dPAA line #2; L5, pb104::mTurquoise2-
1141 b104^dPAA line #3; L6, pUBQ10::mTurquoise2-bHLH104 line #1; L7,
1142 pUBQ10::mTurquoise2-bHLH104 line #2. (C) Quantification of mTurq2-tagged
1143 bHLH104 transgenes in indicated plant lines using RT-qPCR Letters indicating
1144 statistical differences. Statistical significance was assessed by two-way ANOVA
1145 followed by Tukey's HSD test ($p < 0.05$). N = 3 per group. (D) Clustered heatmaps
1146 showing the expression profiles of selected Fe homeostasis genes obtained using
1147 RTqPCR. Heatmaps were generated in RStudio version 4.4.1 using calculated Z-
1148 scores of normalized gene expression values across root and shoot tissues for both
1149 +Fe and –Fe conditions. Purple indicates low expression and yellow indicates high
1150 expression.

1151 **Supplementary Figure S9.** Elemental content analysis of Mn, Zn, and Cu in mature
1152 Arabidopsis thaliana.

1153 Heatmap showing the distribution of iron (Fe) content (in µg/g dry weight) in young
1154 leaves, old leaves, and roots of Arabidopsis transgenic lines, including wild-type (WT),
1155 pb104::b104 (lines #1, #2), pb104::b104^dPAA (line #3), pUBQ10::b104 (lines #1, #2).
1156 Plants were grown hydroponically under iron-sufficient (+Fe) conditions for 27 days,
1157 followed by a 3-day treatment with either +Fe or –Fe media. The color scale indicates
1158 the iron content, with darker blue shades representing higher iron concentrations. Data
1159 represent the mean values from three biological replicates (n = 3). Heatmap intensity
1160 reflects iron concentration (µg/g dry weight) measured by ICP-MS. The plot was
1161 generated using the ggPlantMap package in RStudio. Asterisks indicate genotypes
1162 that differ significantly from WT within the same tissue and treatment condition ($p <$
1163 0.05), as determined by two-way ANOVA and Tukey's post hoc test (n = 3 for each
1164 group).

1165 **Supplementary Figure S10**. Differential expression and GO enrichment across
1166 reproductive stage tissues

1167 (A) Numbers of differentially expressed genes (DEGs) for each line vs WT in root
1168 (Root), young leaves (YL), and old leaves (OL) under Fe(+) and Fe(−). Orange bars
1169 show up-regulated DEGs; blue bars show down-regulated DEGs; values above/below
1170 bars are counts for each category. Total DEGs for each condition are the sum of up-

1171 regulated and down-regulated counts. DEGs were defined at FDR ≤ 0.05 and |log2FC|
1172 ≥ 0.58.

1173 (B) GO Biological Process enrichment for the up-regulated (left panel) and down-
1174 regulated (right panel) DEG sets. Columns correspond to tissue/Fe combinations
1175 (Root, YL, OL × Fe (+), Fe (−)). Each dot represents a significant term (BH FDR ≤
1176 0.05); dot size = number of genes in the term, fill = −log10(FDR), and ring color = Gene
1177 Ratio. Terms shown are the top-ranked per panel; the gene universe comprised all
1178 genes tested in the corresponding comparison. Abbreviations: YL, young leaves; OL,
1179 old leaves.

1180 **Supplementary Figure S11.** Targeted gene expression profiling in reproductive-stage
1181 plants

1182 (A) Plant lines used In this experiment. Abbreviations of lines used: L1, wild-type Col-
1183 0; L2, pb104::mTurquoise2-bHLH104 line #1; L3, pb104::mTurquoise2-bHLH104 line
1184 #2; L4, pb104::mTurquoise2-b104^dPAA line #2; L5, pb104::mTurquoise2-b104^dPAA
1185 line #3; L6, pUBQ10::mTurquoise2-bHLH104 line #1; L7, pUBQ10::mTurquoise2-
1186 bHLH104 line #2.

1187 (B) Experimental design for the dataset shown. Arabidopsis plants were grown
1188 hydroponically under iron-sufficient (+Fe) conditions for 27 days, followed by a 3-day
1189 treatment with either +Fe or –Fe media.

1190 (C) Schematic representation of tissue separation used for RT-qPCR analysis. Young
1191 and old leaves were separated from the roots to examine tissue-specific iron
1192 accumulation and gene expression.

1193 (D) Clustered heatmaps showing the expression profiles of selected Fe homeostasis
1194 genes conditions obtained using RTqPCR in young leaves, old leaves, and roots under
1195 both +Fe and –Fe. Data represent the mean of three biological replicates (n = 3). Z-
1196 scores were calculated from normalized RT-qPCR expression values and visualized
1197 in RStudio version 4.4.1. Yellow indicates high expression; purple indicates low
1198 expression.

1199 **Supplementary figure S12.** Tissue-specific metal accumulation in dPAA line #2
1200 grown under iron-deficient conditions.

1201 (A) Experimental setup: Col-0 and pb104::b104^dPAA line #2 seedlings were grown
1202 hydroponically in Fe-deficient (–Fe) media for 27 days, followed by a 3-day treatment
1203 with either +Fe or –Fe media. Tissue collection occurred at 30 days after sowing
1204 (DAS). (B) Tissue layout: Young leaves, old leaves, and roots were separated to
1205 examine tissue-specific metal accumulation (Fe, Mn, Zn, Cu).(C) Heatmap of metal
1206 content: The distribution of Fe, Mn, Zn, and Cu content (in µg/g dry weight) in dPAA
1207 line #2 and Col-0. The color scale reflects metal concentrations, with darker blue
1208 shades indicating higher content. pb104::b104^dPAA line #2 exhibited significant Fe
1209 accumulation in young leaves after Fe resupply, in contrast to Col-0, where most Fe
1210 remained in the roots. Data represent the mean values from three biological replicates
1211 (n = 3). Elemental content was measured by ICP-MS. The plot was generated using
1212 the ggPlantMap package in RStudio. Asterisks indicate genotypes that differ
1213 significantly from WT within the same tissue and treatment condition ($p < 0.05$), as
1214 determined by two-way ANOVA and Tukey's post hoc test (n = 3 for each group).

1215 **Supplementary Figure S13.** Expression profiles of genes involved in Mn, Zn, and Cu
1216 homeostasis

1217 (A)Plant lines used In this experiment

1218 (B)Clustered heatmap showing expression profiles from RNA sequencing experiment
1219 of genes involved in manganese (Mn), zinc (Zn), and copper (Cu) homeostasis across
1220 root and shoot tissues under +Fe and –Fe conditions. Arabidopsis seedlings were
1221 grown for 10 days after sowing (DAS) under either iron-sufficient (+Fe) or iron-deficient
1222 (–Fe) conditions.

1223 (C)Clustered heatmap showing expression profiles from RNA sequencing experiment
1224 of genes involved in manganese (Mn), zinc (Zn), and copper (Cu) homeostasis in
1225 young leaves, old leaves, and roots under both +Fe and –Fe conditions. Arabidopsis
1226 plants were grown hydroponically under iron-sufficient (+Fe) conditions for 27 days,
1227 followed by a 3-day treatment with either +Fe or –Fe media.

1228 Genes include metal transporters and the Cu homeostasis regulator SPL7. Heatmap
1229 was generated in RStudio version 4.4.1 using calculated Z-scores of normalized gene
1230 expression values. Purple indicates low expression and yellow indicates high
1231 expression.

1232 **Supplementary Figure S14.** Additional independent replicates and anti-mTurq
1233 immunoblots for detection of mTurquoise2-bHLH104 and -bHLH104^dPAA protein in
1234 various transgenic lines.

1235 Genotypes and transgenic lines used in this experiment.

1236 Genotypes and transgenic lines used in this experiment. The mTurquoise2
1237 fluorescent tag is fused at the N-terminus of bHLH104 and b104^dPAA in all transgenic
1238 lines.

1239 Experiment 1: immunoblot of total protein extracted from roots of 10-day-old seedlings
1240 (see also main text figure, Fig. 5B).

1241 Experiment 2: immunoblot of total protein extracted from 10-day-old whole seedlings.

1242 Experiment 3: immunoblot of total protein extracted from 6-day-old whole seedlings.

1243 For each experiment, top panels show the anti-mTurquoise2 blot and bottom panels
1244 show total protein stain as loading control. Molecular weight markers (kDa) are
1245 indicated on the right of each blot. Red arrowheads indicate the expected band
1246 position for the full-length mTurquoise2-bHLH104 fusion protein (~70 kDa). Lower
1247 molecular weight bands detected by the anti-mTurquoise2 antibody likely represent
1248 truncated or partially degraded forms of the mTurquoise2-tagged protein. Across all
1249 three independent experiments, mTurquoise2-b104^dPAA protein is consistently more
1250 abundant than mTurquoise2-bHLH104, supporting that deletion of the PAA sequence
1251 stabilizes bHLH104 protein. The three experiments represent independent biological
1252 samples differing in seedling age (6 or 10 days) and tissue type (whole seedlings or
1253 roots), demonstrating the robustness of the observed protein accumulation pattern.

1254 **Supplementary Figure S15.** Yeast two-hybrid assay results showing protein–protein
1255 interactions between bHLH104 BTSL1 and BTSL2.

1256 bHLH104 interacts with BTSL1 and BTSL2, but not bHLH104dPAA. bHLH104^ΔPAA
1257 retains the ability to heterodimerize with full-length bHLH104, serving as a control for
1258 the presence and expression of the PAA-deleted variant. Full length bHLH104 shows
1259 autoactivation in Y2H. Hence bHLH104-C and bHLH104-C-dPAA were used.

1260 Yeast co-transformed with the AD and BD combinations were spotted in 10-fold
1261 dilution series (A600 = 10–2–10–5) on SD-LW (transformation control) and SD-LWH
1262 plates supplemented with different 3AT concentrations (conc.) as indicated (selection

1263 for protein interaction). Negative controls: empty vectors. Black arrows indicate
1264 interaction.

1265 **Supplementary Figure S16.** Independent replicates of the UbiGate ubiquitination
1266 assay for bHLH104.

1267 Anti-Strep immunoblots from a total of three independent UbiGate experiments
1268 (Experiment 1, see also Fig. 7B; additional Experiment 2 and Experiment 3) supporting
1269 the possible PAA-dependent ubiquitination of bHLH104 by BTS. The anti-Strep
1270 antibody detects Strep-tagged substrate protein (~40 kDa). Brown arrows indicate
1271 non-ubiquitinated substrate. Green arrows indicate a distinct and unique higher
1272 molecular weight band (~70 kDa), present only in the bHLH104-C sample in the
1273 presence of all components, but in none of the control samples nor the bHLH104-
1274 C^dPAA samples consistent with polyubiquitinated bHLH104-C, representing a
1275 molecular weight shift of approximately 30 kDa corresponding to the addition of three
1276 to four ubiquitin moieties. Grey arrows indicate additional higher molecular weight
1277 bands that are not considered specific, as similar bands are present across control
1278 lanes. In both replicates, the ~70 kDa polyubiquitinated band is seen, supporting the
1279 resulting outcome shown in Figure 7B.

1280 **Supplementary Figure S17.** UbiGate assay showing ubiquitination of bHLH115 by
1281 BTS-HC.

1282 UbiGate ubiquitination assay testing whether bHLH115 is ubiquitinated by BTS-HC in
1283 E. coli cells. All four panels are from the same experiment, probed sequentially with
1284 different antibodies after stripping: anti-GST (E2 ligase UBC8 detection, purple box),
1285 anti-Myc (E3 ligase BTS-HC detection, blue box), anti-Strep (substrate bHLH115
1286 detection, green box), and anti-His-UBQ (ubiquitin detection, red box). Lane
1287 compositions are indicated above: +/− denotes presence or absence of E2 ligase
1288 (UBC8), E3 ligase (BTS-HC), and substrate (Strep-tagged bHLH115). The first lane in
1289 each panel contains E2 and E3 without substrate, serving as a substrate-negative
1290 control. The anti-Strep blot (green box) shows the key substrate-specific result: brown
1291 arrows indicate the unmodified bHLH115 substrate, and green arrows indicate higher
1292 molecular weight bands present in the complete reaction lane (+E2, +E3, +substrate)
1293 that are consistent with polyubiquitinated bHLH115 forms. Several non-specific higher
1294 molecular weight bands are present across multiple lanes including controls. However,

1295 the complete reaction lane shows a distinct shift in banding pattern with clear substrate
1296 laddering compared to the E2-minus and E3-minus controls, indicating that
1297 polyubiquitination requires both E2 and E3 components. In the anti-UBQ blot (red box),
1298 the presence of all components (+E2, +E3, +substrate) produces a distinct ubiquitin
1299 banding pattern compared to controls, further supporting substrate ubiquitination.
1300 Violet bracket indicates ubiquitinated E2 ligase (UBC8). Blue bracket indicates
1301 autoubiquitinated E3 ligase (BTS-HC). These results are consistent with previous
1302 reports of BTS-dependent degradation of bHLH115 (Selote et al., 2015; Xing et al.,
1303 2021) and demonstrate the utility of the UbiGate system for testing ubiquitination of
1304 bHLH IVc proteins.

1305 **Supplementary Figure S18.** Validation of Fe deficiency treatment in wild-type plants.

1306 Expression of Fe deficiency marker genes in wild-type Col-0 roots and shoots under
1307 Fe-sufficient (+Fe) and Fe-deficient (−Fe) conditions. RNA-seq data are presented as
1308 transcripts per million (TPM). *IRT1* and *FRO2*, encoding the root Fe uptake transporter
1309 and ferric reductase, respectively, show higher expression under −Fe in roots,
1310 although the difference was not statistically significant due to replicate variability.
1311 *BHLH39* is induced under −Fe compared to +Fe in both roots and shoots. *BHLH100*
1312 is induced under −Fe compared to +Fe predominantly in shoots. These expression
1313 patterns confirm that the Fe deficiency treatment elicited the expected transcriptional
1314 −Fe response in wild-type plants. Data represent mean ± SD (n = 3 biological
1315 replicates). Statistical analysis was performed using one-way ANOVA followed by
1316 Tukey's HSD test ($p < 0.05$). Different letters indicate statistically significant
1317 differences. Note that in the main figure heatmaps (Figure 3), these differences are
1318 not visible due to Z-score normalization being dominated by high expression values in
1319 *pb104::b104^dPAA* lines.

1320 **Supplementary Figure S19.** Original blots for Figure 5B

1321 **Supplementary Table 1.** Primers used in this study.

1322

1323

1324

1325

1326 ## References

1327 **Abuzeineh A, Vert G, Zelazny E** (2022) Birth, life and death of the Arabidopsis IRT1 iron
1328 transporter: the role of close friends and foes. Planta **256**: 112

1329 **Aparicio F, Pallás V** (2017) The coat protein of *Alfalfa mosaic virus* interacts and interferes with the
1330 transcriptional activity of the bHLH transcription factor ILR3 promoting salicylic acid-
1331 dependent defence signalling response. Mol Plant Pathol **18**: 173–186

1332 **Arend D, Lange M, Pape J-M, Weigelt-Fischer K, Arana-Ceballos F, Mücke I, Klukas C,**
1333 **Altmann T, Scholz U, Junker A** (2016) Quantitative monitoring of Arabidopsis thaliana
1334 growth and development using high-throughput plant phenotyping. Sci Data **3**: 160055

1335 **Briat J-F, Curie C, Gaymard F** (2007) Iron utilization and metabolism in plants. Curr Opin Plant
1336 Biol **10**: 276–282

1337 **Cailliatte R, Schikora A, Briat J-F, Mari S, Curie C** (2010) High-Affinity Manganese Uptake by
1338 the Metal Transporter NRAMP1 Is Essential for *Arabidopsis* Growth in Low Manganese
1339 Conditions. Plant Cell **22**: 904–917

1340 **Chen Y-Y, Wang Y, Shin L-J, Wu J-F, Shanmugam V, Tsednee M, Lo J-C, Chen C-C, Wu S-H,**
1341 **Yeh K-C** (2013) Iron Is Involved in the Maintenance of Circadian Period Length in
1342 Arabidopsis. Plant Physiol **161**: 1409–1420

1343 **Cheng H, Qin L, Lee S, Fu X, Richards DE, Cao D, Luo D, Harberd NP, Peng J** (2004)
1344 Gibberellin regulates *Arabidopsis* floral development via suppression of DELLA protein
1345 function. Development **131**: 1055–1064

1346 **Clough SJ, Bent AF** (1998) Floral dip: a simplified method for Agrobacterium-mediated
1347 transformation of Arabidopsis thaliana. Plant J **16**: 735–743

1348 **Connolly EL, Fett JP, Guerinot ML** (2002) Expression of the IRT1 Metal Transporter Is Controlled
1349 by Metals at the Levels of Transcript and Protein Accumulation. Plant Cell **14**: 1347–1357

1350 **Dubeaux G, Neveu J, Zelazny E, Vert G** (2018) Metal Sensing by the IRT1 Transporter-Receptor
1351 Orchestrates Its Own Degradation and Plant Metal Nutrition. Mol Cell **69**: 953-964.e5

1352 **Dutta A, Choudhary P, Caruana J, Raina R** (2017) JMJ 27, an Arabidopsis H3K9 histone
1353 demethylase, modulates defense against *Pseudomonas syringae* and flowering time. Plant J
1354 **91**: 1015–1028

1355 **Eroglu S, Meier B, Von Wirén N, Peiter E** (2016) The Vacuolar Manganese Transporter MTP8
1356 Determines Tolerance to Iron Deficiency-Induced Chlorosis in Arabidopsis. Plant Physiol
1357 **170**: 1030–1045

1358 **Evans R, O'Neill M, Pritzel A, Antropova N, Senior A, Green T, Žídek A, Bates R, Blackwell S,**
1359 **Yim J** (2021) Protein complex prediction with AlphaFold-Multimer. biorxiv 2021.10.
1360 04.463034

1361 **Gao F, Gao F, Robe K, Gaymard F, Izquierdo E, Izquierdo E, Dubos C** (2019) The
1362 Transcriptional Control of Iron Homeostasis in Plants: A Tale of bHLH Transcription
1363 Factors? Front Plant Sci. doi: 10.3389/fpls.2019.00006

1364 **Gao F, Li M, Dubos C** (2024) bHLH121 and clade IVc bHLH transcription factors synergistically
1365 function to regulate iron homeostasis in *Arabidopsis thaliana*. J Exp Bot **75**: 2933–2950

Gelvin SB (2003) *Agrobacterium* -Mediated Plant Transformation: the Biology behind the "Gene-Jockeying" Tool. Microbiol Mol Biol Rev **67**: 16–37

Gietz RD, Schiestl RH (2007) Large-scale high-efficiency yeast transformation using the LiAc/SS carrier DNA/PEG method. Nat Protoc **2**: 38–41

Gratz R, Manishankar P, Ivanov R, Köster P, Mohr I, Trofimov K, Steinhorst L, Meiser J, Meiser J, Mai H-J, et al (2019) CIPK11-Dependent Phosphorylation Modulates FIT Activity to Promote Arabidopsis Iron Acquisition in Response to Calcium Signaling. Dev Cell. doi: 10.1016/j.devcel.2019.01.006

Hindt MN, Akmakjian GZ, Pivarski KL, Punshon T, Baxter I, Salt DE, Guerinot ML (2017) BRUTUS and its paralogs, BTS LIKE1 and BTS LIKE2, encode important negative regulators of the iron deficiency response in Arabidopsis thaliana. Metallomics. doi: 10.1039/c7mt00152e

Hong S-Y, Seo PJ, Ryu JY, Cho S-H, Woo J-C, Park C-M (2013) A Competitive Peptide Inhibitor KIDARI Negatively Regulates HFR1 by Forming Nonfunctional Heterodimers in Arabidopsis Photomorphogenesis. Mol Cells **35**: 25–31

Hüther P, Schandry N, Jandrasits K, Bezrukov I, Becker C (2020) ARADEEPOPSIS, an Automated Workflow for Top-View Plant Phenomics using Semantic Segmentation of Leaf States. Plant Cell **32**: 3674–3688

Jeong J, Guerinot ML (2009) Homing in on iron homeostasis in plants. Trends Plant Sci **14**: 280–285

Jiang M, Niu Y, Wen G, Zhao C, Gao Q, Li G (2024) Evolutionary studies of the basic helix–loop–helix (bHLH) IVc gene family in plants and the role of *AtILR3* in *Arabidopsis* response to ABA stress. Physiol Plant **176**: e14128

Jo L, Kajala K (2024) ggPlantmap: an open-source R package for the creation of informative and quantitative ggplot maps derived from plant images. J Exp Bot **75**: 5366–5376

Jumper J, Evans R, Pritzel A, Green T, Figurnov M, Ronneberger O, Tunyasuvunakool K, Bates R, Žídek A, Potapenko A (2021) Highly accurate protein structure prediction with AlphaFold. nature **596**: 583–589

Knopf MC, Bauer P (2025) Affordable Non-Invasive Machine-Aided Phenotyping Identifies Phenotypic Variation to Soil Stress Across the *Arabidopsis thaliana* Life Cycle. Physiol Plant **177**: e70427

Kobayashi T, Nagasaka S, Senoura T, Itai RN, Nakanishi H, Nishizawa NK (2013) Iron-binding haemerythrin RING ubiquitin ligases regulate plant iron responses and accumulation. Nat Commun. doi: 10.1038/ncomms3792

Kowarschik K, Hoehenwarter W, Marillonnet S, Trujillo M (2018) UbiGate: a synthetic biology toolbox to analyse ubiquitination. New Phytol **217**: 1749–1763

Lampropoulos A, Sutikovic Z, Wenzl C, Maegele I, Lohmann JU, Forner J (2013) GreenGate-a novel, versatile, and efficient cloning system for plant transgenesis. PloS One **8**: e83043

Lešková A, Giehl RFH, Hartmann A, Fargašová A, Von Wirén N (2017) Heavy Metals Induce Iron Deficiency Responses at Different Hierarchic and Regulatory Levels. Plant Physiol **174**: 1648–1668

1407 **Li X, Zhang HM, Ai Q, Liang G, Yu D** (2016) Two bHLH Transcription Factors, bHLH34 and
1408 bHLH104, Regulate Iron Homeostasis in Arabidopsis thaliana. Plant Physiol. doi:
1409 10.1104/pp.15.01827

1410 **Li Y, Lu CK, Li CY, Lei RH, Pu MN, Zhao JH et al** (2021) IRON MAN interacts with BRUTUS
1411 to maintain iron homeostasis in Arabidopsis. Proc Natl Acad Sci U S A. doi:
1412 10.1073/pnas.2109063118

1413 **Liang G, Zhang H, Li X, Ai Q, Yu D** (2017) bHLH transcription factor bHLH115 regulates iron
1414 homeostasis in Arabidopsis thaliana. J Exp Bot **68**: 1743–1755

1415 **Lichtblau DM, Schwarz B, Baby D, Endres C, Sieberg C, Bauer P** (2022) The Iron Deficiency-
1416 Regulated Small Protein Effector FEP3/IRON MAN1 Modulates Interaction of BRUTUS-
1417 LIKE1 With bHLH Subgroup IVc and POPEYE Transcription Factors. Front Plant Sci **13**:
1418 930049

1419 **Lingam S, Mohrbacher J, Brumbarova T, Potuschak T, Potuschak T, Potuschak T, Fink-**
1420 **Straube C, Fink-Straube C, Blondet E, Genschik P, et al** (2011) Interaction between the
1421 bHLH Transcription Factor FIT and ETHYLENE INSENSITIVE3/ETHYLENE
1422 INSENSITIVE3-LIKE1 Reveals Molecular Linkage between the Regulation of Iron
1423 Acquisition and Ethylene Signaling in Arabidopsis. Plant Cell. doi: 10.1105/tpc.111.084715

1424 **Long TA, Tsukagoshi H, Busch W, Lahner B, Salt DE, Benfey PN** (2010) The bHLH
1425 Transcription Factor POPEYE Regulates Response to Iron Deficiency in Arabidopsis Roots.
1426 Plant Cell. doi: 10.1105/tpc.110.074096

1427 **Mai H-J** (2024) PlugNSeq: An Easy, Rapid, and Streamlined mRNA-Seq Data Analysis Pipeline
1428 Empowering Insightful Exploration with Well-Annotated Organisms, Requiring Minimal
1429 Bioinformatic Expertise v1. doi: 10.17504/protocols.io.4r3l2qjo3l1y/v1

1430 **Marschner H** (2012) Marschner's mineral nutrition of higher plants. Academic press

1431 **Maruoka T, Gan E-S, Otsuka N, Shirakawa M, Ito T** (2022) Histone Demethylases JMJ30 and
1432 JMJ32 Modulate the Speed of Vernalization Through the Activation of FLOWERING
1433 LOCUS C in Arabidopsis thaliana. Front Plant Sci **13**: 837831

1434 **Meiser J, Lingam S, Bauer P** (2011) Posttranslational Regulation of the Iron Deficiency Basic
1435 Helix-Loop-Helix Transcription Factor FIT Is Affected by Iron and Nitric Oxide. Plant
1436 Physiol **157**: 2154–2166

1437 **Nagaya S, Kato K, Ninomiya Y, Horie R, Sekine M, Yoshida K, Shinmyo A** (2005) Expression of
1438 Randomly Integrated Single Complete Copy Transgenes Does not Vary in Arabidopsis
1439 thaliana. Plant Cell Physiol **46**: 438–444

1440 **Naranjo-Arcos MA, Maurer F, Meiser J, Meiser J, Pateyron S, Fink-Straube C, Fink-Straube**
1441 **C, Bauer P** (2017) Dissection of iron signaling and iron accumulation by overexpression of
1442 subgroup Ib bHLH039 protein. Sci Rep. doi: 10.1038/s41598-017-11171-7

1443 **Ngigi M, Khan M, Remus R, Gupta SK, Bauer P** (2025) Age-dependent differential iron deficiency
1444 responses of rosette leaves during reproductive stages in *Arabidopsis thaliana*. J Exp Bot
1445 eraf207

1446 **Ngigi MN, Bauer P** (2023) High-Throughput Plant Gene Expression Analysis by 384-Format
1447 Reverse Transcription-Quantitative PCR for Investigating Plant Iron Homeostasis. *In* J Jeong,
1448 ed, Plant Iron Homeost. Methods Protoc. Springer US, New York, NY, pp 1–22

1449 **Nguyen NT, Khan MA, Castro–Guerrero NA, Chia J-C, Vatamaniuk OK, Mari S, Jurisson SS,**
1450 **Mendoza-Cozatl DG** (2022) Iron Availability within the Leaf Vasculature Determines the
1451 Magnitude of Iron Deficiency Responses in Source and Sink Tissues in Arabidopsis. Plant
1452 Cell Physiol **63**: 829–841

1453 **Ortmann S, Marx J, Lampe C, Handrick V, Ehnert T-M, Zinecker S, Reimers M, Bonas U,**
1454 **Erickson JL** (2023) A conserved microtubule-binding region in Xanthomonas XopL is
1455 indispensable for induced plant cell death reactions. PLoS Pathog **19**: e1011263

1456 **Pagni M, Ioannidis V, Cerutti L, Zahn-Zabal M, Jongeneel CV, Hau J, Martin O, Kuznetsov D,**
1457 **Falquet L** (2007) MyHits: improvements to an interactive resource for analyzing protein
1458 sequences. Nucleic Acids Res **35**: W433–W437

1459 **Panda SK, Yamamoto YY** (2019) Redox homeostasis in plants: from signalling to stress tolerance.
1460 Springer

1461 **Pettersen EF, Goddard TD, Huang CC, Couch GS, Greenblatt DM, Meng EC, Ferrin TE** (2004)
1462 UCSF Chimera—a visualization system for exploratory research and analysis. J Comput
1463 Chem **25**: 1605–1612

1464 **Pottier M, Dumont J, Masclaux-Daubresse C, Thomine S** (2018) Autophagy is essential for
1465 optimal translocation of iron to seeds in Arabidopsis. J Exp Bot. doi: 10.1093/jxb/ery388

1466 **Pullin J, Rodríguez-Celma J, Franceschetti M, Mundy JEA, Svistunenko DA, Bradley JM, Le**
1467 **Brun NE, Balk J** (2025) Iron-sensing and redox properties of the hemerythrin-like domains
1468 of Arabidopsis BRUTUS and BRUTUS-LIKE2 proteins. Nat Commun **16**: 3865

1469 **Raffeiner M, Zhu S, González-Fuente M, Üstün S** (2023) Interplay between autophagy and
1470 proteasome during protein turnover. Trends Plant Sci **28**: 698–714

1471 **Rampey RA, Woodward AW, Hobbs BN, Tierney MP, Lahner B, Salt DE, Bartel B** (2006) An
1472 Arabidopsis Basic Helix-Loop-Helix Leucine Zipper Protein Modulates Metal Homeostasis
1473 and Auxin Conjugate Responsiveness. Genetics **174**: 1841–1857

1474 **Rodríguez-Celma J, Connorton JM, Kruse I, Green RT, Franceschetti M, Chen Y-T, Cui Y,**
1475 **Ling H-Q, Yeh K-C, Balk J** (2019) Arabidopsis BRUTUS-LIKE E3 ligases negatively
1476 regulate iron uptake by targeting transcription factor FIT for recycling. Proc Natl Acad Sci U
1477 S A. doi: 10.1073/pnas.1907971116

1478 **Salomé PA, Oliva M, Weigel D, Krämer U** (2012) Circadian clock adjustment to plant iron status
1479 depends on chloroplast and phytochrome function. EMBO J **32**: 511–523

1480 **Samira R, Li B, Kliebenstein D, Li C, Davis E, Gillikin JW, Long TA** (2018) The bHLH
1481 transcription factor ILR3 modulates multiple stress responses in Arabidopsis. Plant Mol Biol
1482 **97**: 297–309

1483 **Schwarz B, Bauer P** (2020) FIT, a regulatory hub for iron deficiency and stress signaling in roots,
1484 and FIT-dependent and -independent gene signatures. J Exp Bot **71**: 1694–1705

1485 **Selote D, Selote D, Samira R, Matthiadis A, Gillikin JW, Long TA** (2015) Iron-Binding E3 Ligase
1486 Mediates Iron Response in Plants by Targeting Basic Helix-Loop-Helix Transcription
1487 Factors. Plant Physiol. doi: 10.1104/pp.114.250837

1488 **Sharma R, Yeh K** (2020) The dual benefit of a dominant mutation in Arabidopsis *IRON*
1489 *DEFICIENCY TOLERANT1* for iron biofortification and heavy metal phytoremediation. Plant
1490 Biotechnol J **18**: 1200–1210

1491 **Shen C, Yang Y, Liu K, Zhang L, Guo H, Sun T, Wang H** (2016) Involvement of endogenous
1492 salicylic acid in iron-deficiency responses in Arabidopsis. J Exp Bot **67**: 4179–4193

1493 **Shinkawa H, Kobayashi T, Murota A, Kamijima A, Nishizawa NK** (2025) Stability and function
1494 of rice OsHRZ ubiquitin ligases are regulated at multiple sites by the iron–zinc balance. Plant
1495 J **122**: e70258

1496 **Thrower JS** (2000) Recognition of the polyubiquitin proteolytic signal. EMBO J **19**: 94–102

1497 **Vert G, Grotz N, Dédaldéchamp F, Gaymard F, Guerinot ML, Briat J-F, Curie C** (2002) IRT1,
1498 an Arabidopsis Transporter Essential for Iron Uptake from the Soil and for Plant Growth.
1499 Plant Cell **14**: 1223–1233

1500 **Wang F, Zhu D, Huang X, Li S, Gong Y, Yao Q, Fu X, Fan L-M, Deng XW** (2009) Biochemical
1501 Insights on Degradation of *Arabidopsis* DELLA Proteins Gained From a Cell-Free Assay
1502 System. Plant Cell **21**: 2378–2390

1503 **Wang JZ, Du Z, Payattakool R, Yu PS, Chen C-F** (2007) A new method to measure the semantic
1504 similarity of GO terms. Bioinformatics **23**: 1274–1281

1505 **Wang P, Nolan TM, Clark NM, Jiang H, Montes-Serey C, Guo H, Bassham DC, Walley JW,**
1506 **Yin Y** (2021) The F-box E3 ubiquitin ligase BAF1 mediates the degradation of the
1507 brassinosteroid-activated transcription factor BES1 through selective autophagy in
1508 Arabidopsis. Plant Cell **33**: 3532–3554

1509 **Waters BM, Grusak MA** (2008) Whole-plant mineral partitioning throughout the life cycle in
1510 *Arabidopsis thaliana* ecotypes Columbia, Landsberg *erecta* , Cape Verde Islands, and the
1511 mutant line *ysl1ysl3*. New Phytol **177**: 389–405

1512 **Wild M, Davière J-M, Regnault T, Sakvarelidze-Achard L, Carrera E, Lopez Diaz I, Cayrel A,**
1513 **Dubeaux G, Vert G, Achard P** (2016) Tissue-Specific Regulation of Gibberellin Signaling
1514 Fine-Tunes Arabidopsis Iron-Deficiency Responses. Dev Cell **37**: 190–200

1515 **Xing Y, Xu N, Bhandari DD, Lapin D, Sun X, Luo X, Wang Y, Cao J, Wang H, Coaker G, et al**
1516 (2021) Bacterial effector targeting of a plant iron sensor facilitates iron acquisition and
1517 pathogen colonization. Plant Cell **33**: 2015–2031

1518 **Yi Y, Guerinot ML** (1996) Genetic evidence that induction of root Fe(III) chelate reductase activity
1519 is necessary for iron uptake under iron deficiency†. Plant J **10**: 835–844

1520 **Zhang J, Zhang J, Liu B, Li M, Feng D, Jin H, Wang P, Liu J, Liu J, Liu J, et al** (2015) The
1521 bHLH Transcription Factor bHLH104 Interacts with IAA-LEUCINE RESISTANT3 and
1522 Modulates Iron Homeostasis in Arabidopsis. Plant Cell. doi: 10.1105/tpc.114.132704

1523 **Zhao J, Li Y, Ping H, Lei R, Pan B, Liang G** (2026) Arabidopsis BRUTUS, BRUTUS-LIKE, and
1524 bHLH IVc subgroup proteins coordinate iron homeostasis in the root and shoot. Plant Cell
1525 koag006

1526 **Zhao Q, Ren Y-R, Wang Q-J, Wang X-F, You C-X, Hao Y-J** (2016) Ubiquitination-Related
1527 MdBT Scaffold Proteins Target a bHLH Transcription Factor for Iron Homeostasis. Plant
1528 Physiol **172**: 1973–1988

1529

Figure 1

PAA sequence in bHLH104 enables E3 ligase interaction and degradation

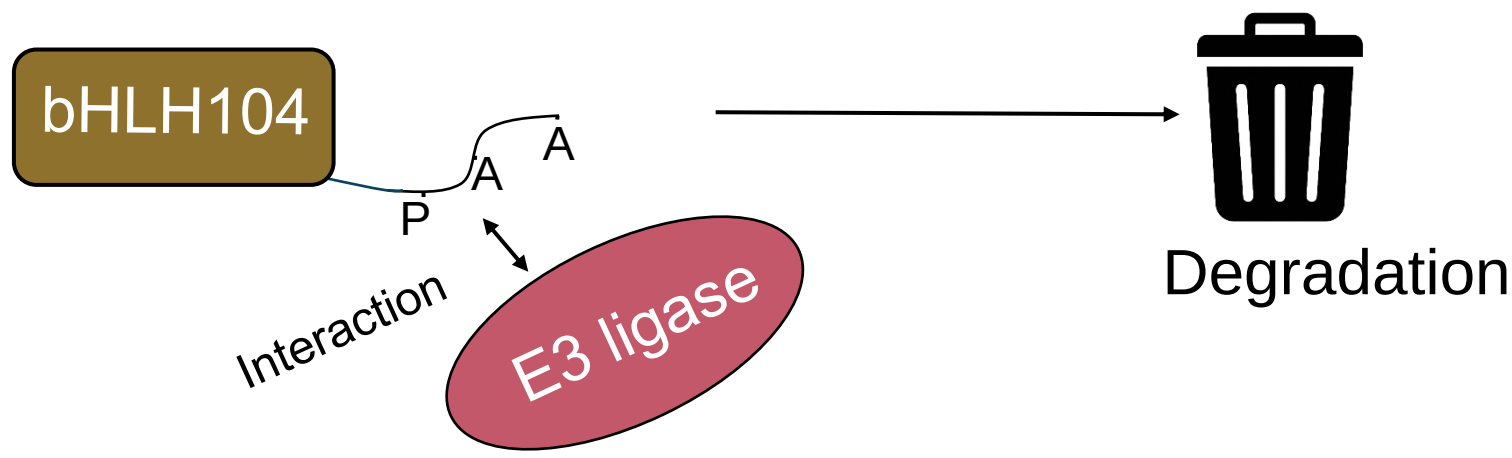

Figure 1. Conceptual model of bHLH104 regulation by its conserved PAA sequence.
In the full-length bHLH104 protein, the PAA sequence forms the interaction interface with an E3 ligase, likely enabling ubiquitination and proteasomal degradation of bHLH104.

Figure 2

A
pb104::b104
pbHLH104
mTURQ2
bHLH104
pb104::b104 ^dPAA
pbHLH104
mTURQ2
bHLH104dPAA
200 bp

B
#1 #2 #1 #2 #3 #4
WT pb104::b104 pb104::b104^dPAA

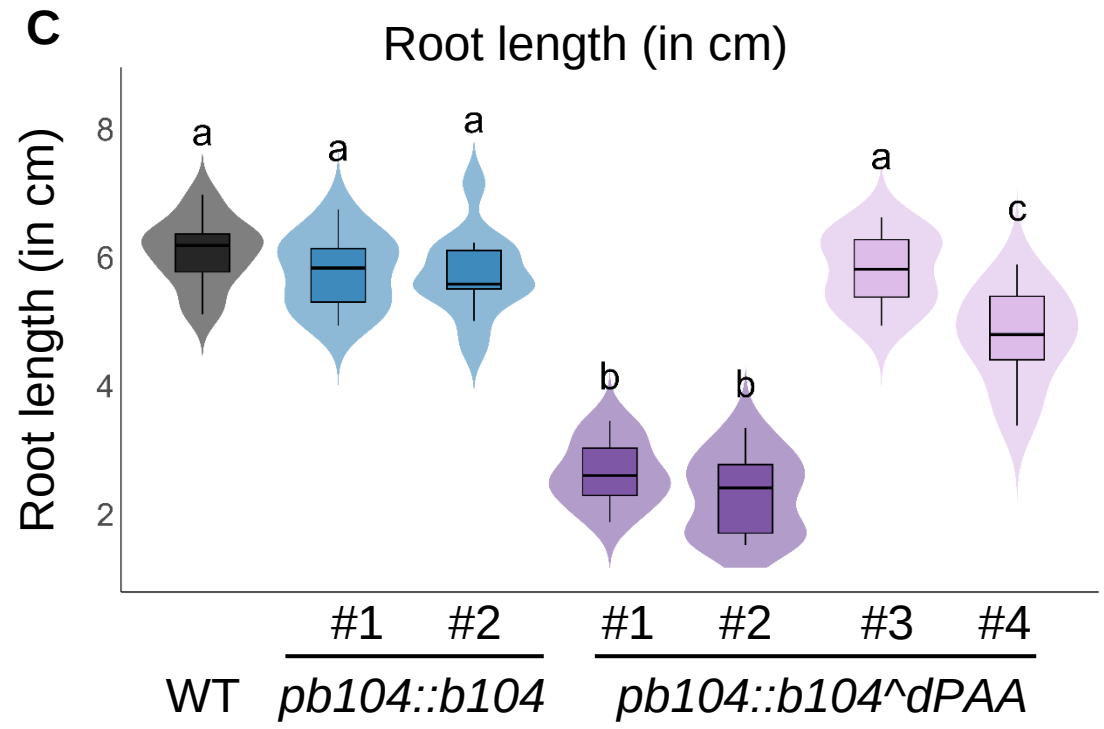
C
Root length (in cm)
Root length (in cm)
8
6
4
2
a a a b b a c
#1 #2 #1 #2 #3 #4
WT pb104::b104 pb104::b104^dPAA

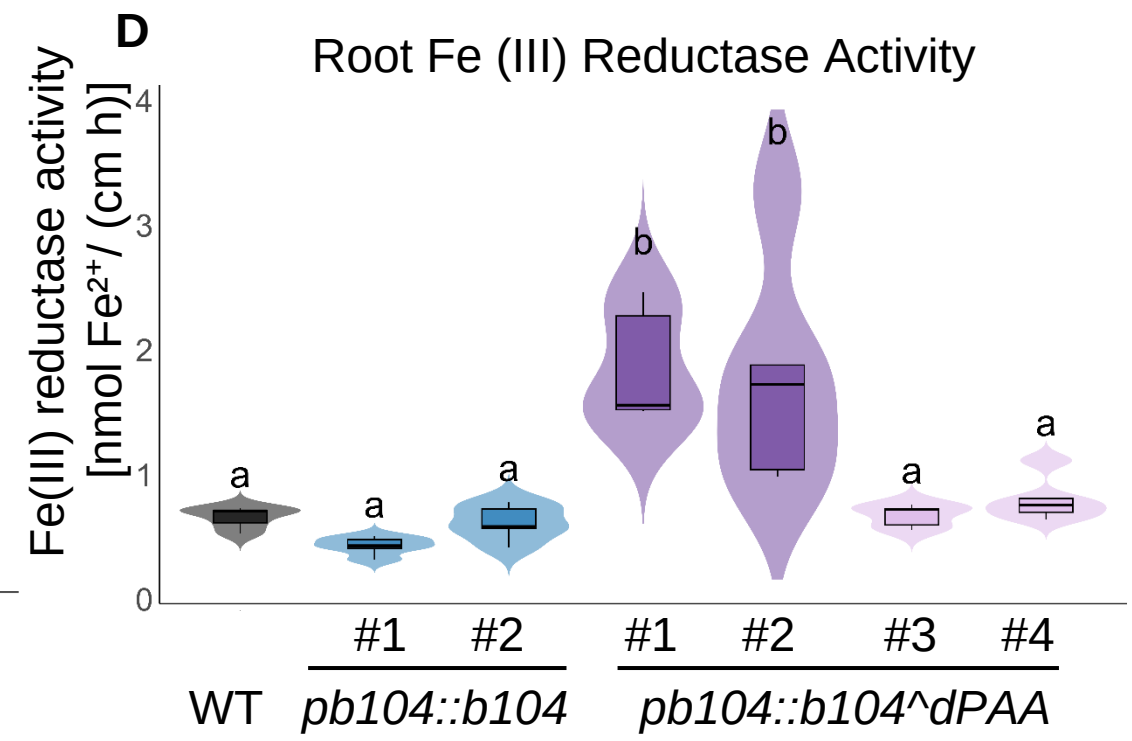
D
Root Fe (III) Reductase Activity
Fe(III) reductase activity
[nmol Fe2+ / (cm h)]
4
3
2
1
0
a a a b b a a
#1 #2 #1 #2 #3 #4
WT pb104::b104 pb104::b104^dPAA

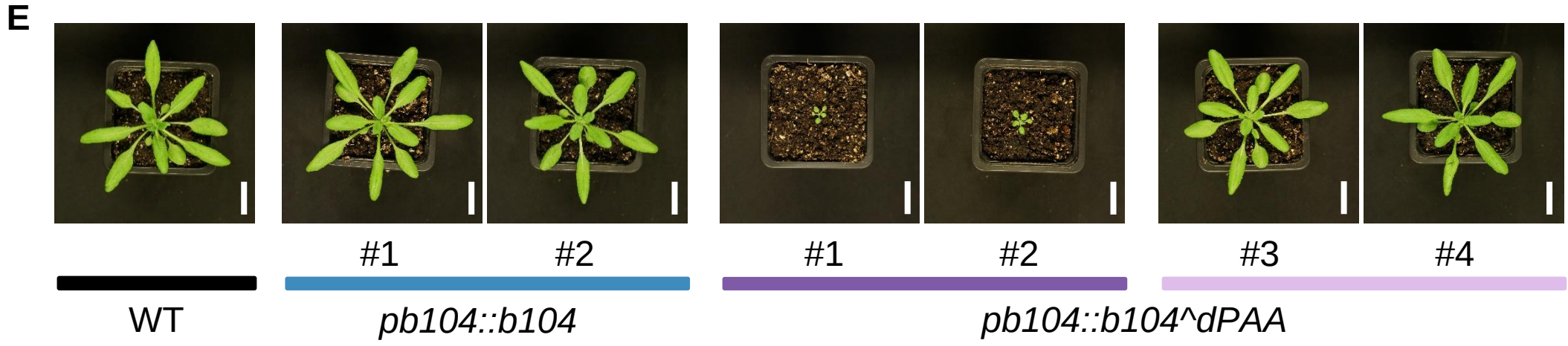
E
#1 #2 #1 #2 #3 #4
WT pb104::b104 pb104::b104^dPAA

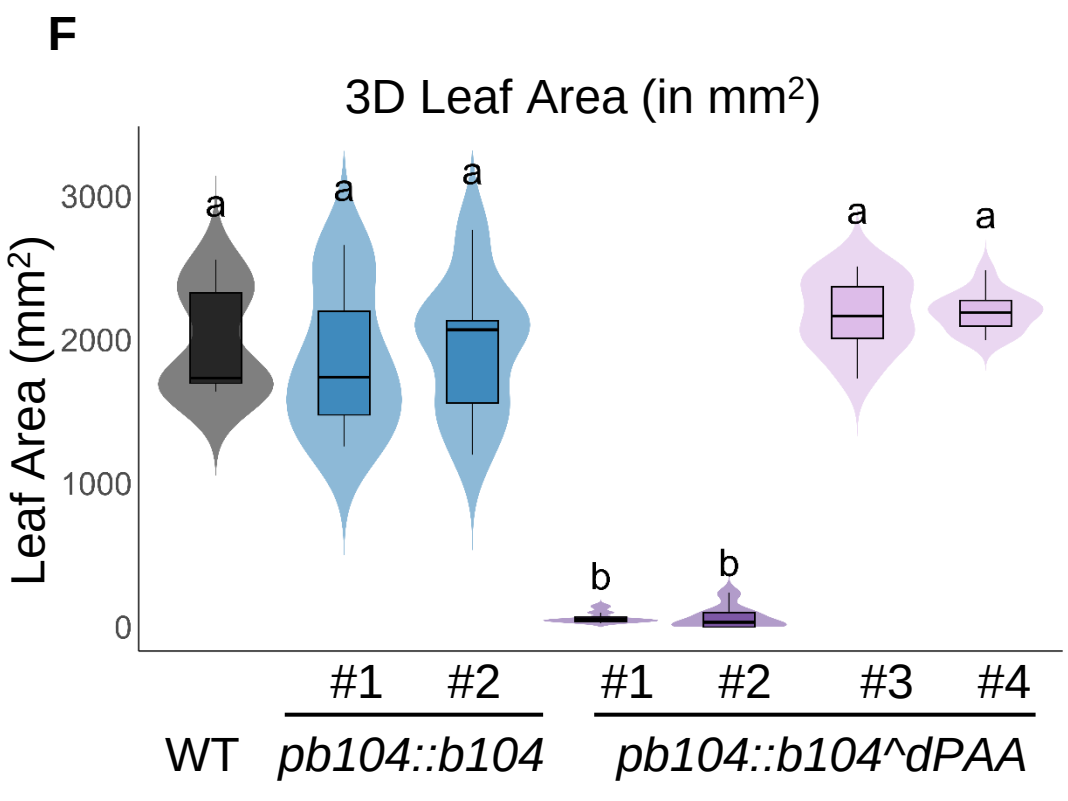
F
3D Leaf Area (in mm2)
Leaf Area (mm2)
3000
2000
1000
0
a a a b b a a
#1 #2 #1 #2 #3 #4
WT pb104::b104 pb104::b104^dPAA

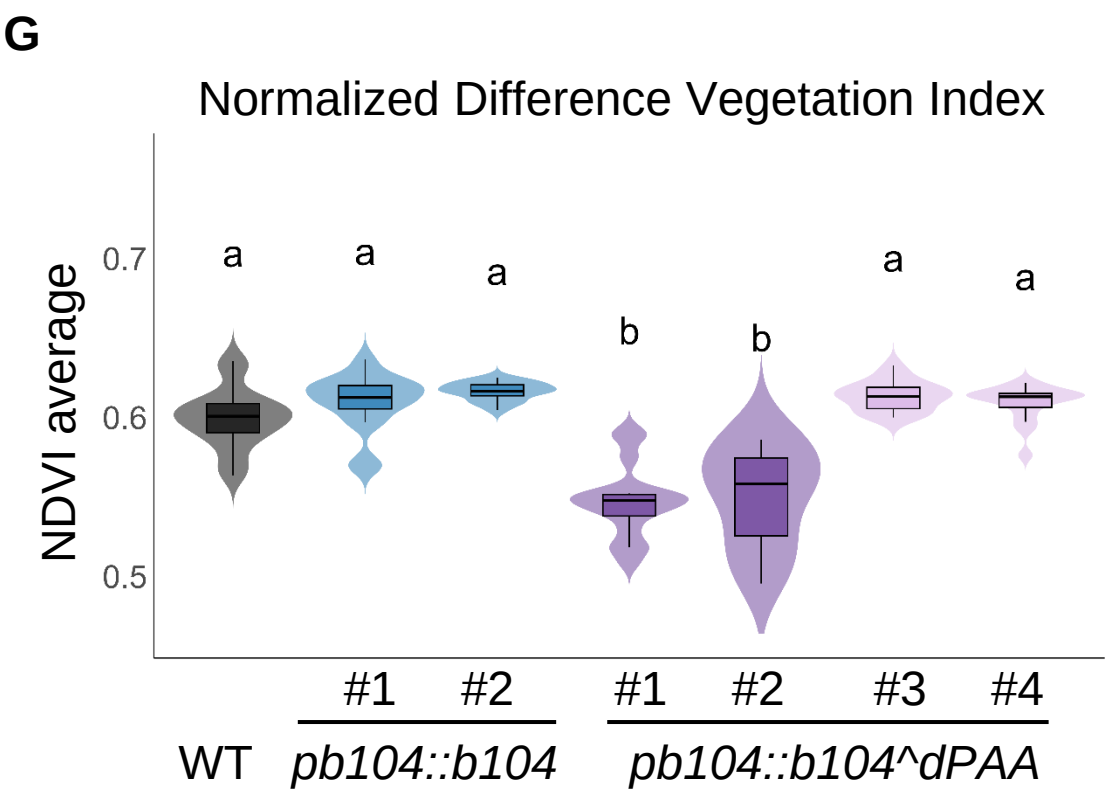
G
Normalized Difference Vegetation Index
NDVI average
0.7
0.6
0.5
a a a b b a a
#1 #2 #1 #2 #3 #4
WT pb104::b104 pb104::b104^dPAA

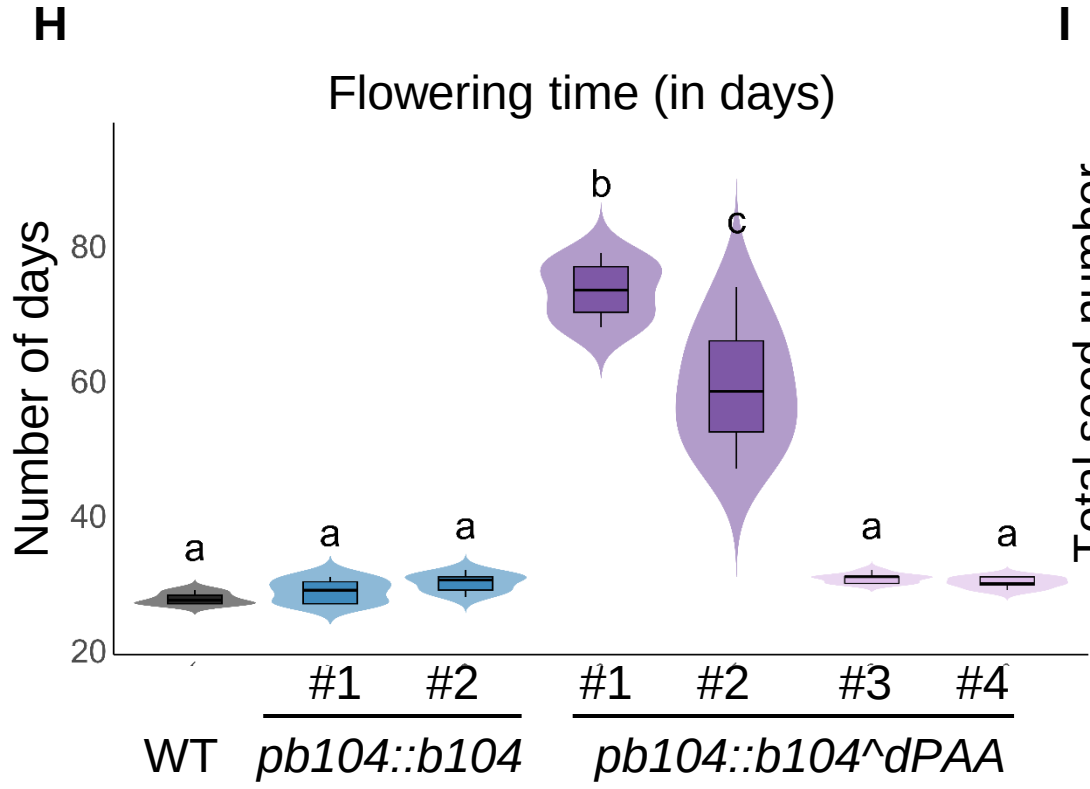
H
Flowering time (in days)
Number of days
80
60
40
20
a a a b c a a
#1 #2 #1 #2 #3 #4
WT pb104::b104 pb104::b104^dPAA

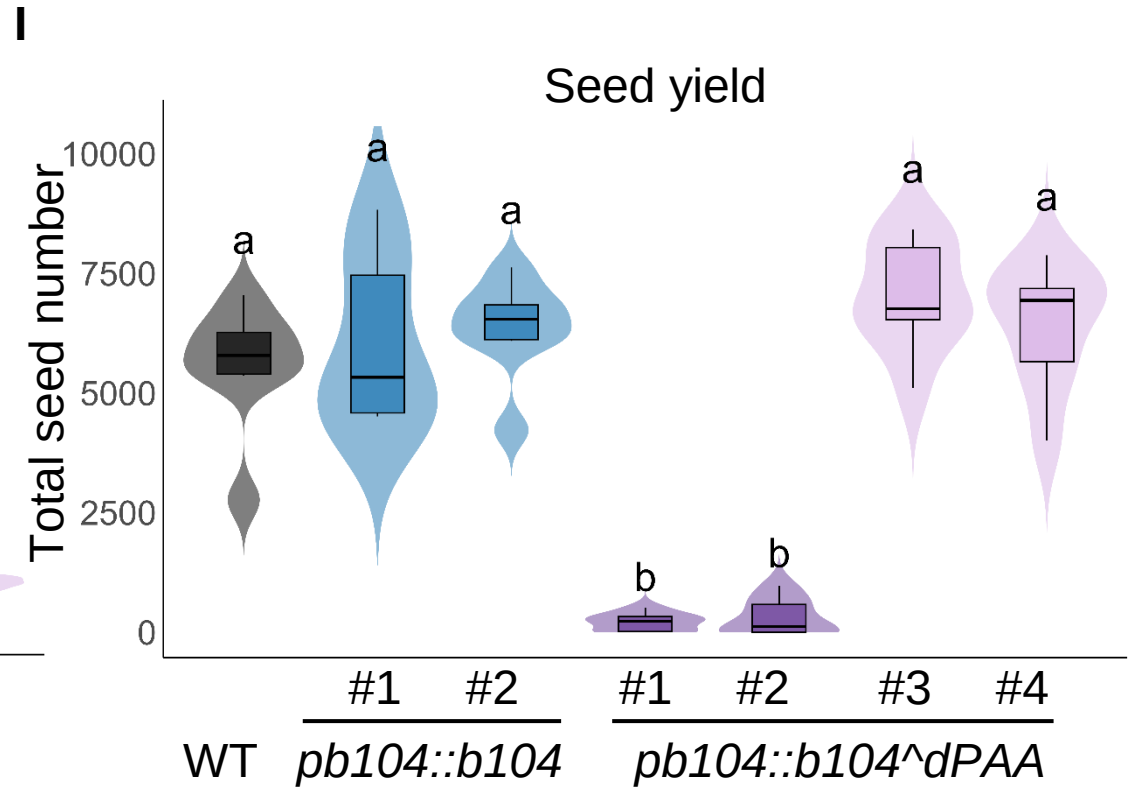
I
Seed yield
Total seed number
10000
7500
5000
2500
0
a a a b b a a
#1 #2 #1 #2 #3 #4
WT pb104::b104 pb104::b104^dPAA

Figure 2. Transgenic expression of bHLH104 lacking the PAA sequence leads to growth alterations and physiological changes in Arabidopsis.
((A) Schematic representation of constructs used to generate transgenic lines expressing either full-length bHLH104 (pb104::b104) or a C-terminal deletion variant lacking the conserved three–amino acid PAA sequence (pb104::b104^dPAA). Both constructs are driven by the native bHLH104 promoter (2,069 bp) and fused at the N-terminus to an mTurquoise2 fluorescent tag. The deleted PAA sequence in b104^dPAA is indicated by a red cross at the C-terminus. Scale bar = 200 bp.
(B) Representative images of 10-day-old seedlings grown on +Fe medium (scale bar = 2 cm).
(C) Primary root length of 12-day-old seedlings grown vertically on Hoagland medium supplemented with Fe.
(D) Fe reductase activity in roots of 10-day-old seedlings grown under +Fe. Activity was quantified spectrophotometrically as Fe(II)–ferrozine complex formation and normalized to total root length.
(E) Representative images of four-week-old soil-grown plants (scale bar = 2 cm). Shown are Col-0 (WT), two independent pb104::b104 lines (#1, #2), and four independent pb104::b104^dPAA lines (#1–4).
(F–G) Quantitative analysis of aboveground phenotypes using the Phenospex PlantEye system: (F) 3D leaf area (mm^2); (G) NDVI (Normalized Difference Vegetation Index)
(H) Flowering time, recorded as days to bolting.
(I) Seed number per plant, estimated from total seed weight based on mean weight per 100 seeds.
Data represent means ± SD (n = 7–12 biological replicates per line). Statistical analysis was performed using two-way ANOVA followed by Tukey's post hoc test. Different letters indicate statistically significant differences at $p < 0.05$.

Figure 3

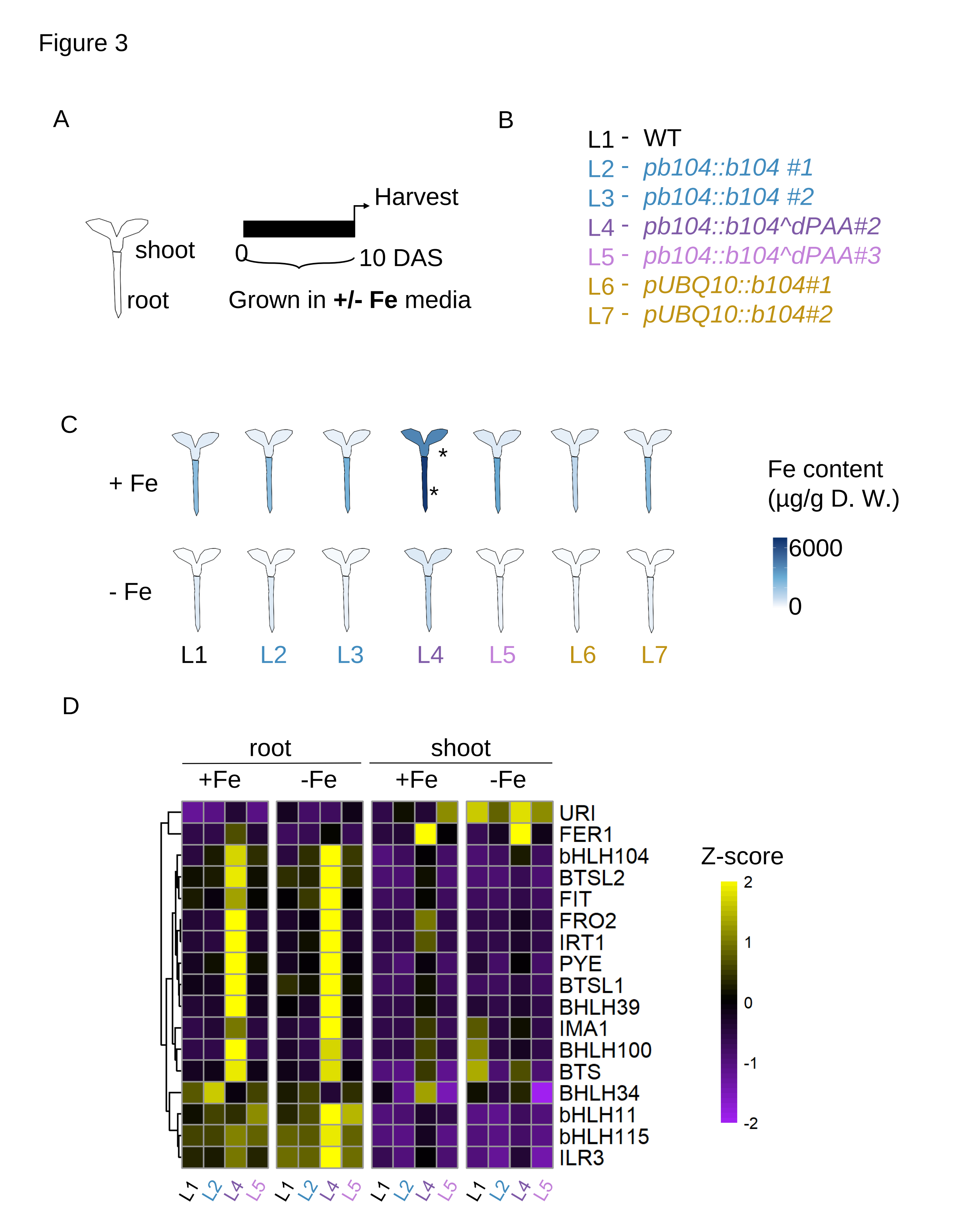
A
shoot
root
Harvest
0
10 DAS
Grown in +/- Fe media
B
L1 - WT
L2 - pb104::b104 #1
L3 - pb104::b104 #2
L4 - pb104::b104^dPAA#2
L5 - pb104::b104^dPAA#3
L6 - pUBQ10::b104#1
L7 - pUBQ10::b104#2
C
+ Fe
- Fe
*
*
L1
L2
L3
L4
L5
L6
L7
Fe content
(µg/g D. W.)
6000
0
D
root
shoot
+Fe
-Fe
+Fe
-Fe
URI
FER1
bHLH104
BTSL2
FIT
FRO2
IRT1
PYE
BTSL1
BHLH39
IMA1
BHLH100
BTS
BHLH34
bHLH11
bHLH115
ILR3
L1 L2 L4 L5 L1 L2 L4 L5 L1 L2 L4 L5 L1 L2 L4 L5
Z-score
2
1
0
-1
-2

Figure 3. Transgenic lines expressing bHLH104^dPAA exhibit increased iron accumulation and altered iron homeostasis gene expression in seedling stage.

(A) Schematic representation of the experimental design. *Arabidopsis* seedlings were grown for 10 days after sowing (DAS) under either iron-sufficient (+Fe) or iron-deficient (–Fe) conditions. Shoot and root tissues were collected separately for ICP-MS and gene expression analyses. (B) Genotypes used in this study. (C) Iron content in shoot and root tissues of seedlings grown under +Fe and –Fe conditions, measured by ICP-MS. Data represent the mean of three biological replicates (n = 3). Heat map intensity reflects iron concentration (µg/g dry weight). Color shading was rendered using the R package ggplantmap, with darker blue indicating higher Fe accumulation. Notably*, pb104::b104^dPAA* lines show increased Fe accumulation in roots and shoots under +Fe conditions.(D) Clustered heatmaps showing the expression profiles (RNA sequencing) of selected Fe homeostasis genes. Heatmaps were generated in RStudio version 4.4.1 using calculated Z-scores of normalized gene expression values across tissues for both +Fe and –Fe conditions. Purple indicates low expression and yellow indicates high expression. Asterisks indicate genotypes that differ significantly from WT within the same tissue and treatment condition ($p < 0.05$), as determined by two-way ANOVA and Tukey's post hoc test (n = 3 for each group).

Figure 4

A

L1 - WT
L2 - *pb104::b104 #1*
L3 - *pb104::b104 #2*
L4 - *pb104::b104^dPAA#2*
L5 - *pb104::b104^dPAA#3*
L6 - *pUBQ10::b104#1*
L7 - *pUBQ10::b104#2*

B

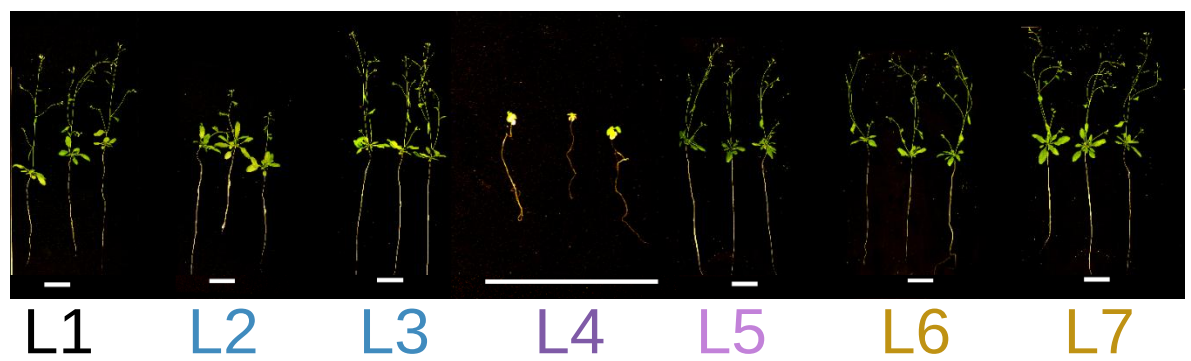

C

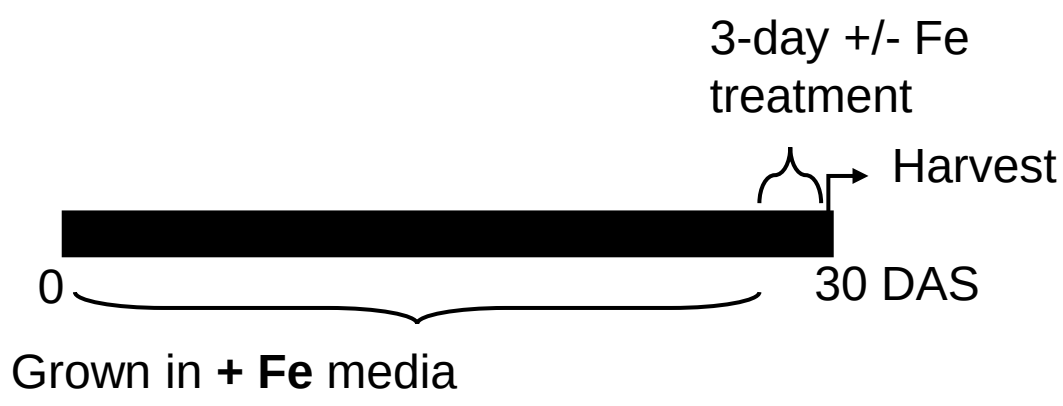

D

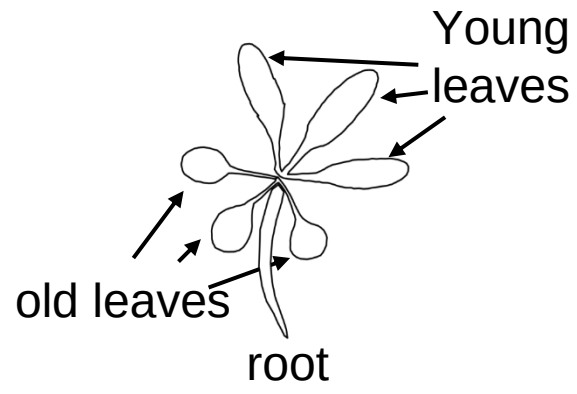

E

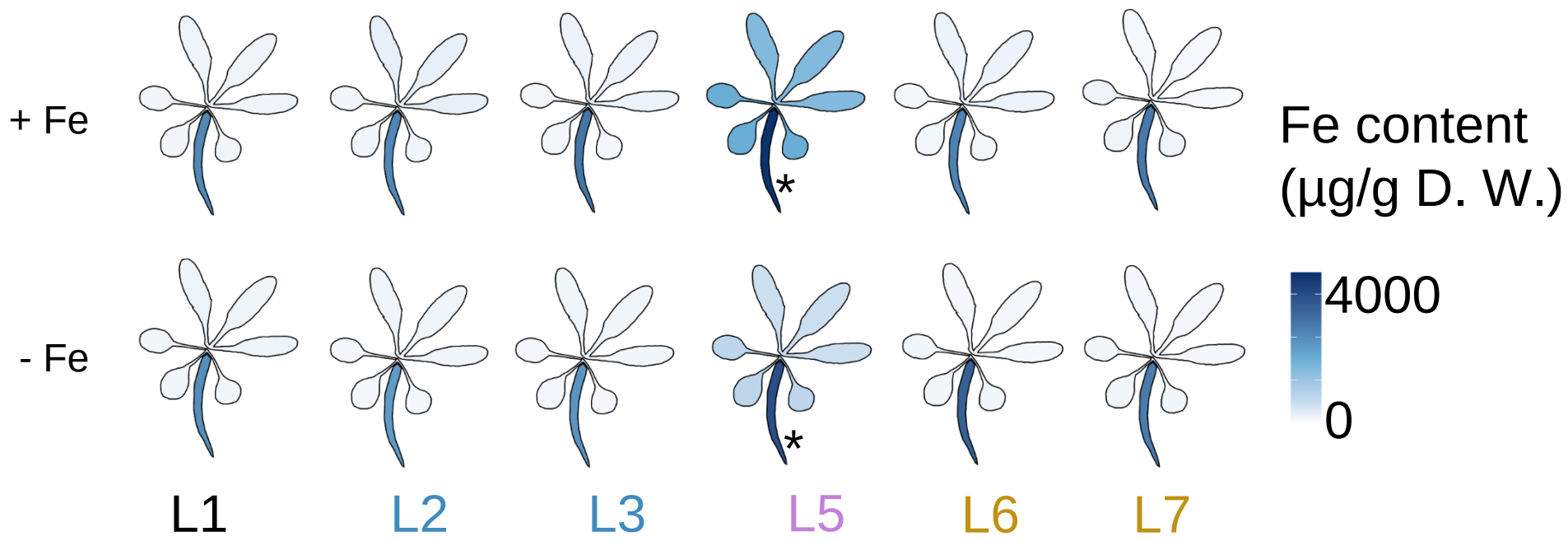

F

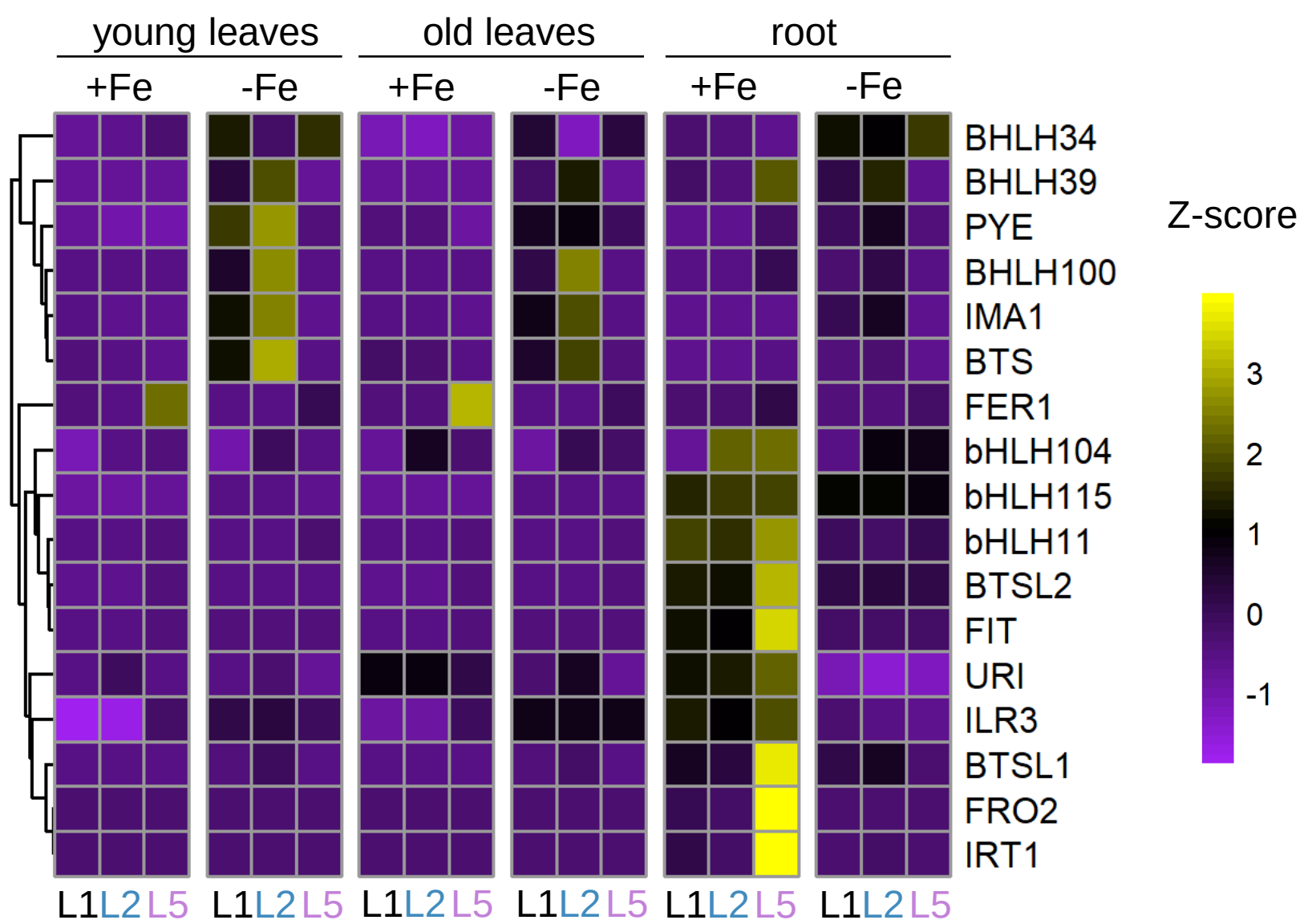

Figure 4. Elevated shoot iron accumulation and altered Fe deficiency responses in reproductive-stage bHLH104^dPAA transgenic lines.

(A) Plant lines used In this experiment
(B) Representative images of 30-days-old Arabidopsis plants grown in hydroponic system (scale bar = 5 cm). Among grown plant lines, *pb104::b104^dPAA #2* (L4) grew poorly and was not used in ICPMS and gene expression analysis.
(C) Experimental design for the dataset shown. Arabidopsis plants were grown hydroponically under iron-sufficient (+Fe) conditions for 27 days, followed by a 3-day treatment with either +Fe or –Fe media.
(D) Schematic representation of tissue separation used for both ICP-MS and RT-qPCR analysis. Young and old leaves were separated from the roots to examine tissue-specific iron accumulation and gene expression. The same tissue layout is used to represent heatmaps in the ICP-MS dataset.
(E) Iron content in young leaves, old leaves, and roots under +Fe and –Fe conditions, measured by ICP-MS. Data represent mean values from three biological replicates (n = 3). Heat map intensity reflects iron concentration (µg/g dry weight). Color shading was generated using the R package ggplantmap, with deeper blue indicating higher Fe content. Asterisks indicate genotypes that differ significantly from WT within the same tissue and treatment condition ($p < 0.05$), as determined by two-way ANOVA and Tukey's post hoc test (n = 3 for each group).
(F) Clustered heatmaps showing the expression profiles (RNA sequencing) of selected Fe homeostasis genes in young leaves, old leaves, and roots under both +Fe and –Fe conditions. Data represent the mean of three biological replicates (n = 3). Z-scores were calculated from normalized RNA expression values and visualized in RStudio version 4.4.1. Yellow indicates high expression; purple indicates low expression.

Figure 5

A

L1 - WT
L2 - *pb104::b104 #1*
L3 - *pb104::b104 #2*
L4 - *pb104::b104^dPAA#1*
L5 - *pb104::b104^dPAA#2*
L6 - *pb104::b104^dPAA#3*
L7 - *pb104::b104^dPAA#4*
L8 - *pUBQ10::b104#1*
L9 - *pUBQ10::b104#2*

B

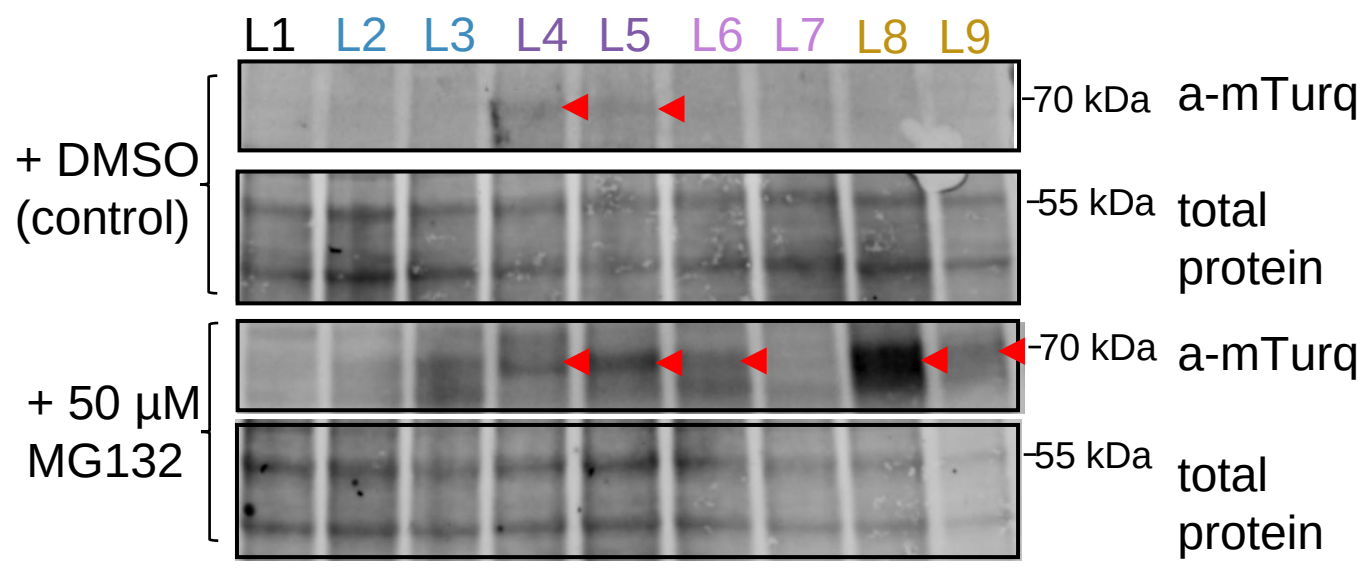

C

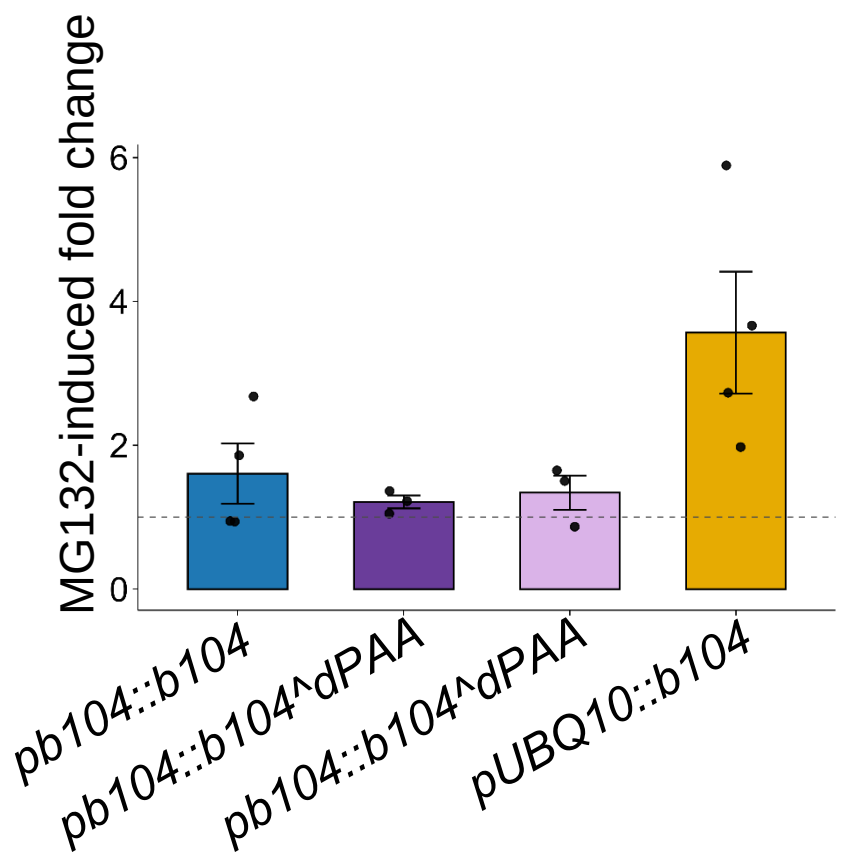

D

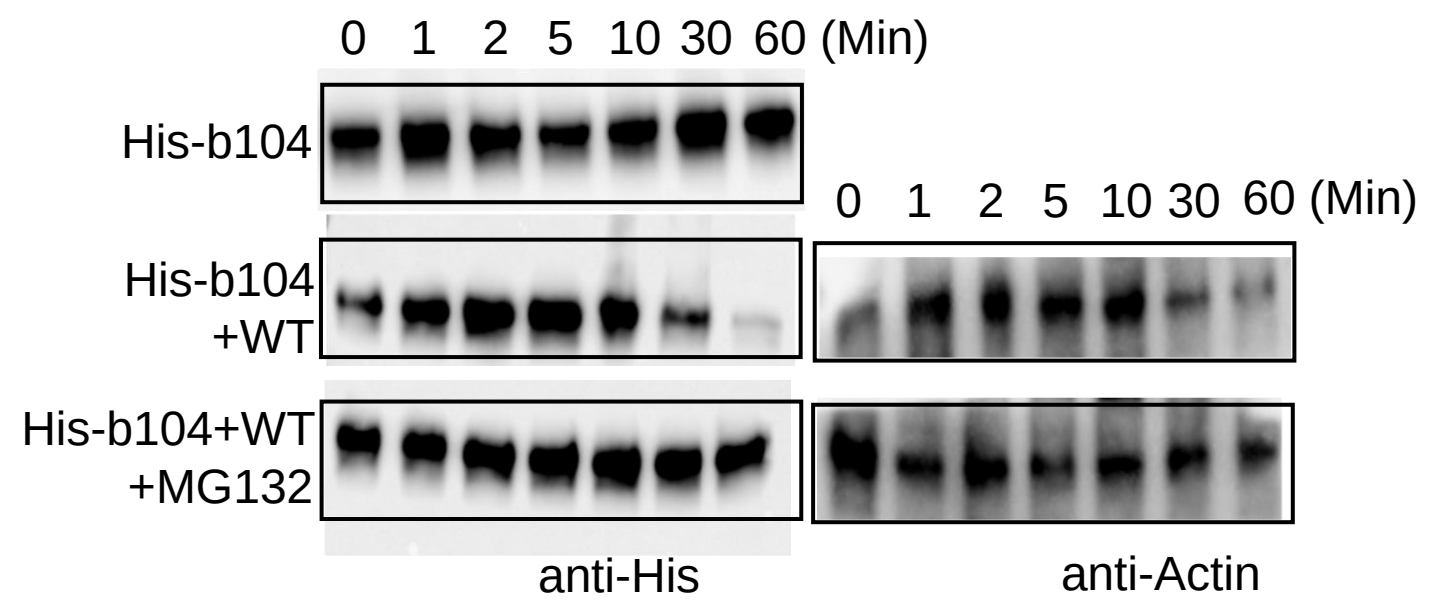

E

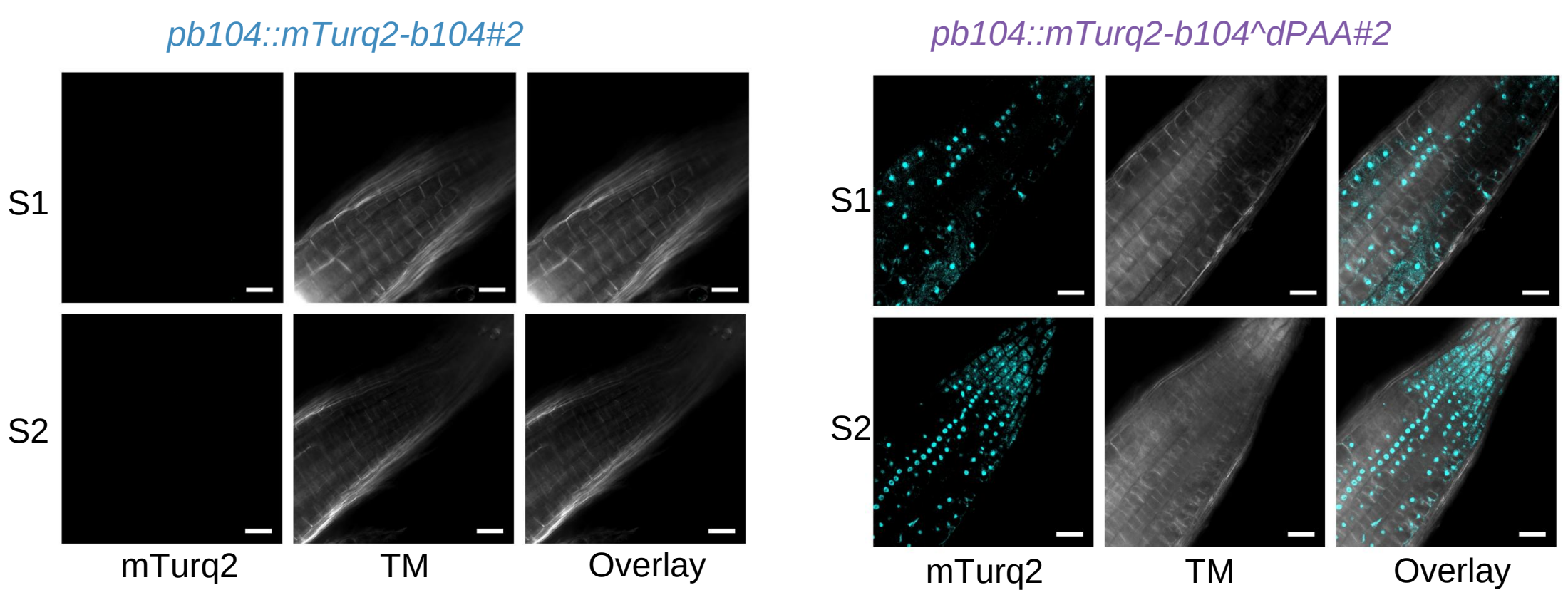

Figure 5. The PAA short sequence mediates bHLH104 protein stability and affects its abundance in Arabidopsis.

(A) Genotypes and transgenic lines used in this experiment.

(B) Immunoblot analysis of mTurquoise2-tagged bHLH104 and b104^dPAA in different transgenic lines treated with either DMSO (control) or 50 µM MG132. Total protein and anti-mTurquoise2 blots are shown. Samples are labeled from #L1 to #L9. The transgenic lines exhibiting increased protein abundance correspond to those that displayed altered growth phenotypes in Figure 1, suggesting a link between protein stability and the observed developmental responses. Red arrows indicate the expected band position for mTurquoise2-bHLH104 fusion protein. Additional blots for replicate studies are provided in Supplementary Figure S14. Original uncropped blot is shown in Supplementary Figure S19.

(C) Relative protein levels of mTurquoise-tagged bHLH104 were determined by Western blot. Band intensities were normalized to total protein, and fold-change was calculated as the ratio of MG132-treated to DMSO-treated samples. Bars represent mean ± SEM; individual data points are shown.

(D) Cell-free degradation assay showing in vitro degradation of His-tagged bHLH104 protein when incubated with protein extracts from 10-day-old Col-0 (WT) *Arabidopsis thaliana* seedlings. His-bHLH104 was expressed in *E. coli* and remained stable on its own, but degraded upon incubation with the plant extracts, indicating proteasome-mediated degradation. Total protein from whole seedlings was extracted using standard protein extraction procedures. Samples were collected at the indicated time points and analyzed by immunoblotting with anti-His and anti-Actin antibodies. MG132 treatment stabilizes bHLH104, indicating proteasome-dependent degradation.

(E) Confocal microscopy of mTurquoise2 fluorescence in roots of transgenic Arabidopsis seedlings expressing full-length bHLH104 (left) or b104^dPAA (right). Images show two representative seedlings (S1 and S2) per genotype. Arabidopsis thaliana seedlings were at the germination stage, 5 days old, corresponding to 2 days after stratification, and grown on +Fe medium. TM, transmitted light; Overlay, merged mTurq2 and TM channels. Scale bar = 25 µm; excitation at 458 nm; emission collected from 493–613 nm.

Figure 6

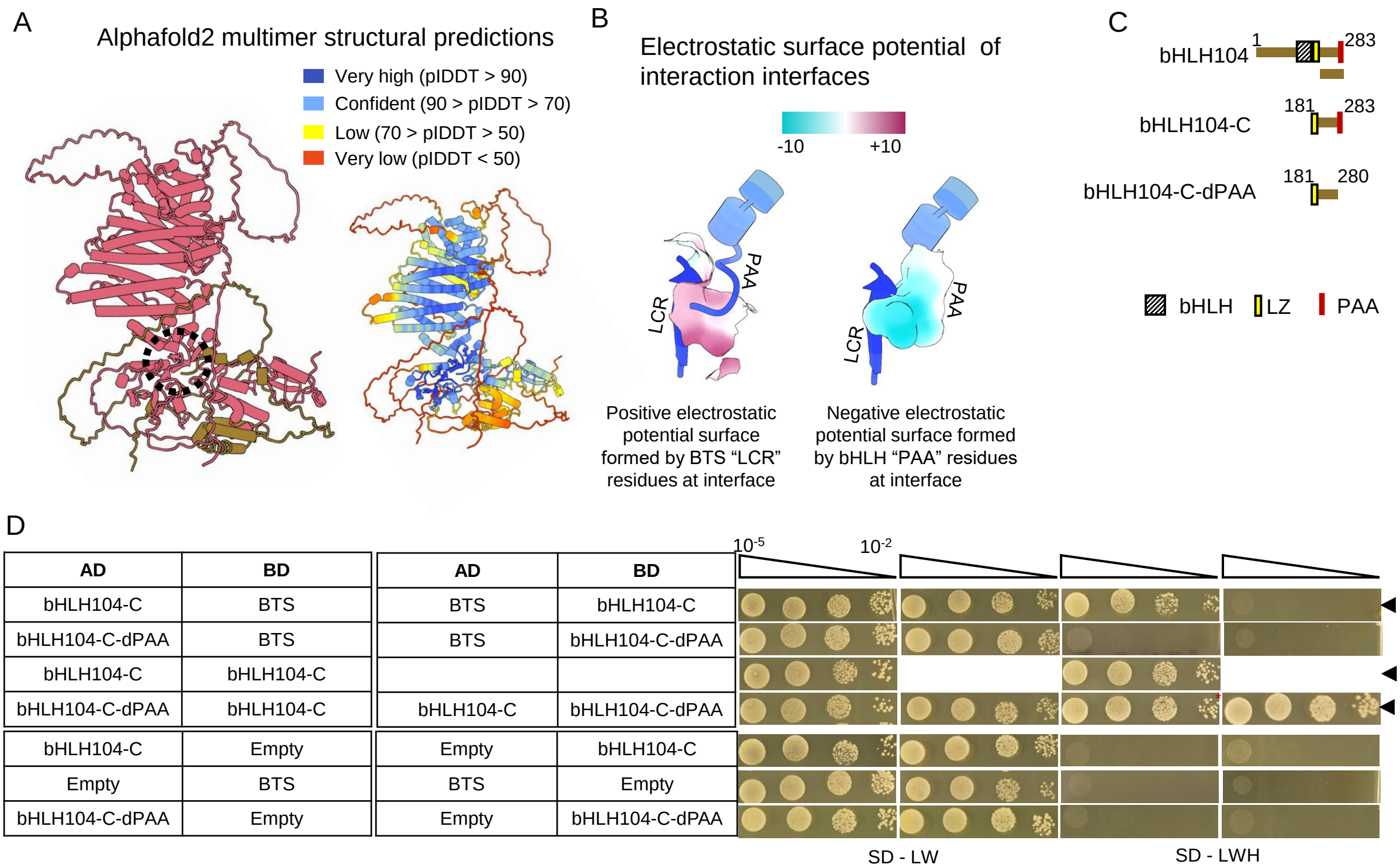

Figure 6. The PAA short sequence is required for bHLH104 interaction with BTS.
(A) Structural prediction of the bHLH104–BTS complex using AlphaFold2 Multimer (Evans et al., 2021; Jumper et al., 2021). Left: Chain-colored model showing BTS (rose color) and bHLH104 (bronze color). Right: Per-residue confidence model with pLDDT scores color-coded as very high (pLDDT > 90), confident (90 > pLDDT > 70), low (70 > pLDDT > 50), and very low (pLDDT < 50). Dashed circle marks the interaction interface formed by BTS and bHLH104.
(B) Electrostatic surface potential modeling (Pettersen et al., 2004) reveals a negatively charged region near the proline–alanine–alanine (PAA) sequence in bHLH104 that complements a positively charged surface in the leucine–cysteine–arginine (LCR) domain of BTS. The electrostatic scale ranges from –10 (purple) to +10 (cyan) kT/e.
(C) Schematic representation of full-length bHLH104, bHLH104-C and bHLH104-C-dPAA used for Y2H and UbiGate assays. C-terminal parts lack the N-terminus and the DNA-binding basic Helix Loop Helix (bHLH) domain. LZ is Leuzine zipper domain. Numbers indicate amino acid positions.
(D) Yeast two-hybrid assays testing protein–protein interactions between bHLH104-C^dPAA and BTS. bHLH104-C and BTS heterodimerization and bHLH104-C homodimerization serve as positive controls. Note that C-terminal bHLH104 fragments were used since full length bHLH104 shows autoactivation in Y2H (Lichtblau et al. 2022). Black arrows indicate positive interaction due to colony growth in the selective condition.

Figure 7

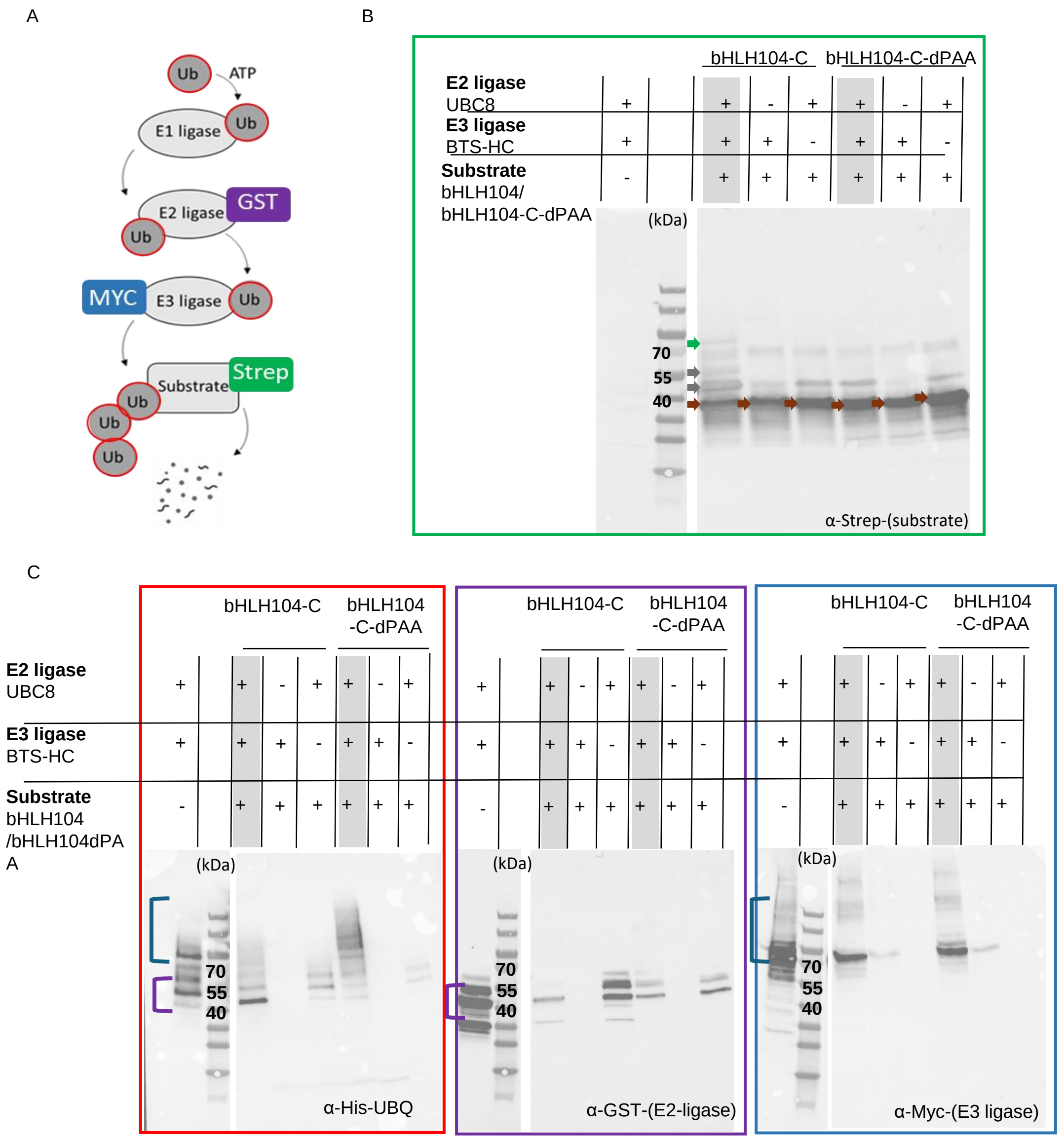

Figure 7. The PAA short sequence leads to a specific bHLH104-C band in the UbiGate system testing for BTS-mediated ubiquitination of bHLH104 in E. coli cells.

(A) Schematic overview of the ubiquitin/26S proteasome pathway. Each component was expressed in E. coli using the UbiGate system (Kowarschik et al., 2018). Recombinant bHLH104-C or bHLH104-C^dPAA proteins (Strep-tagged) were used as substrates. BTS-HC served as the E3 ligase (Myc-tagged), in combination with UBC8 as E2 ligase (GST-tagged), an E1 activating enzyme, and ubiquitin (His-tagged).

(B) The relevant immunoblot for assessing substrate ubiquitination is the anti-Strep blot. The anti-Strep antibody detects predominantly the Strep-tagged substrate protein in as an expected band corresponding to a non-ubiquitinated form (~40 kDa; brown arrows). Only in the presence of all components, there are multiple higher than 40 kDa protein bands, indicative of a protein ubiquitination ladder (Kowarschik et al., 2018), with one particular unique form (~70 kDa) potentially corresponding to polyubiquitinated bHLH104-C (green arrow corresponding to ~70 kDa plus molecular weight shift of approximately 30 kDa corresponding to the addition of three to four ubiquitin moieties of ~8.6 kDa each; grey arrows indicating additional higher molecular weight bands indicating a ubiquitination ladder pattern). The 70 kDa band is absent in the relevant controls, either bHLH104-C^dPAA lane under identical conditions or in control samples lacking individual components. Strep bands are also detectable in control lanes, these are not considered ubiquitination signals. The assay has been performed three times with similar outcome of the unique 70 kDa band which might point to the polyubiquitinated bHLH104-C target (additional replicates in Supplementary Figure S16).

(C) Shown are three types of control immunoblots confirming expression of all proteins for ubiquitination activity of the E3 ligase in the UbiGate assay. All panels are from the same membrane, sequentially probed with different antibodies after stripping. Anti-GST detects E2 ligase (GST-UBC8); anti-Myc detects E3 ligase (Myc-BTS-HC); anti-His-UBQ detects total ubiquitin conjugates (His-Ub). Violet bracket indicates autoubiquitinated E2 ligase; blue bracket indicates autoubiquitinated E3 ligase. Bands in control lanes of the anti-ubiquitin blot represent E2 and E3 autoubiquitination, which is independent of substrate ubiquitination.

Figure 8

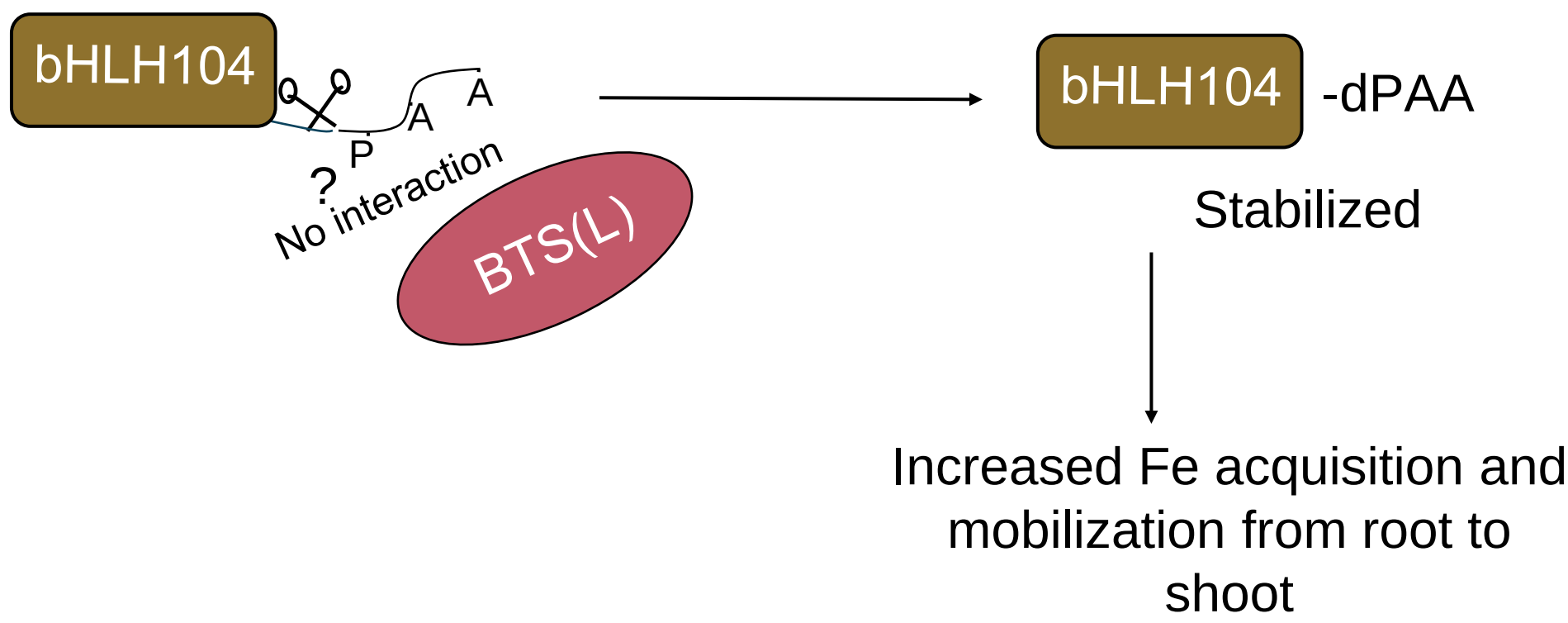

Figure 8. Working model of bHLH104 regulation through the C-terminal PAA sequence and its impact on Fe homeostasis.
The C-terminal PAA sequence in bHLH104 mediates interaction with BTS-type E3 ligases, targeting the protein for proteasomal degradation. Deletion of the PAA motif (b104^dPAA) disrupts this interaction, leading to protein stabilization. The increased abundance of stabilized b104^dPAA enhances Fe acquisition responses in *Arabidopsis*.

Supplementary Figure S1

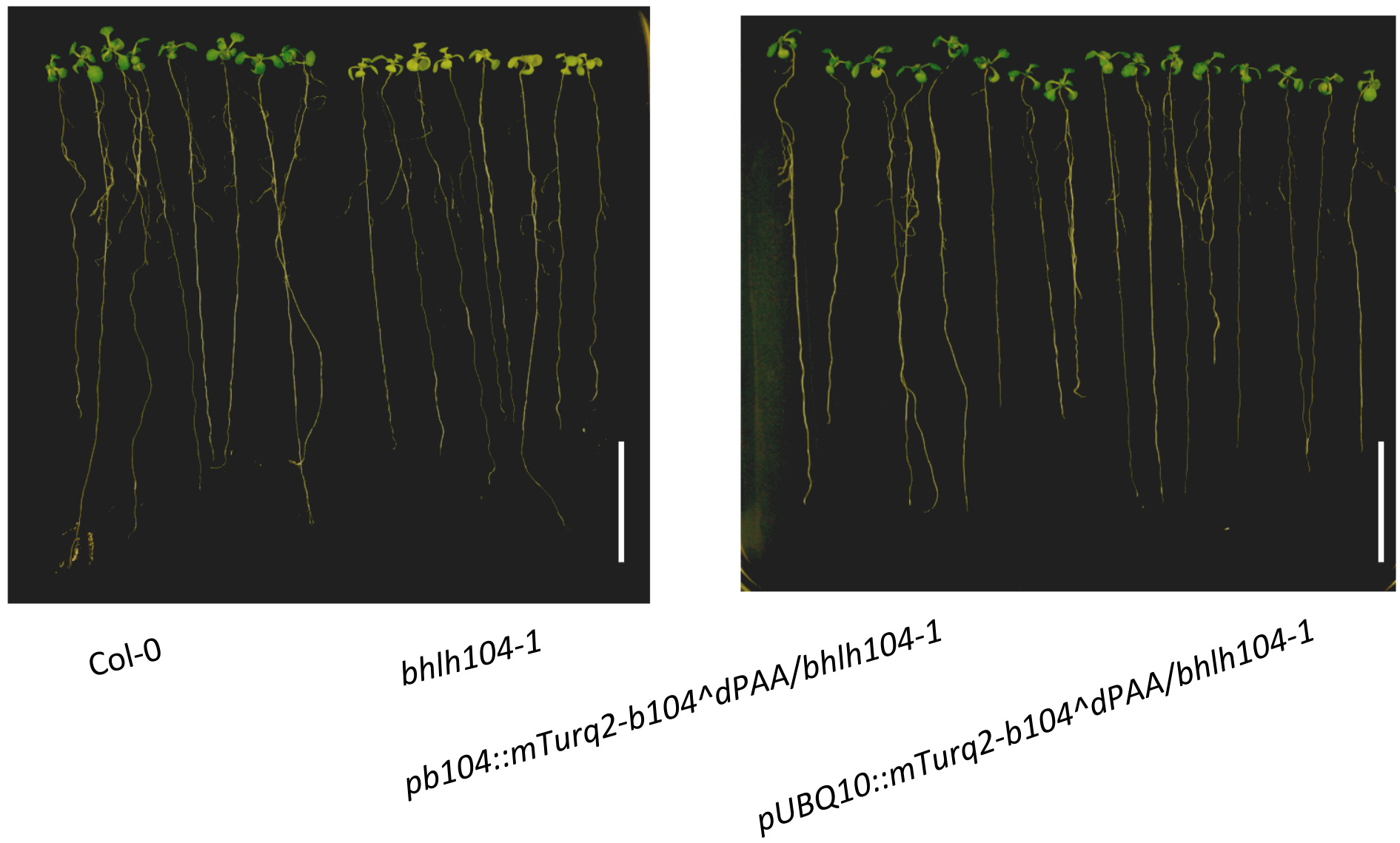

Supplementary Figure S1. mTurquoise2-tagged bHLH104^dPAA complements the *bhlh104-1* phenotype under Fe deficiency.
Representative images of 12-day-old seedlings grown on iron-deficient (–Fe) medium. Left panel: wild-type Col-0 and *bhlh104-1*. Right panel: *pb104::mTurq2-b104^dPAA/bhlh104-1* and *pUBQ10::mTurq2-b104^dPAA/bhlh104-1* complementation lines. The *bhlh104-1* displays chlorotic leaves compared to Col-0 under iron deficiency. Expression of mTurquoise2-tagged bHLH104^dPAA under either the native bHLH104 promoter or the UBQ10 promoter restores leaf health in the *bhlh104-1* background, demonstrating that the mTurquoise2-tagged protein is biologically functional. Scale bars: 2 cm.

Supplementary Figure S2

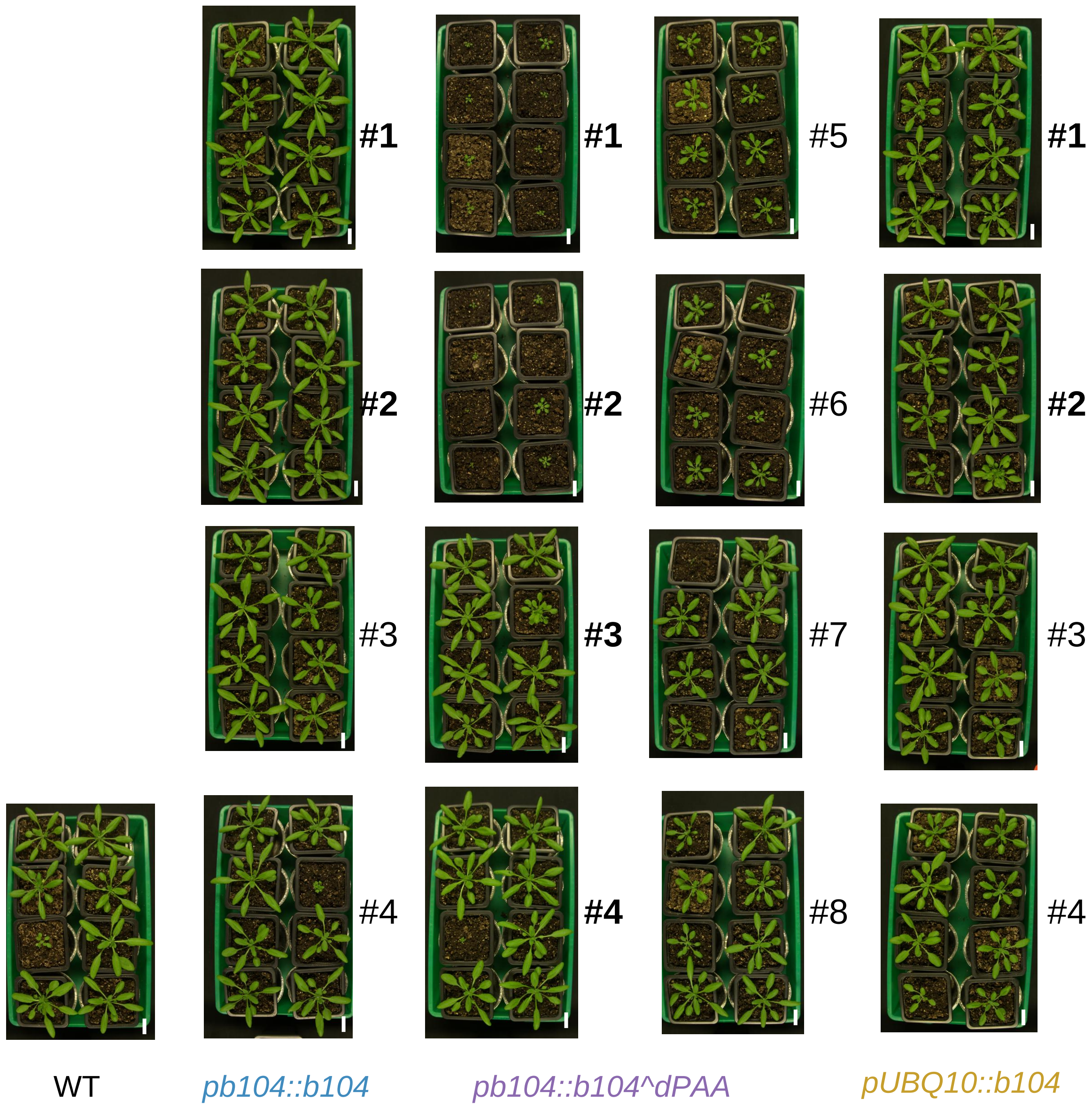

Supplementary Figure S2. Preliminary phenotypic screen of independent transgenic *Arabidopsis* lines expressing bHLH104 or bHLH104^dPAA.
26 days old plants of Col-0 wild type (WT), *pb104::b104* (4 independent lines), *pb104::b104^dPAA* (8 independent lines), and *pUBQ10::b104* lines (4 independent lines), were grown under same conditions. Each tray contained eight plants derived from an independent T1 transgenic line. Lines selected for further analysis in the main study are indicated: *pb104::b104 lines* #1 and #2, and *pb104::b104^dPAA lines #1–#4* and *pUBQ10::b104* lines #1 and #2, scale bar = 2 cm.

Supplementary Figure S3

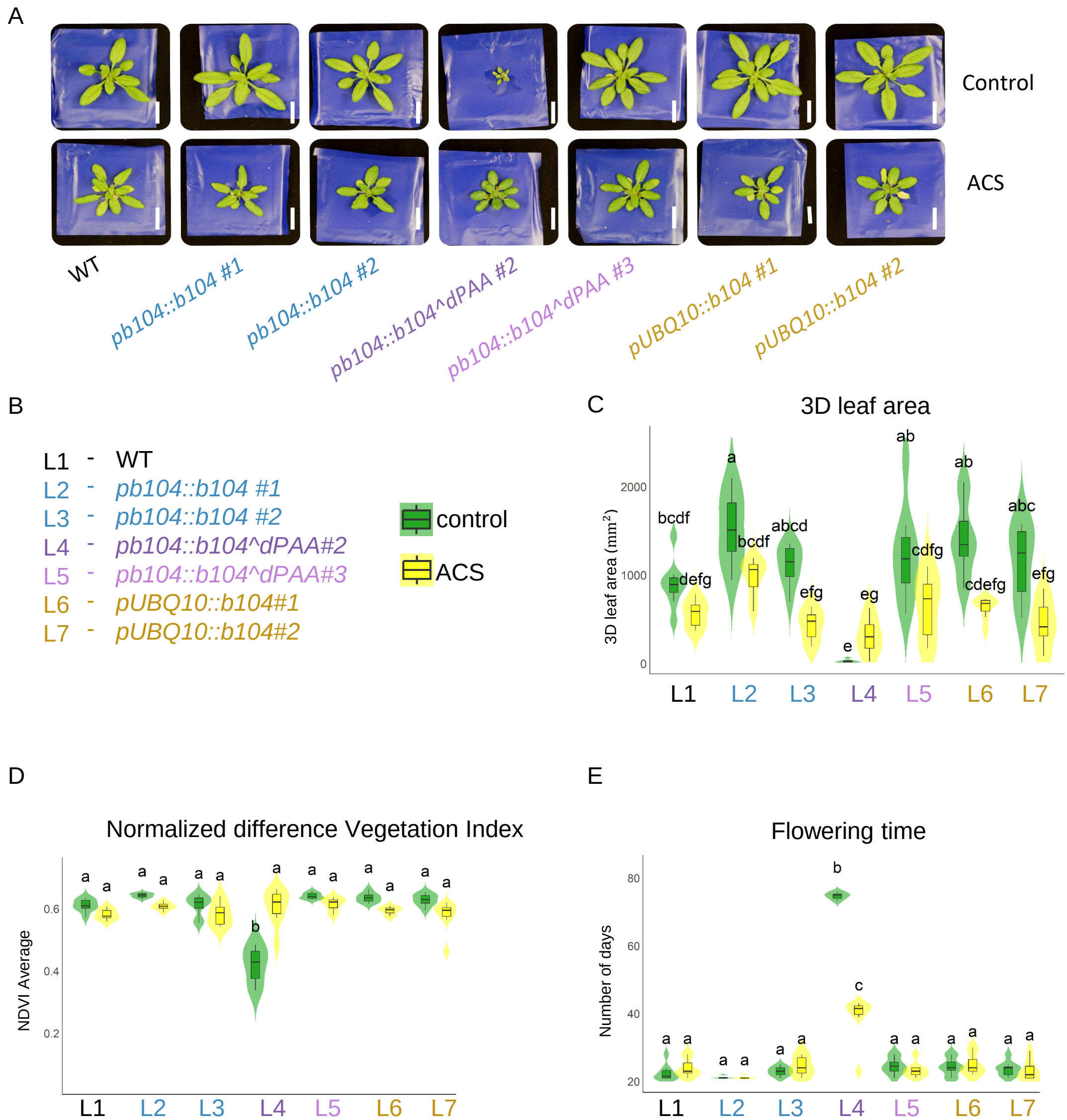

Supplementary Figure S3. Response of bHLH104^dPAA transgenic lines to iron-limiting conditions in alkaline calcareous soil (ACS).
Arabidopsis thaliana transgenic lines were grown in either control soil (pH 5.9) or alkaline calcareous soil (ACS, pH 8.1).(A) Photos of four-week-old plants grown in control and ACS soil conditions.(B) List of plant lines used in this experiment, numbered from L1 to L7. scale bar = 2 cm (C) 3D leaf area measurements: Plants were evaluated for leaf expansion and overall growth in both conditions.(D) NDVI (Normalized Difference Vegetation Index): NDVI values were measured to assess photosynthetic activity in response to ACS conditions.(E) Flowering time: Flowering time was compared between control and ACS conditions, with letters indicating statistical differences. Statistical significance was assessed by two-way ANOVA followed by Tukey's HSD test ($p < 0.05$). N = 8 plants per line.

Supplementary Figure S4

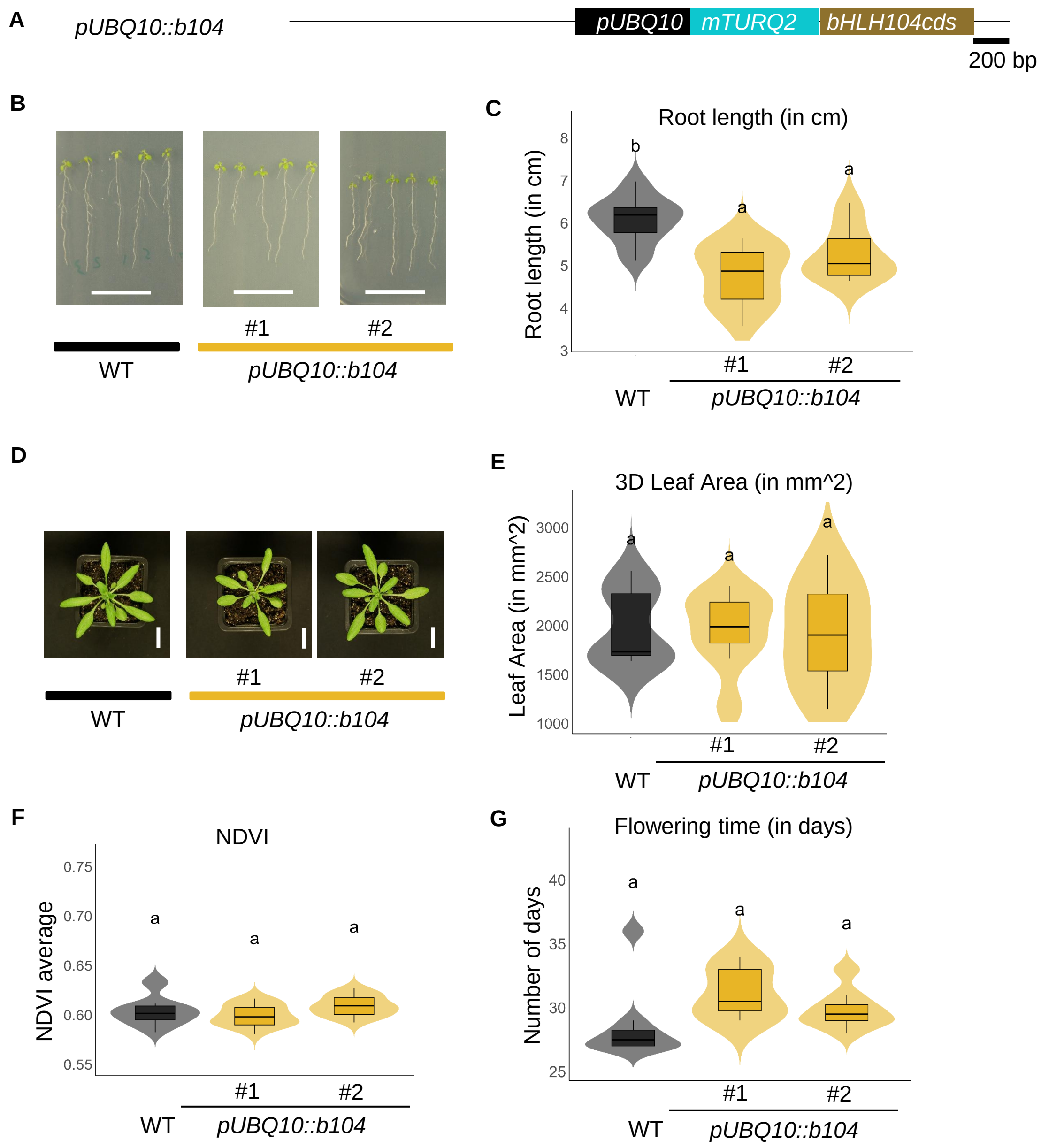

Supplmentary Figure S4. Constitutive expression of bHLH104 did not alter growth and physiological traits in Arabidopsis.

(A) Schematic representation of the construct used to generate transgenic lines expressing full-length bHLH104 (*pUBQ10::bHLH104*). The construct is driven by the ubiquitin 10 (UBQ10) promoter and is fused at the N-terminus to the mTurquoise2 fluorescent tag. Scale bar = 200 bp.

(B-C) Photos and root length quantification data of 12-day-old seedlings grown vertically on Hoagland medium supplemented with iron (+Fe). Scale bar =2 cm

(D) Representative images of 4-week-old Arabidopsis plants grown in soil. Shown are Col-0 (WT) and two independent *pUBQ10::b104* lines (#1, #2). Scale bar = 2 cm

(E–F) Quantitative analysis of aboveground phenotypes acquired using the Phenospex PlantEye system: (E) 3D leaf area (mm^2); (F) NDVI (Normalized Difference Vegetation Index).

(G) Flowering time, measured manually as the number of days to bolting.

Data represent means ± SD (n = 7–12 biological replicates per line). Statistical analysis was performed using two-way ANOVA followed by Tukey's post hoc test. Different letters indicate statistically significant differences at $p < 0.05$.

Supplementary Figure S5

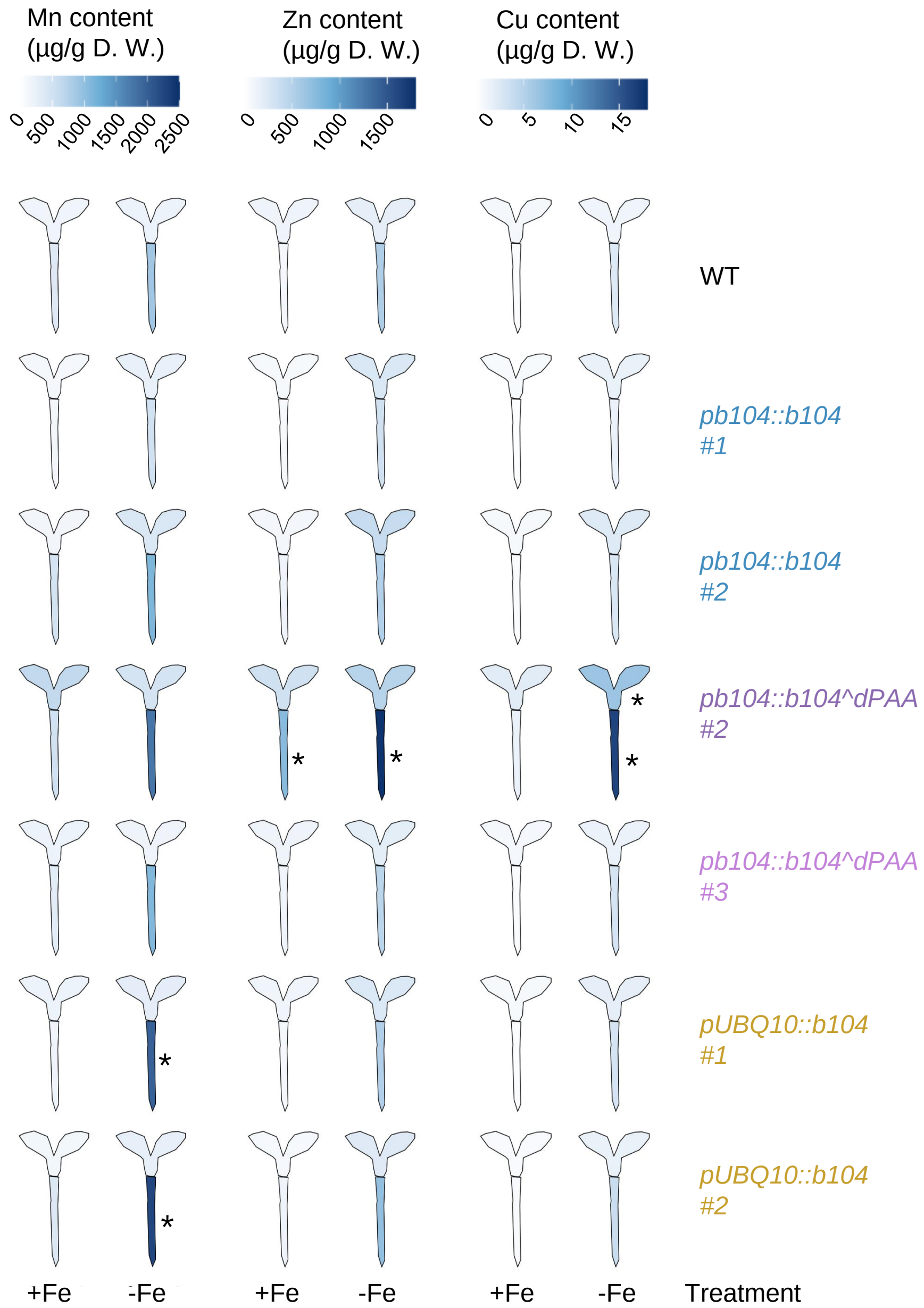

Supplementary Figure S5. Elemental content analysis of Mn, Zn, and Cu in 10-day old Arabidopsis seedlings.

Heatmap showing the distribution of Mn, Zn, and Cu content (in µg/g dry weight) across different *Arabidopsis* seedlings, including wild-type (WT), pb104::b104 (lines #1, #2), *pb104::b104^dPAA* (lines #2, #3), *pUBQ10::b104* (lines #1, #2). The color scale indicates the range of elemental concentrations from low (light blue) to high (dark blue). Seedlings were grown in Hoagland media with or without 50 mM Fe supplementation. Data were collected from 10-day-old seedlings, with elemental content measurements obtained via ICP-MS analysis. Three biological replicates per line were used. The plot was generated using the ggPlantMap package in RStudio. Asterisks indicate genotypes that differ significantly from WT within the same tissue and treatment condition ($p < 0.05$), as determined by two-way ANOVA and Tukey's post hoc test ($n = 3$ for each group).

Supplementary Figure S6

A

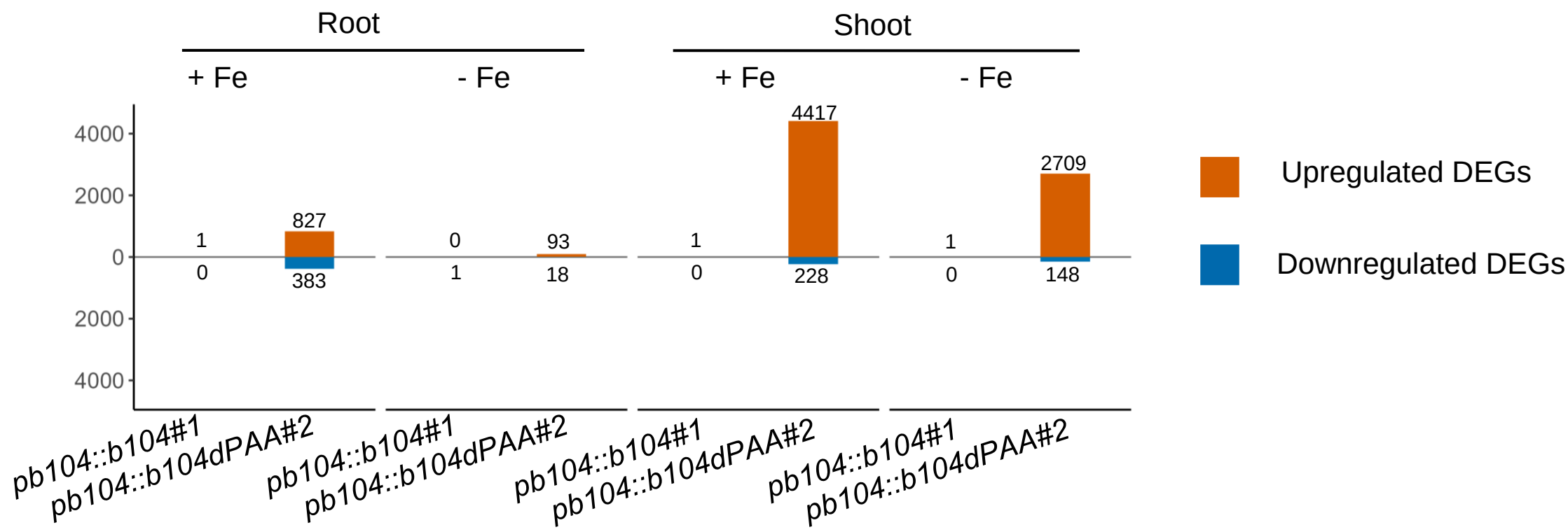

B

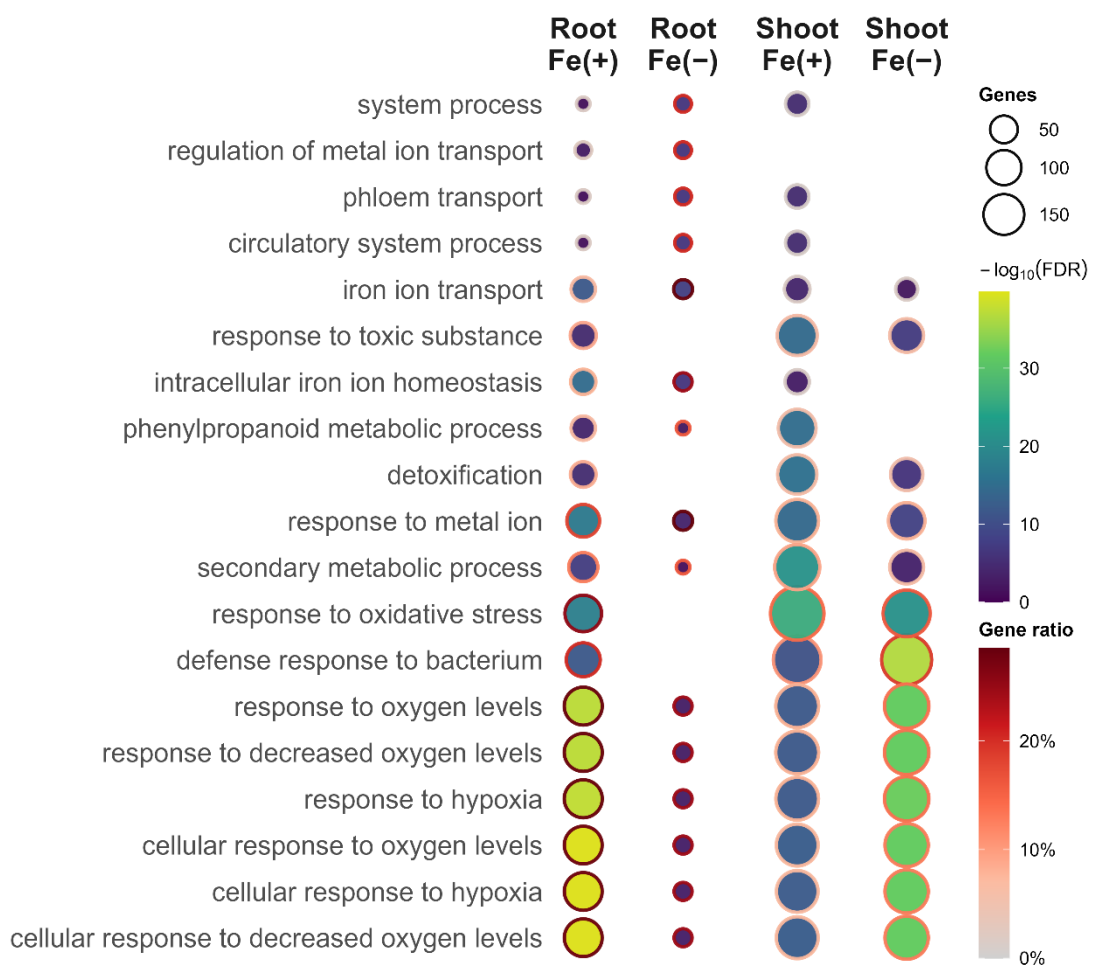

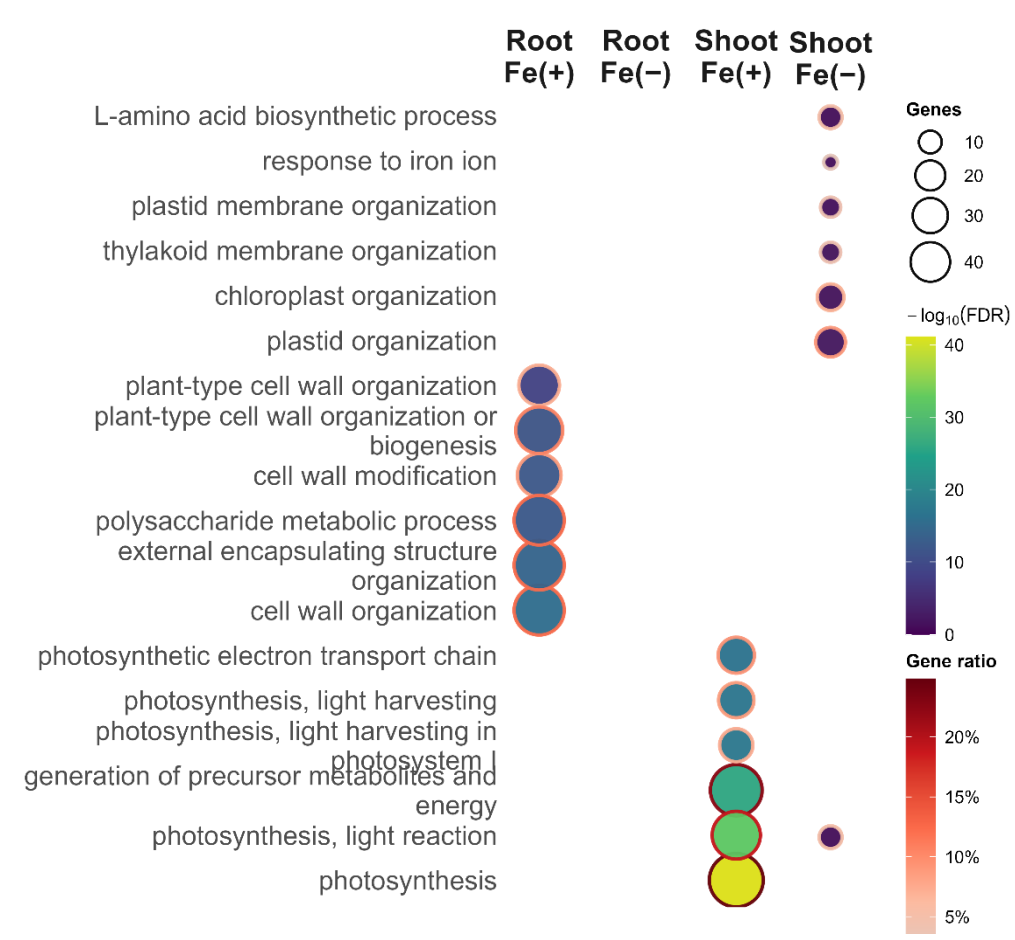

Supplementary Figure S6: Differential expression and GO enrichment across seedling tissues.

(A) Counts of differentially expressed genes (DEGs) for each line vs WT in root and shoot under Fe(+) and Fe(−). Orange = up-regulated; blue = down-regulated; numbers above/below bars indicate counts for each category. Total DEGs for each condition are the sum of up-regulated and down-regulated counts. DEGs were defined at FDR ≤ 0.05 and |log2FC| ≥ 0.58. X-axis labels show the abbreviated line IDs.

(B) GO Biological Process enrichment for the up-regulated (left panel) and down-regulated (right panel) DEG sets. Columns correspond to tissue/Fe combinations (Root Fe(+), Root Fe(−), Shoot Fe(+), Shoot Fe(−)). Each dot represents a significant term (BH FDR ≤ 0.05); dot size = number of genes in the term, fill = −log10(FDR), and ring color = GeneRatio. Terms plotted are the top-ranked per panel; the gene universe was all genes tested in the corresponding comparison.

Supplementary Figure S7

A

L1 - WT
L2 - *pb104::b104 #1*
L4 - *pb104::b104^dPAA#2*
L5 - *pb104::b104^dPAA#3*

B

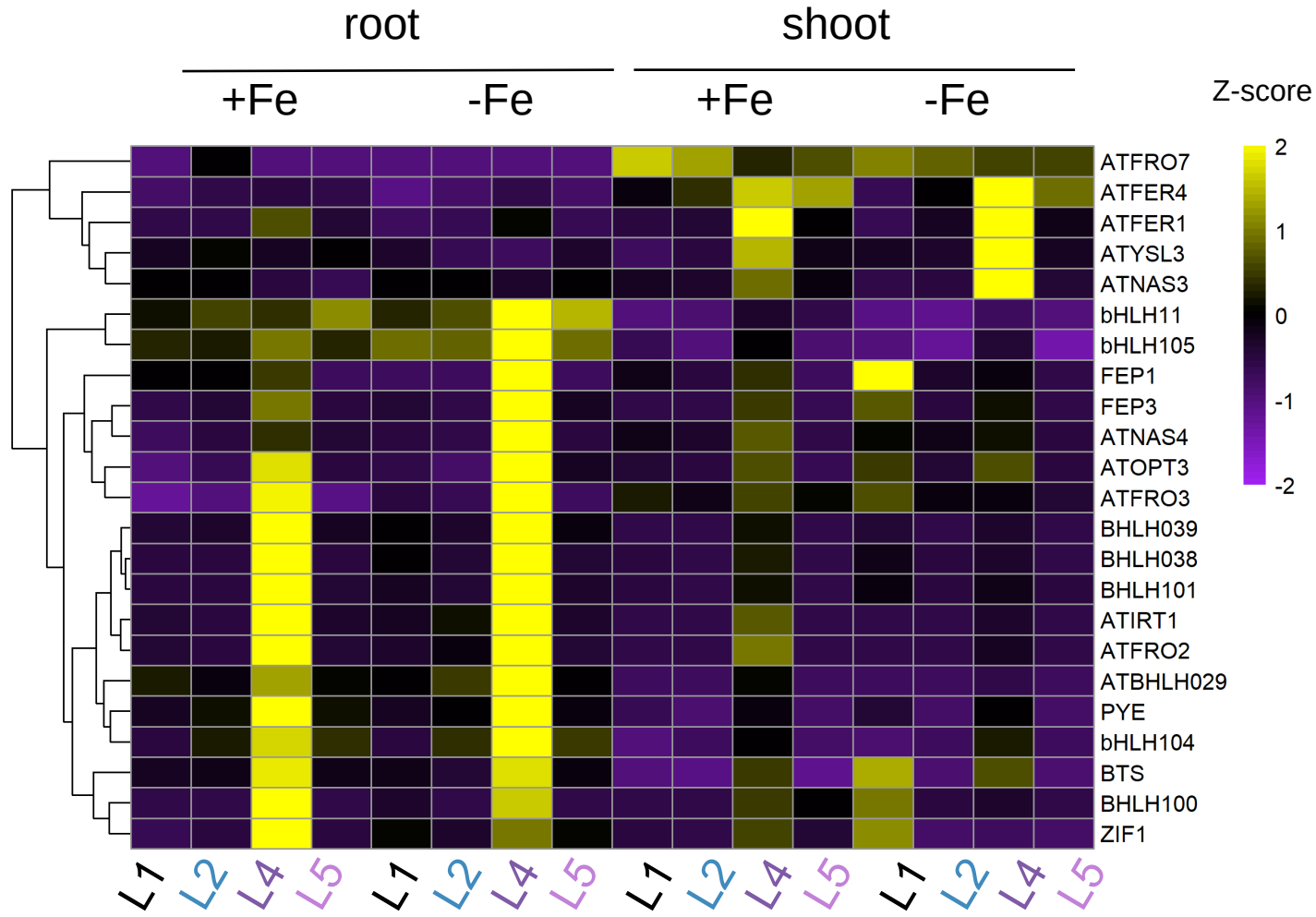

C

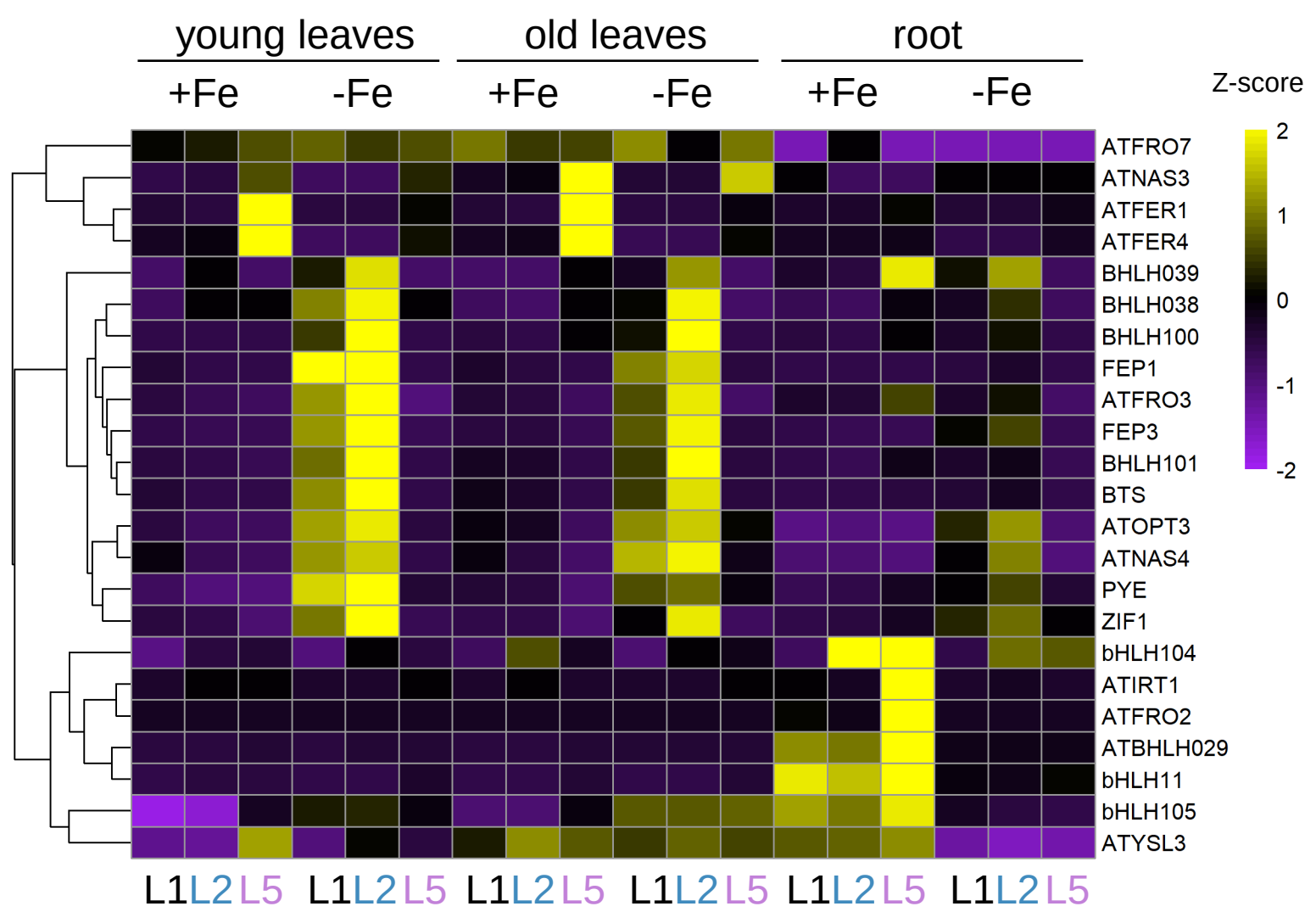

Supplementary Figure S7. Expression profiles of 23 selected Fe homeostasis genes involved in Fe acquisition and mobilization

(A)Plant lines used In this experiment

(B)Clustered heatmap showing expression profiles of 23 Fe homeostasis genes (gene selection based on Ngigi et al., 2025; Schwarz et al., 2020) obtained using RNA sequencing in root and shoot tissues under +Fe and –Fe conditions. Arabidopsis seedlings were grown for 10 days after sowing (DAS) under either iron-sufficient (+Fe) or iron-deficient (–Fe) conditions.

(C)Clustered heatmap showing expression profiles of 23 Fe homeostasis genes (gene selection based on Ngigi et al., 2025; Schwarz et al., 2020) obtained using RNA sequencing in young leaves, old leaves, and roots under both +Fe and –Fe conditions. *Arabidopsis* plants were grown hydroponically under iron-sufficient (+Fe) conditions for 27 days, followed by a 3-day treatment with either +Fe or –Fe media.

Heatmap was generated in RStudio version 4.4.1 using calculated Z-scores of normalized gene expression values. Purple indicates low expression and yellow indicates high expression.

Supplementary Figure S8

A

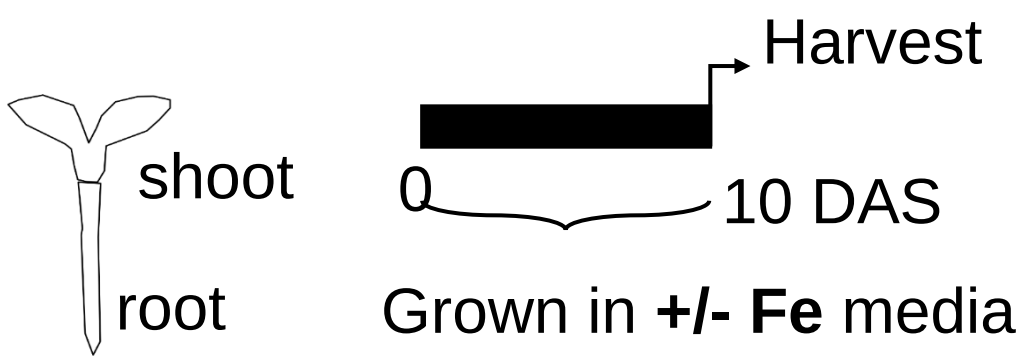

B

L1 - WT
L2 - *pb104::b104 #1*
L3 - *pb104::b104 #2*
L4 - *pb104::b104^dPAA#2*
L5 - *pb104::b104^dPAA#3*
L6 - *pUBQ10::b104#1*
L7 - *pUBQ10::b104#2*

C

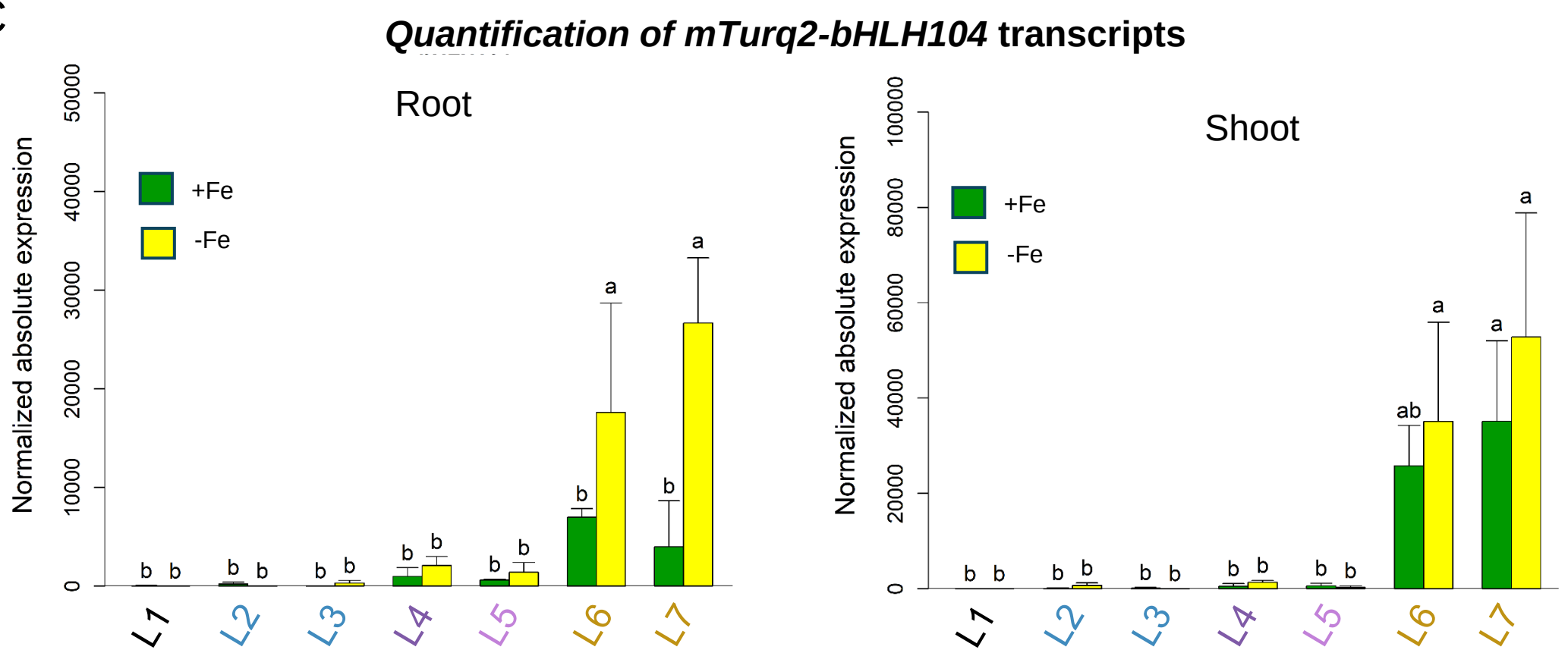

D

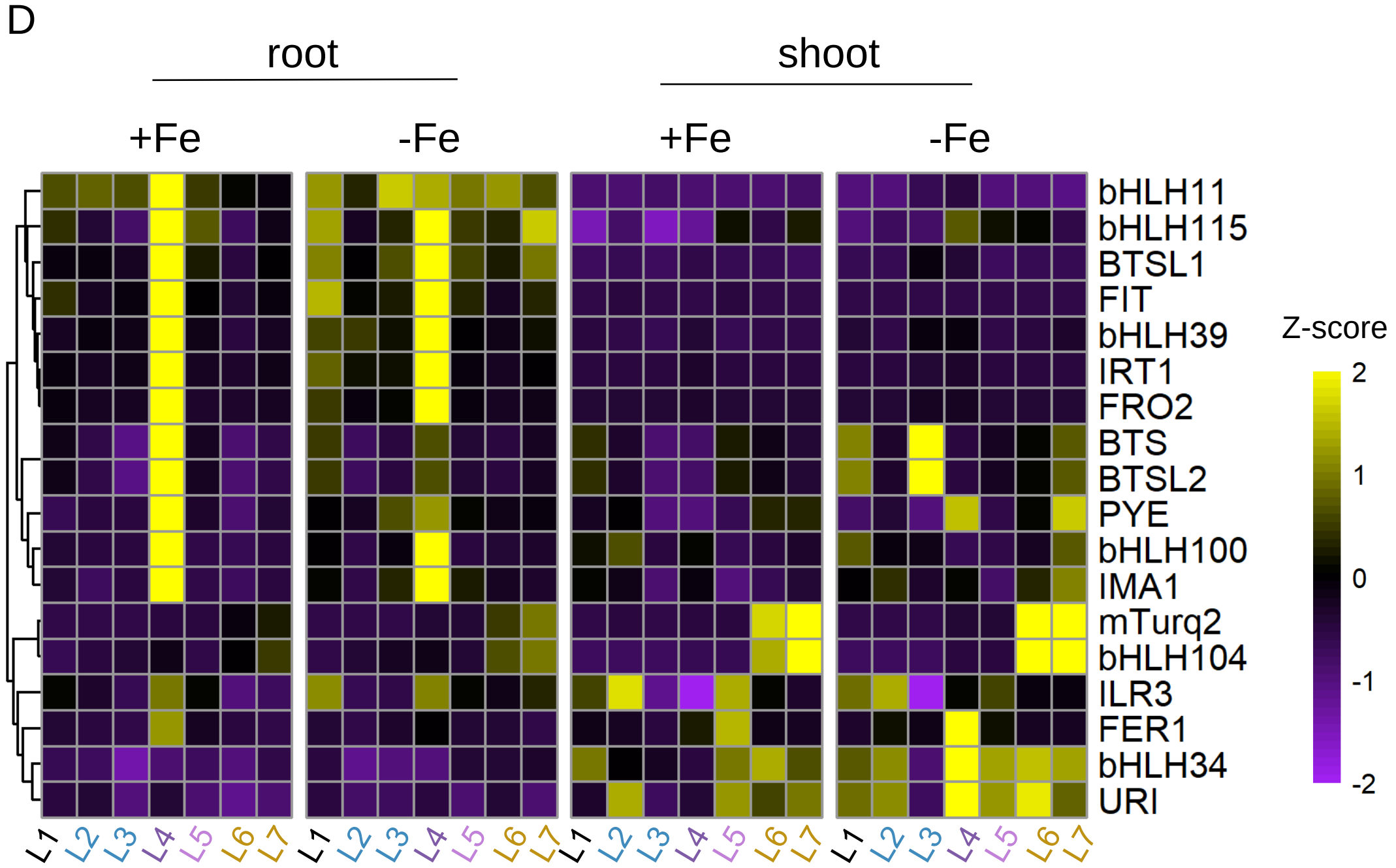

Supplementary Figure S8. Targeted gene expression profiling in seedlings.
(A) Schematic representation of the experimental design. Arabidopsis seedlings were grown for 10 days after sowing (DAS) under either iron-sufficient (+Fe) or iron-deficient (–Fe) conditions. Shoot and root tissues were collected separately for RT-qPCR analyses. (B) Genotypes used in this study. Abbreviations of lines used: L1, wild-type Col-0; L2, *pb104::mTurquoise2-bHLH104 line #1*; L3, *pb104::mTurquoise2-bHLH104 line #2*; L4, *pb104::mTurquoise2-b104^dPAA line #2*; L5, *pb104::mTurquoise2-b104^dPAA line #3*; L6, *pUBQ10::mTurquoise2-bHLH104 line #1*; L7, *pUBQ10::mTurquoise2-bHLH104 line #2*. (C) Quantification of mTurq2-tagged bHLH104 transgenes in indicated plant lines using RT-qPCR Letters indicating statistical differences. Statistical significance was assessed by two-way ANOVA followed by Tukey's HSD test ($p < 0.05$). N = 3 per group. (D) Clustered heatmaps showing the expression profiles of selected Fe homeostasis genes obtained using RTqPCR. Heatmaps were generated in RStudio version 4.4.1 using calculated Z-scores of normalized gene expression values across root and shoot tissues for both +Fe and –Fe conditions. Purple indicates low expression and yellow indicates high expression.

Supplementary Figure S9

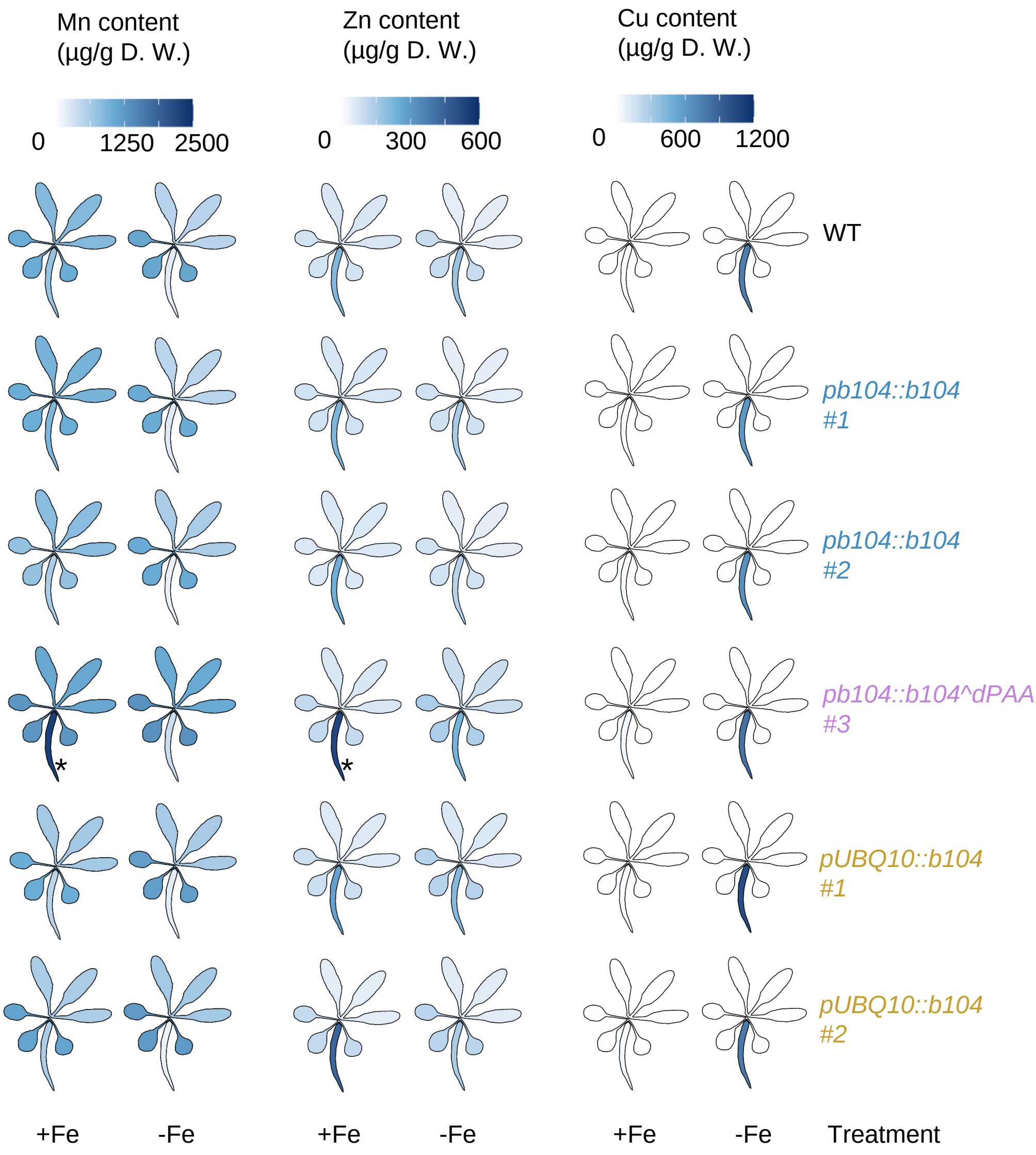

Supplementary Figure S9. Elemental content analysis of Mn, Zn, and Cu in mature *Arabidopsis thaliana*.
Heatmap showing the distribution of iron (Fe) content (in µg/g dry weight) in young leaves, old leaves, and roots of *Arabidopsis* transgenic lines, including wild-type (WT), *pb104::b104* (lines #1, #2), *pb104::b104^dPAA* (line #3), *pUBQ10::b104* (lines #1, #2). Plants were grown hydroponically under iron-sufficient (+Fe) conditions for 27 days, followed by a 3-day treatment with either +Fe or –Fe media. The color scale indicates the iron content, with darker blue shades representing higher iron concentrations. Data represent the mean values from three biological replicates (n = 3). Heatmap intensity reflects iron concentration (µg/g dry weight) measured by ICP-MS. The plot was generated using the ggPlantMap package in RStudio. Asterisks indicate genotypes that differ significantly from WT within the same tissue and treatment condition ($p < 0.05$), as determined by two-way ANOVA and Tukey's post hoc test (n = 3 for each group).

Supplementary Figure S10

A

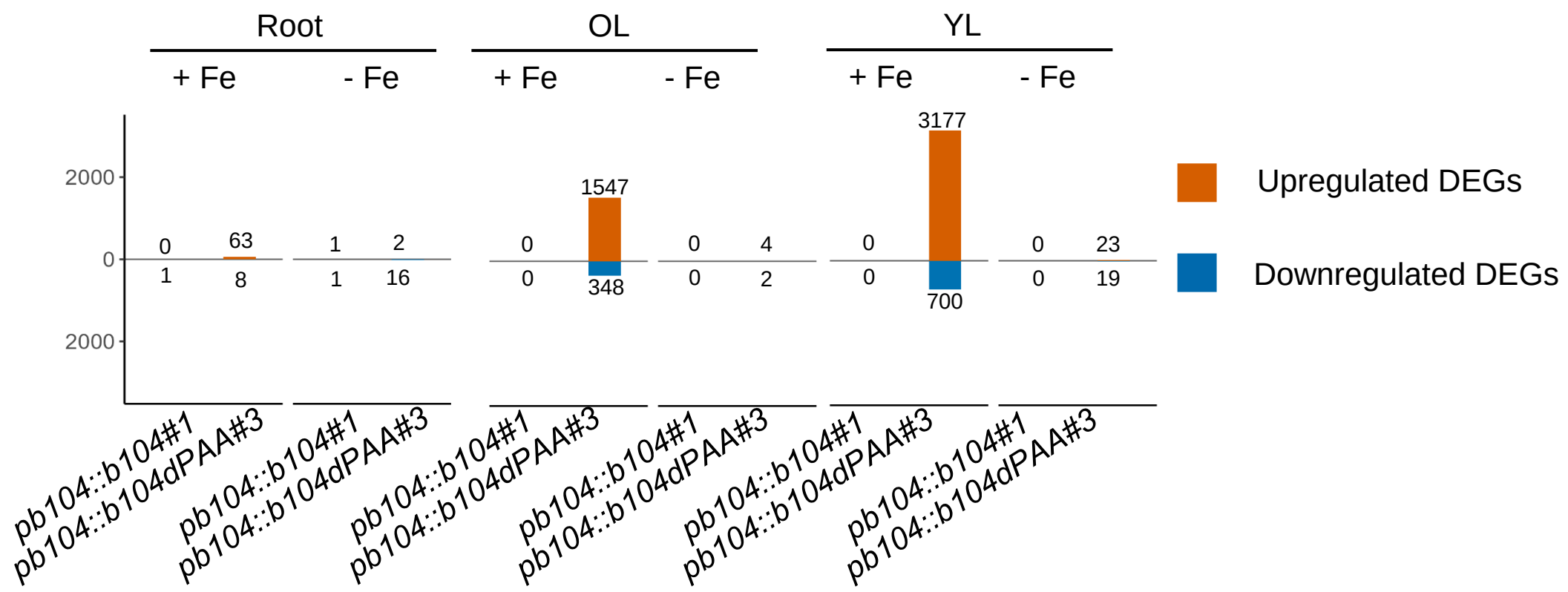

B

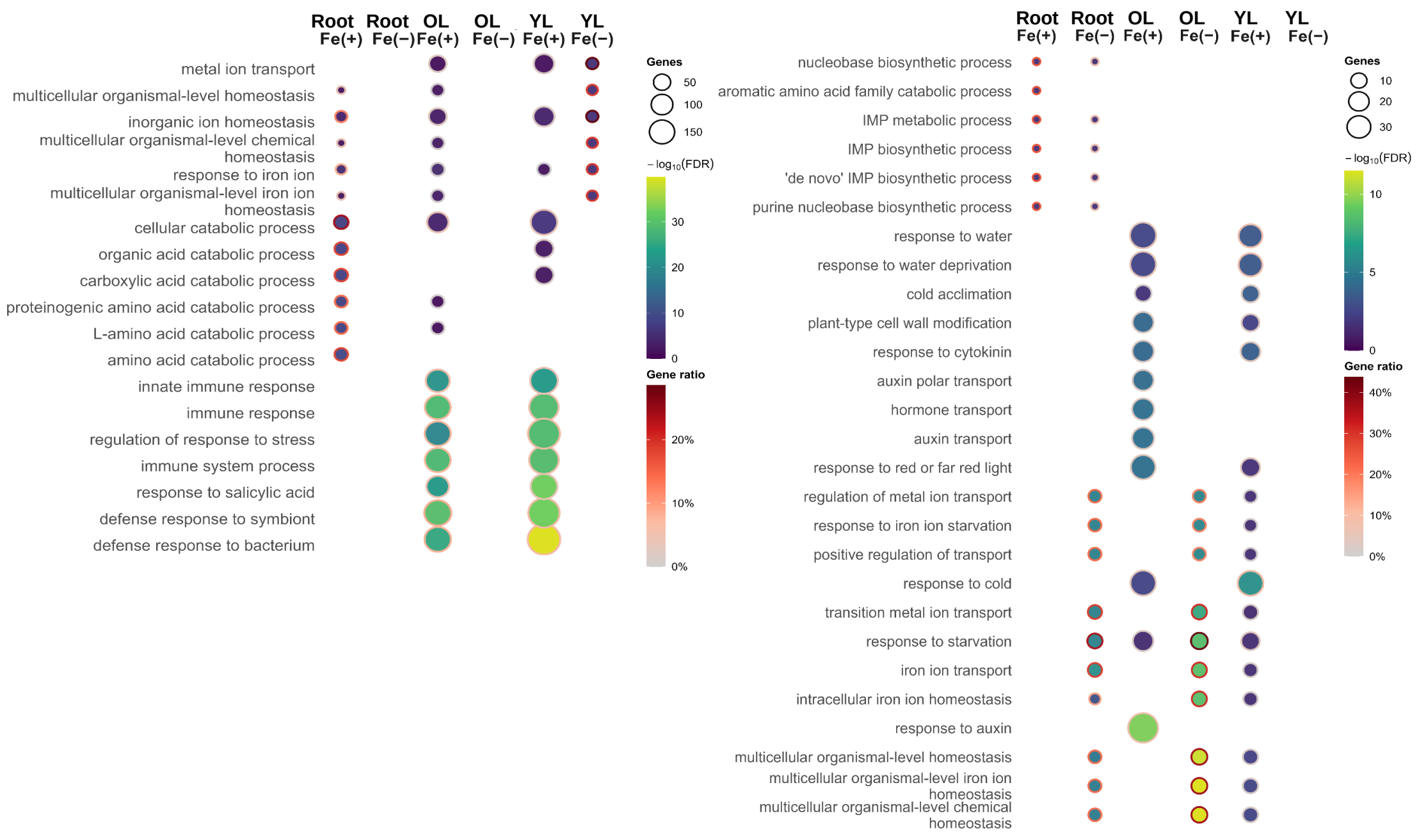

Supplementary Figure S10: Differential expression and GO enrichment across reproductive stage tissues

(A) Numbers of differentially expressed genes (DEGs) for each line vs WT in root (Root), young leaves (YL), and old leaves (OL) under Fe(+) and Fe(−). Orange bars show up-regulated DEGs; blue bars show down-regulated DEGs; values above/below bars are counts for each category. Total DEGs for each condition are the sum of up-regulated and down-regulated counts. DEGs were defined at FDR ≤ 0.05 and |log2FC| ≥ 0.58.

(B) GO Biological Process enrichment for the up-regulated (left panel) and down-regulated (right panel) DEG sets. Columns correspond to tissue/Fe combinations (Root, YL, OL × Fe(+), Fe(−)). Each dot represents a significant term (BH FDR ≤ 0.05); dot size = number of genes in the term, fill = −log10(FDR), and ring color = GeneRatio. Terms shown are the top-ranked per panel; the gene universe comprised all genes tested in the corresponding comparison. Abbreviations: YL, young leaves; OL, old leaves.

Supplementary Figure S11

A

L1 - WT
L2 - *pb104::b104 #1*
L3 - *pb104::b104 #2*
L4 - *pb104::b104^dPAA#2*
L5 - *pb104::b104^dPAA#3*
L6 - *pUBQ10::b104#1*
L7 - *pUBQ10::b104#2*

B

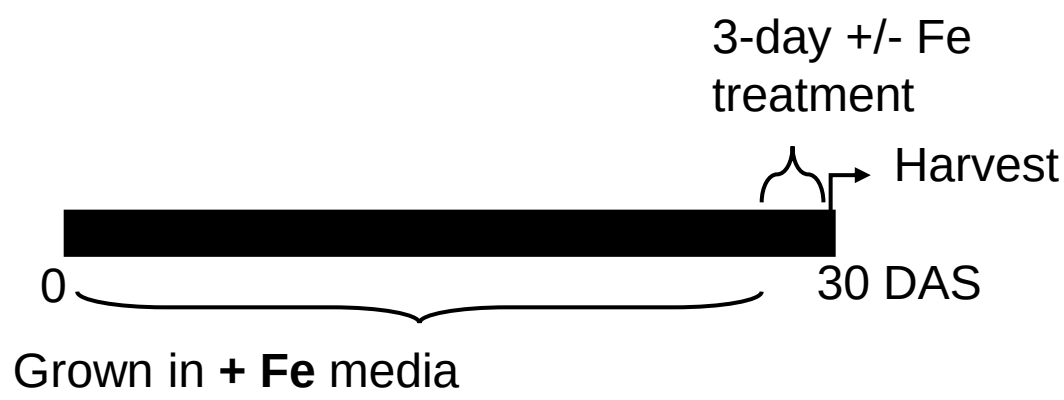

C

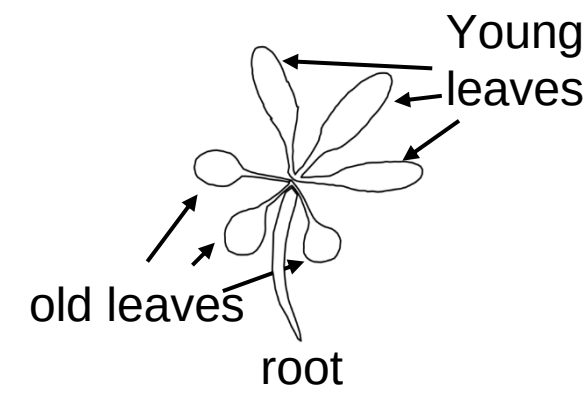

D

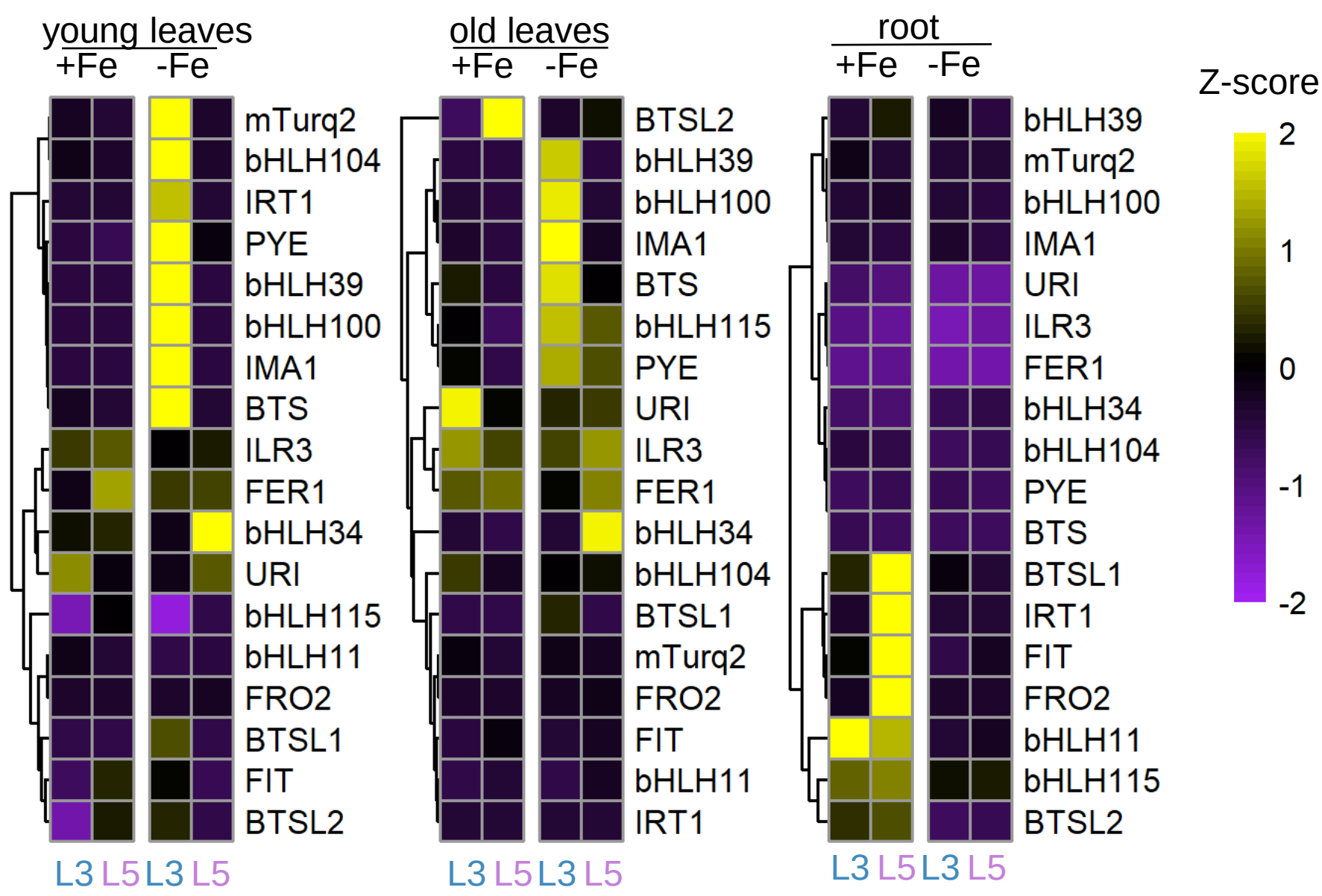

Supplementary Figure S11. Targeted gene expression profiling in reproductive-stage plants

(A) Plant lines used In this experiment. Abbreviations of lines used: L1, wild-type Col-0; L2, *pb104::mTurquoise2-bHLH104 line #1*; L3, *pb104::mTurquoise2-bHLH104 line #2*; L4, *pb104::mTurquoise2-b104^dPAA line #2*; L5, *pb104::mTurquoise2-b104^dPAA line #3*; L6, *pUBQ10::mTurquoise2-bHLH104 line #1*; L7, *pUBQ10::mTurquoise2-bHLH104 line #2*.

(B) Experimental design for the dataset shown. *Arabidopsis* plants were grown hydroponically under iron-sufficient (+Fe) conditions for 27 days, followed by a 3-day treatment with either +Fe or –Fe media.

(C) Schematic representation of tissue separation used for RT-qPCR analysis. Young and old leaves were separated from the roots to examine tissue-specific iron accumulation and gene expression.

(D) Clustered heatmaps showing the expression profiles of selected Fe homeostasis genes conditions obtained using RTqPCR in young leaves, old leaves, and roots under both +Fe and –Fe. Data represent the mean of three biological replicates (n = 3). Z-scores were calculated from normalized RT-qPCR expression values and visualized in RStudio version 4.4.1. Yellow indicates high expression; purple indicates low expression.

Supplementary Figure S12

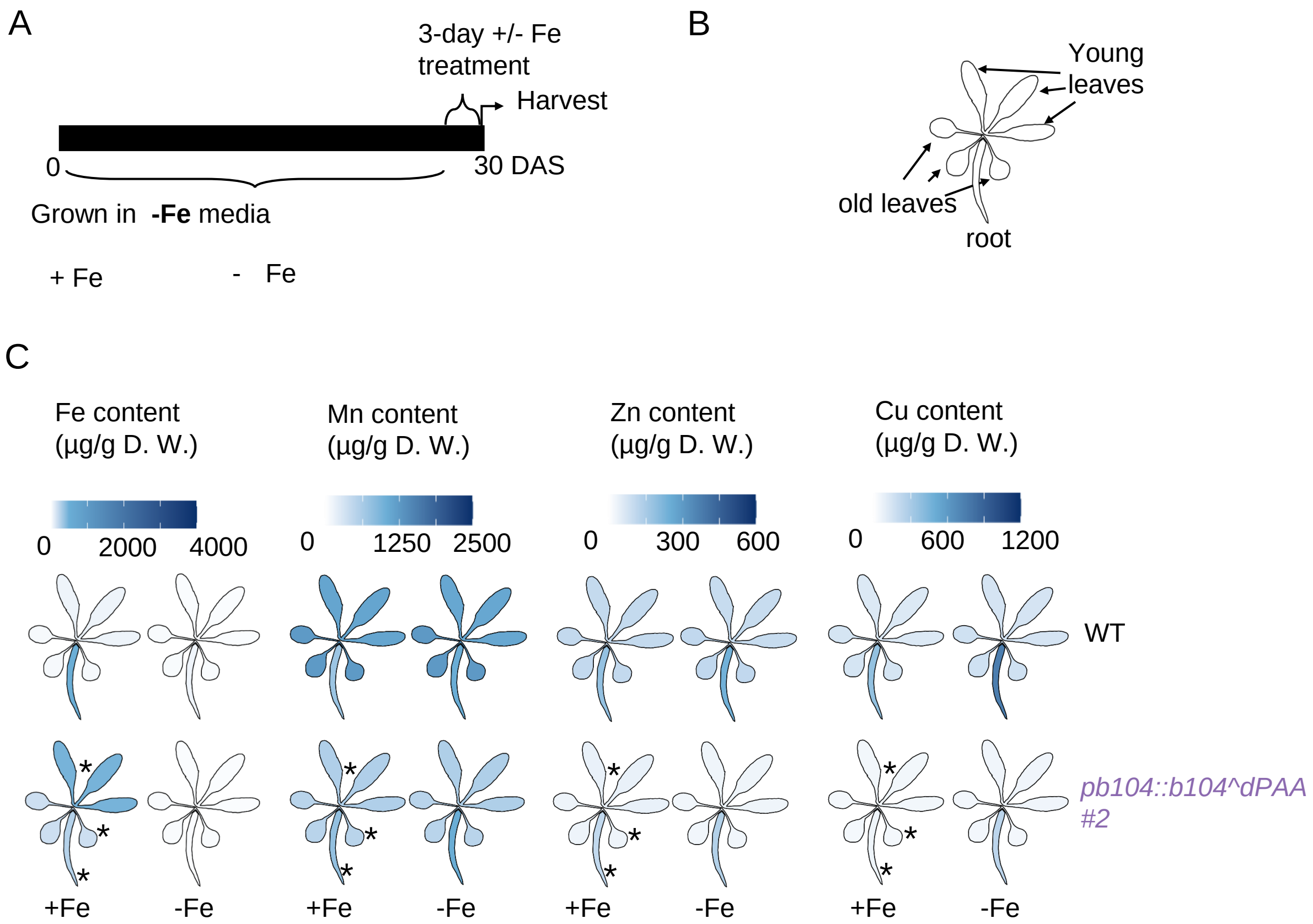

Supplementary figure S12. Tissue-specific metal accumulation in dPAA line #2 grown under iron-deficient conditions.
(A) Experimental setup: Col-0 and *pb104::b104^dPAA line #2* seedlings were grown hydroponically in Fe-deficient (–Fe) media for 27 days, followed by a 3-day treatment with either +Fe or –Fe media. Tissue collection occurred at 30 days after sowing (DAS).(B) Tissue layout: Young leaves, old leaves, and roots were separated to examine tissue-specific metal accumulation (Fe, Mn, Zn, Cu).(C) Heatmap of metal content: The distribution of Fe, Mn, Zn, and Cu content (in µg/g dry weight) in dPAA line #2 and Col-0. The color scale reflects metal concentrations, with darker blue shades indicating higher content. *pb104::b104^dPAA line #2* exhibited significant Fe accumulation in young leaves after Fe resupply, in contrast to Col-0, where most Fe remained in the roots. Data represent the mean values from three biological replicates (n = 3). Elemental content was measured by ICP-MS. The plot was generated using the ggPlantMap package in RStudio. Asterisks indicate genotypes that differ significantly from WT within the same tissue and treatment condition ($p < 0.05$), as determined by two-way ANOVA and Tukey's post hoc test (n = 3 for each group).

Supplementary Figure S13

A

L1 - WT
L2 - *pb104::b104 #1*
L4 - *pb104::b104^dPAA#2*
L5 - *pb104::b104^dPAA#3*

B

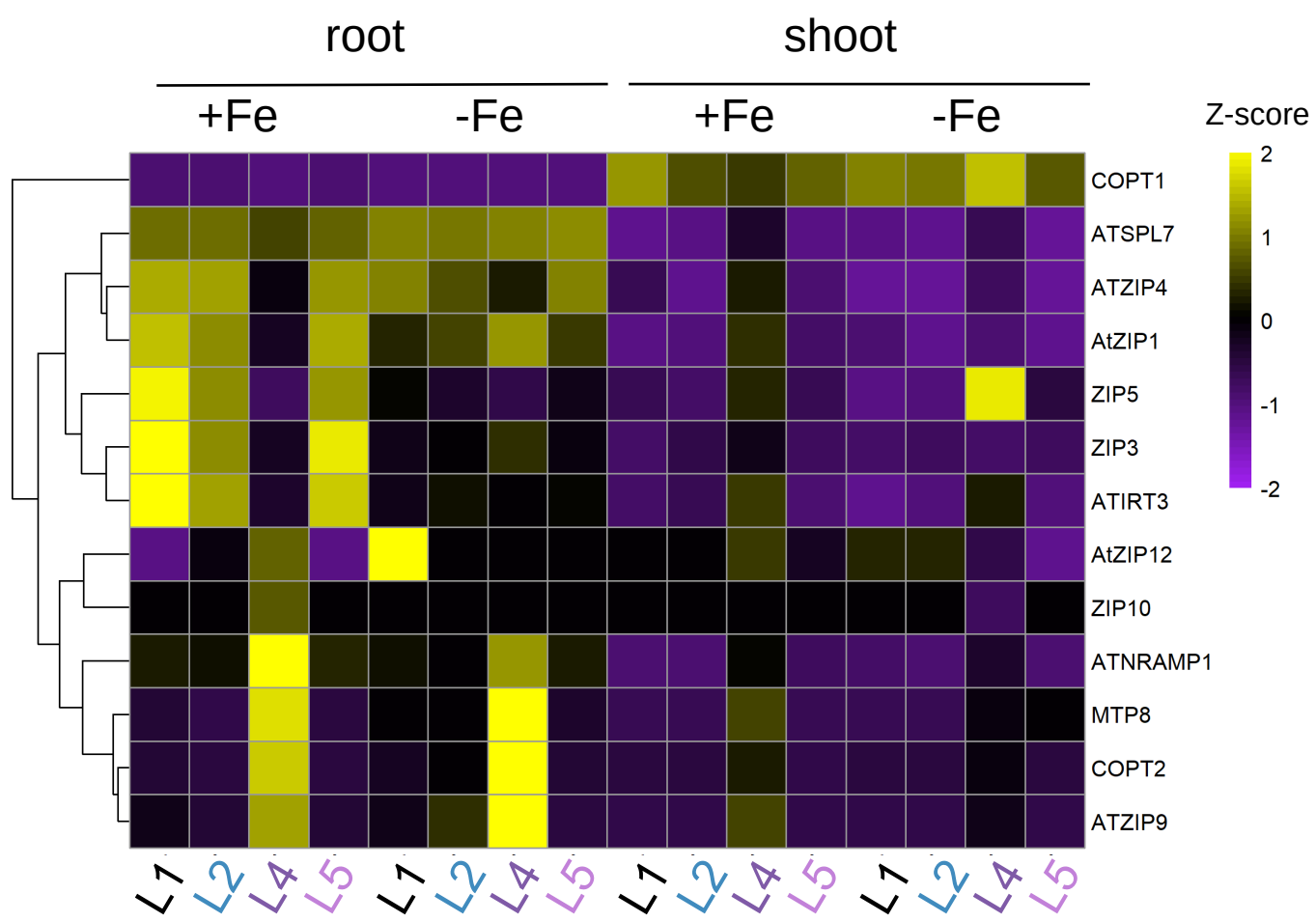

C

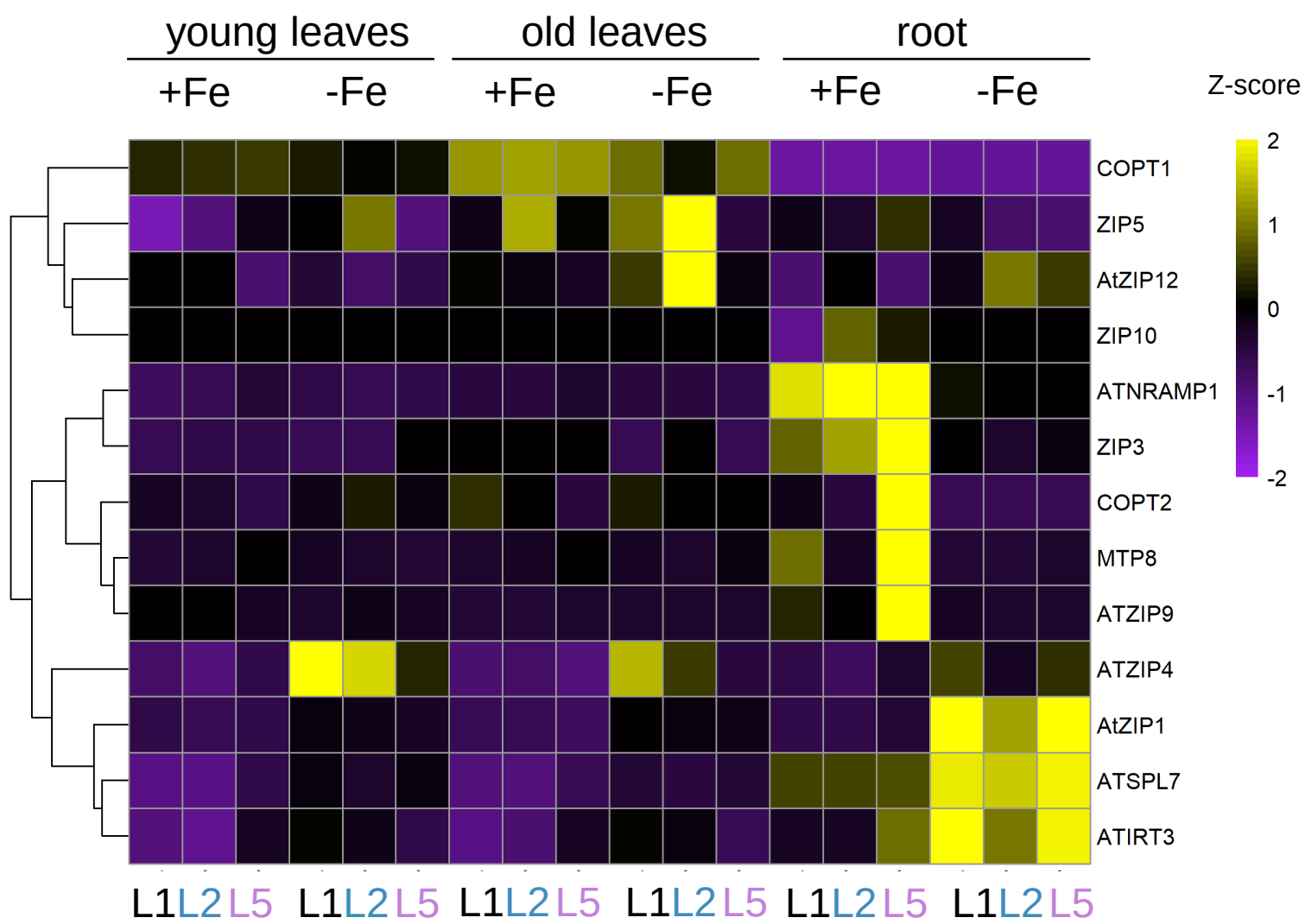

Supplementary Figure S13. Expression profiles of genes involved in Mn, Zn, and Cu homeostasis

(A)Plant lines used In this experiment

(B)Clustered heatmap showing expression profiles from RNA sequencing experiment of genes involved in manganese (Mn), zinc (Zn), and copper (Cu) homeostasis across root and shoot tissues under +Fe and –Fe conditions. Arabidopsis seedlings were grown for 10 days after sowing (DAS) under either iron-sufficient (+Fe) or iron-deficient (–Fe) conditions.

(C)Clustered heatmap showing expression profiles from RNA sequencing experiment of genes involved in manganese (Mn), zinc (Zn), and copper (Cu) homeostasis in young leaves, old leaves, and roots under both +Fe and –Fe conditions. *Arabidopsis* plants were grown hydroponically under iron-sufficient (+Fe) conditions for 27 days, followed by a 3-day treatment with either +Fe or –Fe media.

Genes include metal transporters and the Cu homeostasis regulator SPL7. Heatmap was generated in RStudio version 4.4.1 using calculated Z-scores of normalized gene expression values. Purple indicates low expression and yellow indicates high expression.

Supplementary Figure S14

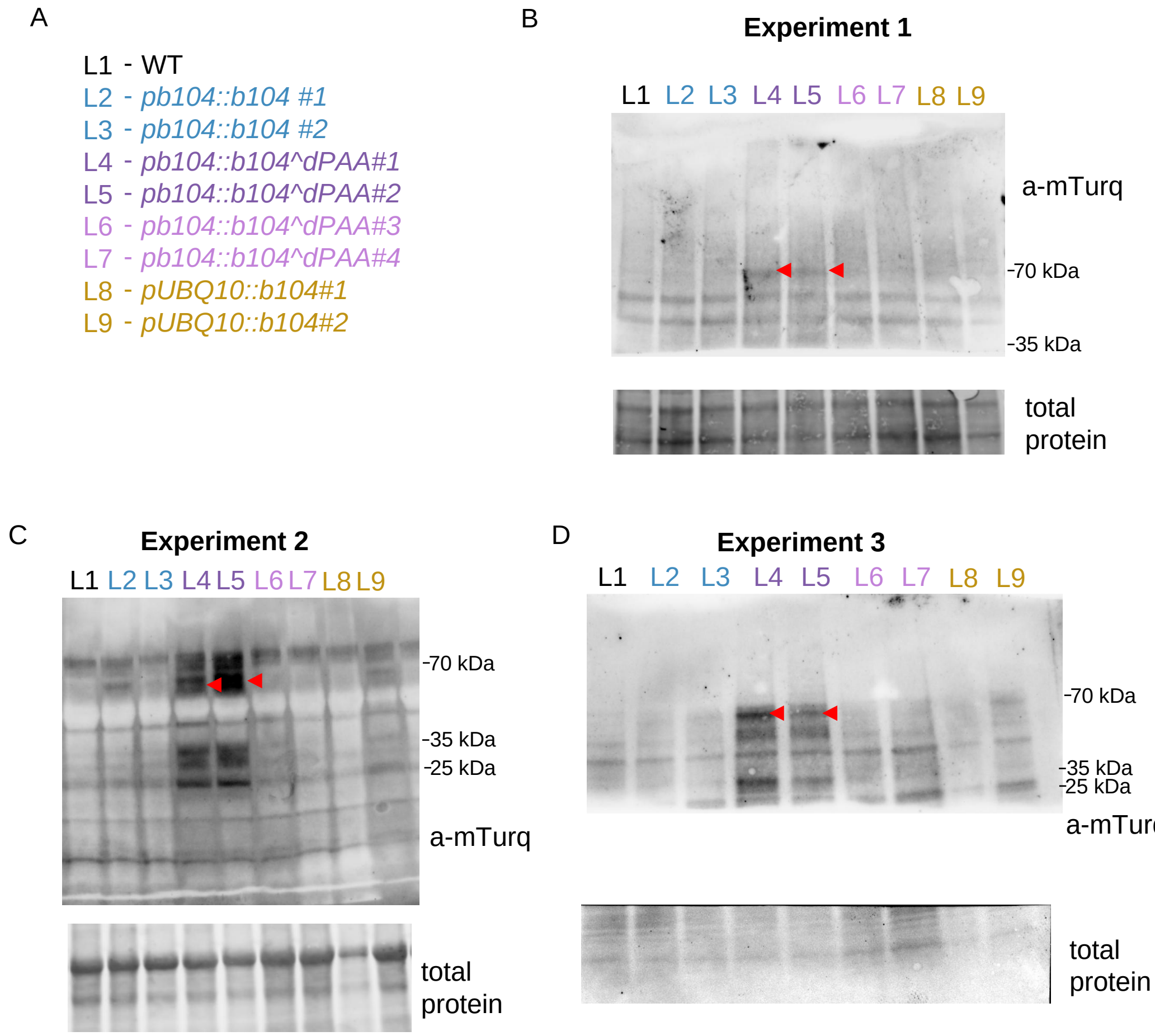

Supplementary Figure S14. Additional independent replicates and anti-mTurq immunoblots for detection of mTurquoise2-bHLH104 and -bHLH104^dPAA protein in various transgenic lines.
Genotypes and transgenic lines used in this experiment.

(A) Genotypes and transgenic lines used in this experiment. The mTurquoise2 fluorescent tag is fused at the N-terminus of bHLH104 and b104^dPAA in all transgenic lines.

(B) Experiment 1: immunoblot of total protein extracted from roots of 10-day-old seedlings (see also main text figure, Fig. 5B).

(C) Experiment 2: immunoblot of total protein extracted from 10-day-old whole seedlings.

(D) Experiment 3: immunoblot of total protein extracted from 6-day-old whole seedlings.

For each experiment, top panels show the anti-mTurquoise2 blot and bottom panels show total protein stain as loading control. Molecular weight markers (kDa) are indicated on the right of each blot. Red arrowheads indicate the expected band position for the full-length mTurquoise2-bHLH104 fusion protein (~70 kDa). Lower molecular weight bands detected by the anti-mTurquoise2 antibody likely represent truncated or partially degraded forms of the mTurquoise2-tagged protein. Across all three independent experiments, mTurquoise2-b104^dPAA protein is consistently more abundant than mTurquoise2-bHLH104, supporting that deletion of the PAA sequence stabilizes bHLH104 protein. The three experiments represent independent biological samples differing in seedling age (6 or 10 days) and tissue type (whole seedlings or roots), demonstrating the robustness of the observed protein accumulation pattern.

Supplementary Figure S15

AD	BD	AD	BD
bHLH104-C	BTSL1	BTSL1	bHLH104-C
bHLH104-C	BTSL2	BTSL2	bHLH104-C
bHLH104-C-dPAA	BTSL1	BTSL1	bHLH104-C-dPAA
bHLH104-C-dPAA	BTSL2	BTSL2	bHLH104-C-dPAA
Empty	BTSL1	BTSL1	Empty
Empty	BTSL2	BTSL2	Empty
bHLH104-C	Empty	Empty	bHLH104-C
bHLH104-C-dPAA	Empty	Empty	bHLH104-C-dPAA

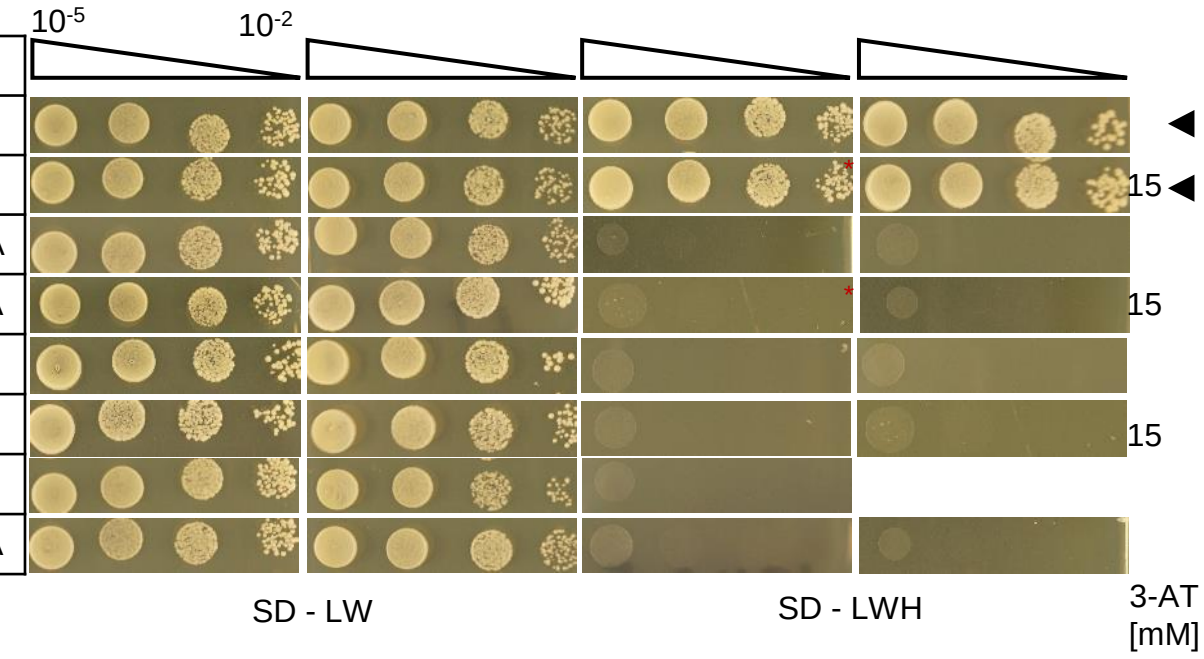

Supplementary Figure S15: Yeast two-hybrid assay results showing protein–protein interactions between bHLH104 BTSL1 and BTSL2.
bHLH104 interacts with BTSL1 and BTSL2, but not bHLH104dPAA. bHLH104^ΔPAA retains the ability to heterodimerize with full-length bHLH104, serving as a control for the presence and expression of the PAA-deleted variant. Full length bHLH104 shows autoactivation in Y2H. Hence bHLH104-C and bHLH104-C-dPAA were used.
Yeast co-transformed with the AD and BD combinations were spotted in 10-fold dilution series (A600 = 10–1–10–4) on SD-LW (transformation control) and SD-LWH plates supplemented with different 3AT concentrations (conc.) as indicated (selection for protein interaction). Negative controls: empty vectors. Black arrows indicate interaction.

Supplementary Figure S16

Experiment 2

	bHLH104-C					bHLH104-C-dPAA			
E2 ligase UBC8	+	+	-	+		+	+	-	+
E3 ligase BTS-HC	+	+	+	-		+	+	+	-
Substrate bHLH104 /bHLH104dPAA	-	+	+	+		-	+	+	+

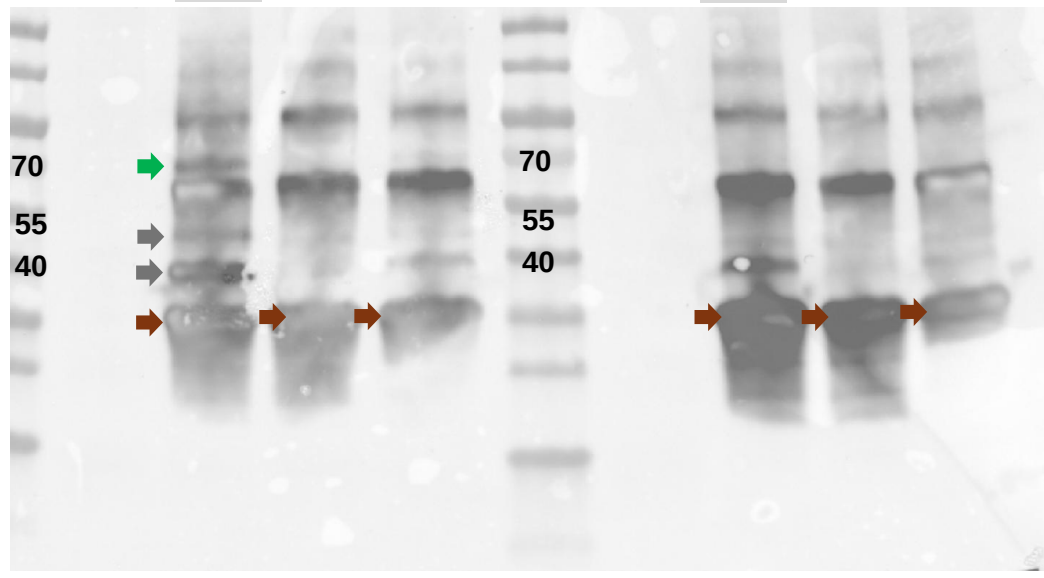

Experiment 3

	bHLH104-C					bHLH104-C-dPAA			
E2 ligase UBC8	+		+	-	+	+	-	+	
E3 ligase BTS-HC	+		+	+	-	+	+	-	
Substrate bHLH104 /bHLH104dPAA	-		+	+	+	+	+	+	

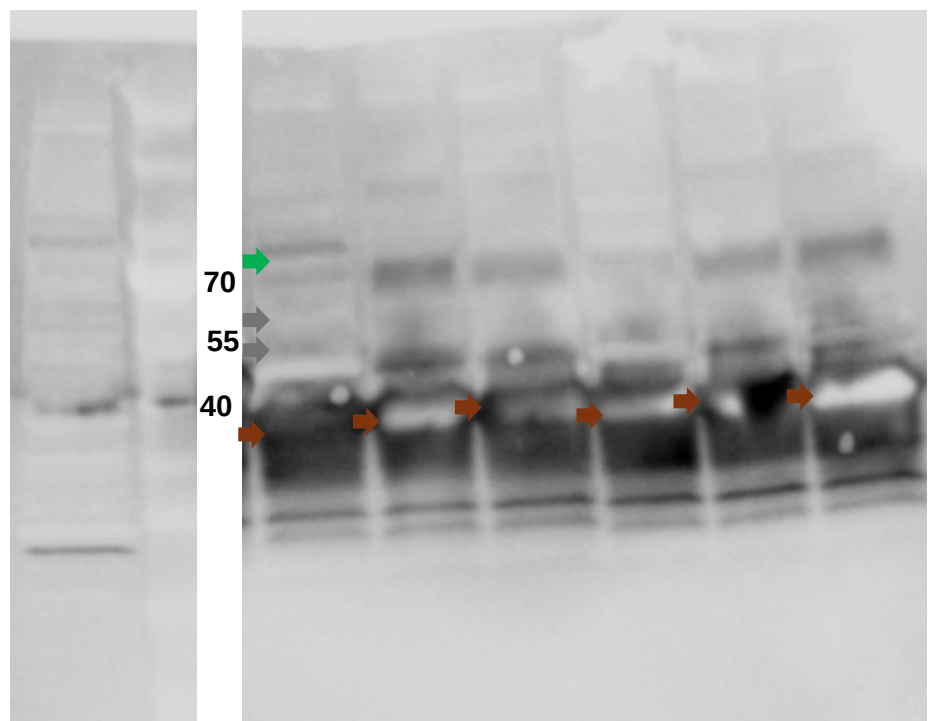

Supplementary Figure S16. Independent replicates of the UbiGate ubiquitination assay for bHLH104. Anti-Strep immunoblots from a total of three independent UbiGate experiments (Experiment 1, see also Fig. 7B; additional Experiment 2 and Experiment 3) supporting the possible PAA-dependent ubiquitination of bHLH104 by BTS. The anti-Strep antibody detects Strep-tagged substrate protein (~40 kDa). Brown arrows indicate non-ubiquitinated substrate. Green arrows indicate a distinct and unique higher molecular weight band (~70 kDa), present only in the bHLH104-C sample in the presence of all components, but in none of the control samples nor the bHLH104-C^dPAA samples consistent with polyubiquitinated bHLH104-C, representing a molecular weight shift of approximately 30 kDa corresponding to the addition of three to four ubiquitin moieties. Grey arrows indicate additional higher molecular weight bands that are not considered specific, as similar bands are present across control lanes. In both replicates, the ~70 kDa polyubiquitinated band is seen, supporting the resulting outcome shown in Figure 7B.

Supplementary Figure S17

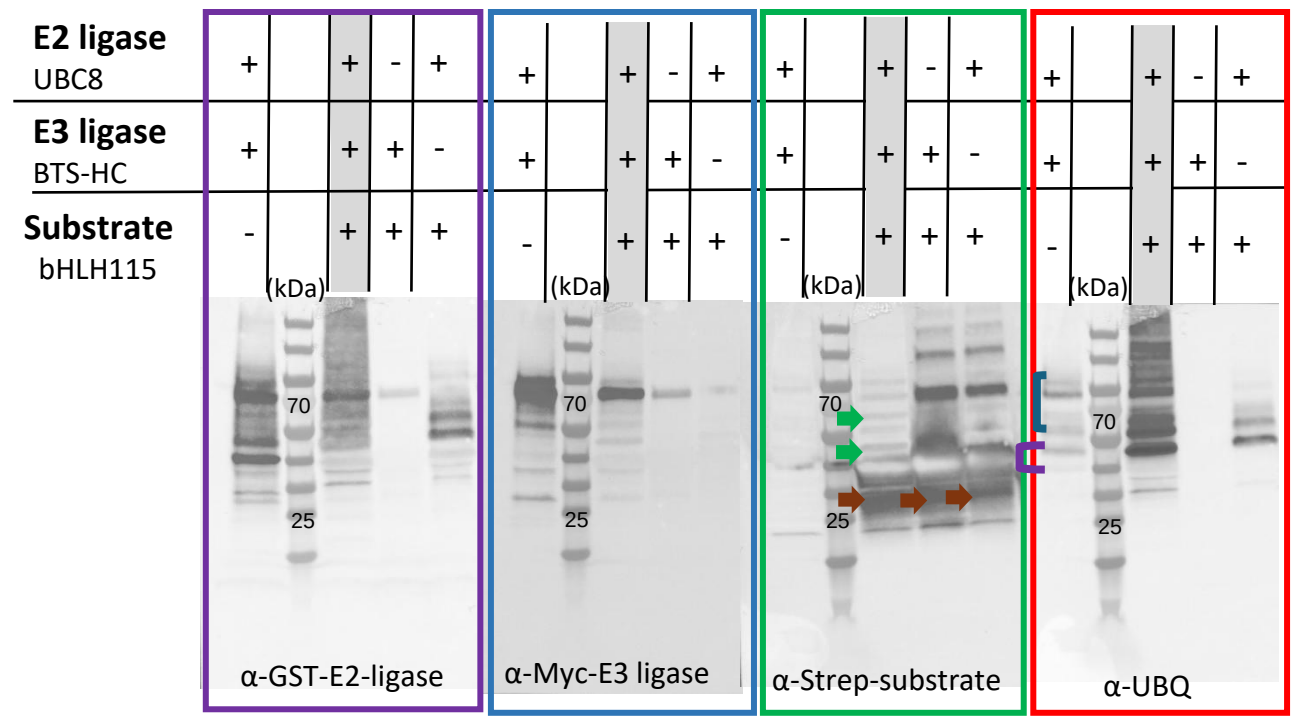

Supplementary Figure S17: UbiGate assay showing ubiquitination of bHLH115 by BTS-HC.

UbiGate ubiquitination assay testing whether bHLH115 is ubiquitinated by BTS-HC in E. coli cells. All four panels are from the same experiment, probed sequentially with different antibodies after stripping: anti-GST (E2 ligase UBC8 detection, purple box), anti-Myc (E3 ligase BTS-HC detection, blue box), anti-Strep (substrate bHLH115 detection, green box), and anti-His-UBQ (ubiquitin detection, red box). Lane compositions are indicated above: +/− denotes presence or absence of E2 ligase (UBC8), E3 ligase (BTS-HC), and substrate (Strep-tagged bHLH115). The first lane in each panel contains E2 and E3 without substrate, serving as a substrate-negative control. The anti-Strep blot (green box) shows the key substrate-specific result: brown arrows indicate the unmodified bHLH115 substrate (~25 kDa), and green arrows indicate higher molecular weight bands present in the complete reaction lane (+E2, +E3, +substrate) that are consistent with polyubiquitinated bHLH115 forms. Several non-specific higher molecular weight bands are present across multiple lanes including controls. However, the complete reaction lane shows a distinct shift in banding pattern with clear substrate laddering compared to the E2-minus and E3-minus controls, indicating that polyubiquitination requires both E2 and E3 components. In the anti-UBQ blot (red box), the presence of all components (+E2, +E3, +substrate) produces a distinct ubiquitin banding pattern compared to controls, further supporting substrate ubiquitination. Violet bracket indicates ubiquitinated E2 ligase (UBC8). Blue bracket indicates autoubiquitinated E3 ligase (BTS-HC). These results are consistent with previous reports of BTS-dependent degradation of bHLH115 (Selote et al., 2015; Xing et al., 2021) and demonstrate the utility of the UbiGate system for testing ubiquitination of bHLH IVc proteins.

Supplementary Figure S18

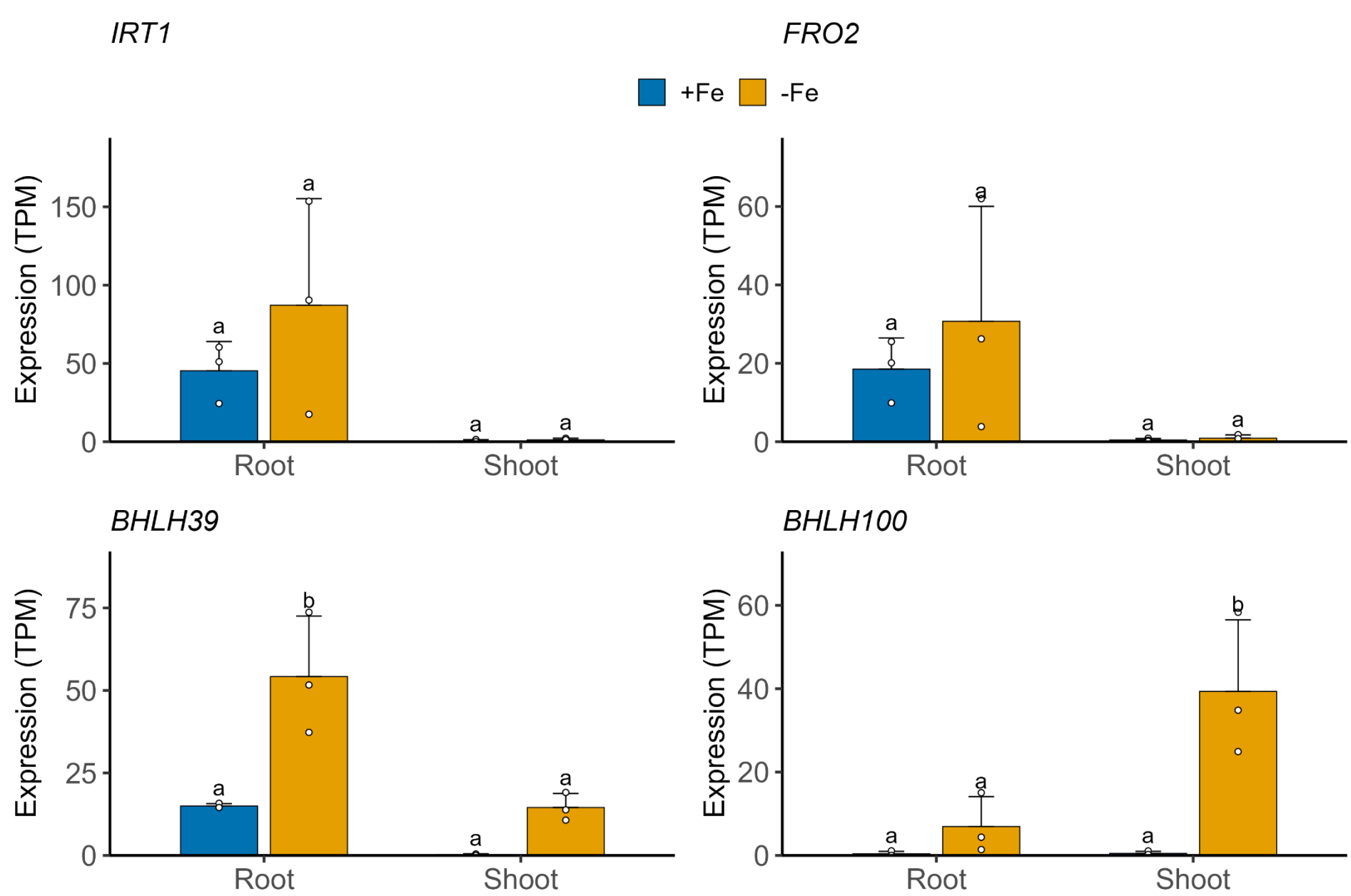

Supplementary Figure S18. Validation of Fe deficiency treatment in wild-type plants. Expression of Fe deficiency marker genes in wild-type Col-0 roots and shoots under Fe-sufficient (+Fe) and Fe-deficient (−Fe) conditions. RNA-seq data are presented as transcripts per million (TPM). IRT1 and FRO2, encoding the root Fe uptake transporter and ferric reductase, respectively, show higher expression under −Fe in roots, although the difference was not statistically significant due to replicate variability. BHLH39 is induced under −Fe compared to +Fe in both roots and shoots. BHLH100 is induced under −Fe compared to +Fe predominantly in shoots. These expression patterns confirm that the Fe deficiency treatment elicited the expected transcriptional −Fe response in wild-type plants. Data represent mean ± SD (n = 3 biological replicates). Statistical analysis was performed using one-way ANOVA followed by Tukey's HSD test ($p < 0.05$). Different letters indicate statistically significant differences. Note that in the main figure heatmaps (Figure 3), these differences are not visible due to Z-score normalization being dominated by high expression values in pb104::b104^dPAA lines**.**

Supplementary Figure S19

Original blots for Figure 5B

L1 - WT
L2 - *pb104::b104 #1*
L3 - *pb104::b104 #2*
L4 - *pb104::b104^dPAA#1*
L5 - *pb104::b104^dPAA#2*
L6 - *pb104::b104^dPAA#3*
L7 - *pb104::b104^dPAA#4*
L8 - *pUBQ10::b104#1*
L9 - *pUBQ10::b104#2*

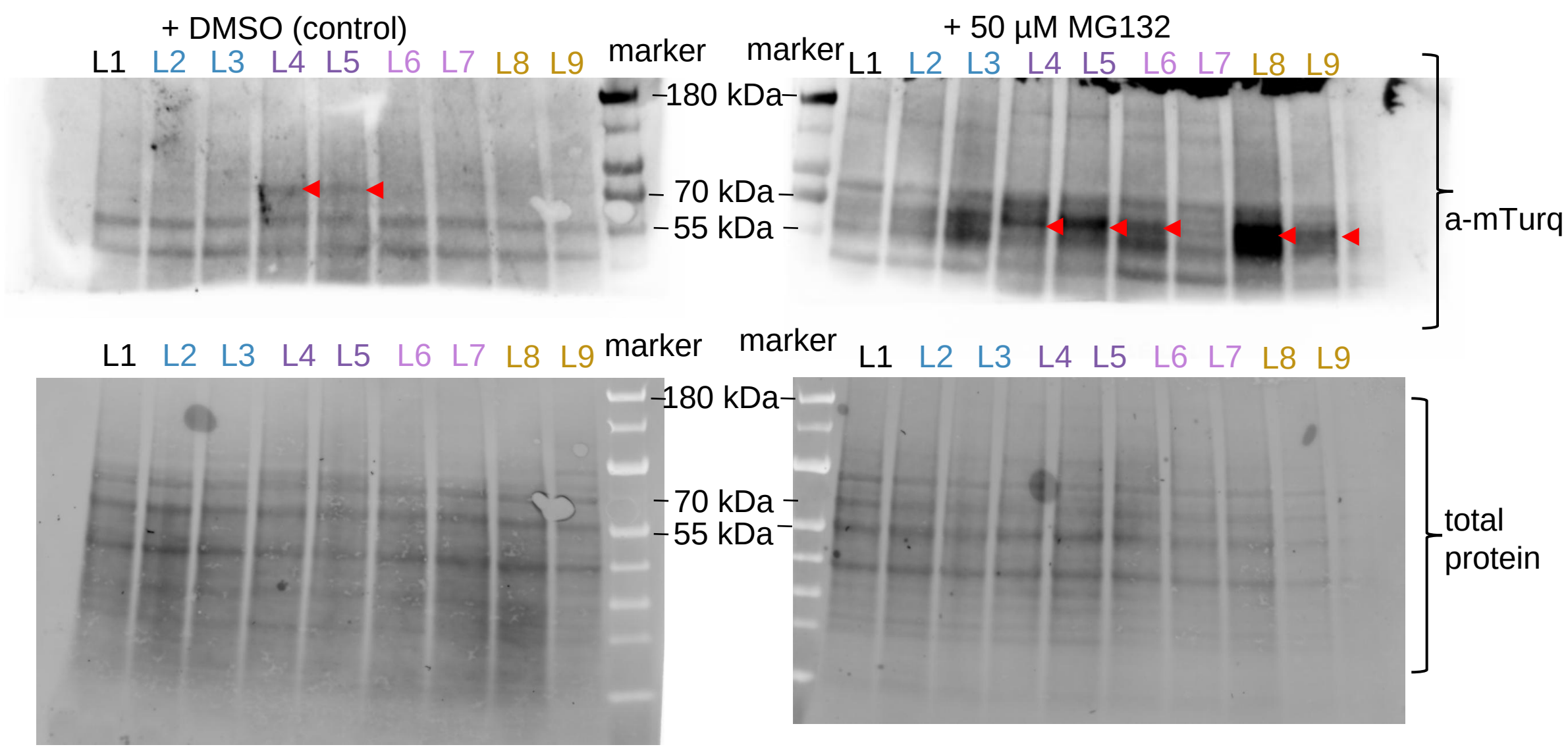

Red arrows indicate the expected band position for mTurquoise2-bHLH104 fusion protein

Supplementary Table 1. Primers used in this study.			
fw = forward, rev = reverse, d = delta a.k.a. deletion, -C = C-term, (att)B1/B2 = Gateway B attachment sites for BP reaction.			
Primer name	**Sequence**	**Purpose**	**Origin**
Amplification of full-length CDS or deletion constructs for Y2H			
bHLH104-C_B1 fw	GGGGACAAGTTTGTACAAAAAAGCAGGCTTCATGGCTCT	cloning of bHLH104-C (attB1)	lichtblau 2023
bHLH104-C-d_B2 rev	GGGGACCACTTTGTACAAGAAAGCTGGGTCTTAAGGCCTGAGTTCTTGAT	cloning of bHLH104-C-d (attB2)	This study
bHLH104_B2 rev	GGGGACCACTTTGTACAAGAAAGCTGGGTCTTAAGCAGCAGGAGGCCTG	cloning of bHLH104-C (attB2)	lichtblau 2022
Cloning bHLH104 promoter and CDS for transgenic lines			
bHLH104 fw	aacaggtctcaggctggatgtatccttctctcgacg	Cloning of bHLH104/bHLH104-d CDS	This study
bHLH104 rev	aacaggtctcactgaAGCAGCAGGAGGCCTGA	Cloning of bHLH104 CDS	This study
bHLH104-d rev	aacaggtctcactgaAGGCCTGAGTTCTTGAT	Cloning of bHLH104-d CDS	This study
pbHLH104 fw	AACAGGTCTCAACCTCTAGCTCTGAGAAGCGGCATC	Cloning of bHLH104 promoter	
pbHLH104 rev	AACAGGTCTCATGTTTTGAGAGTCTCCAAACAAATT	Cloning of bHLH104 promoter	This study
Amplification of full-length CDS or deletion constructs for Ubigate			
BTS-HC fw	ttgaagacaaaATGGCAGAACG	Cloning BTS HC fragment	This study
BTS-HC_rev	ttgaagacaaaagcTTAGCTGCTGGTG	Cloning BTS HC fragment	This study
optbhlh104-C fw	GGGGACAAGTTTGTACAAAAAAGCAGGCTTCATGACCGATAAACCGG	Cloning bHLH104 in pUGTP1 (attB1)	This study
optbhlh104 rev	GGGGACCACTTTGTACAAGAAAGCTGGGTCTTATGCTGCAGGCGGA	Cloning bHLH104 in pUGTP1 (attB2)	This study
optbhlh104d rev	GGGGACCACTTTGTACAAGAAAGCTGGGTCTTACGGACGCAGTTCT	Cloning bHLH104 in pUGTP1 (attB2)	This study
RT-qPCR primers			
EFc_fw	TATGGGATCAAGAAACTCACAAT	for RTqPCR	
EFc_rev	CTGGATGTACTCGTTGTTAGGC	for RTqPCR	
EFg_fw	TCCGAACAATACCAGAACTACG	for RTqPCR	
EFg_rev	CCGGGACATATGGAGGTAAG	for RTqPCR	
FIT_fw	CCCTGTTTCATAGACGAGAAC	for RTqPCR	
FIT_rev	ATCCTTCATACGCCCTCTCC	for RTqPCR	
IRT1_fw	AAGCTTTGATCACGGTTGG	for RTqPCR	
IRT1_rev	TTAGGTCCCATGAACTCCG	for RTqPCR	
FRO2_fw	CTTGGTCATCTCCGTGAGC	for RTqPCR	
FRO2_rev	AAGATGTTGGAGATGGACGG	for RTqPCR	
BHLH39_fw	GACGGTTTCTCGAAGCTTG	for RTqPCR	
BHLH39_rev	GGTGGCTGCTTAACGTAACAT	for RTqPCR	
BTS_fw	CGGGGAAGGACTAGGAATCG	for RTqPCR	
BTS_rev	CAGCAGATGGGGCAATTTGT	for RTqPCR	
PYE_fw	GTTCCCAGGACTTCCCATTT	for RTqPCR	
PYE_rev	GTGTCTGGGGATCAGGTTGT	for RTqPCR	
BHLH104_fw	GGTTGAGGAGGGAGAAGCTAAATG	for RTqPCR	
BHLH104_rev	ACGGATTGCATCATCGAGTATAGC	for RTqPCR	
ILR3_fw	GCATGTAGAGAGAAGCAGCGAC	for RTqPCR	
ILR3_rev	TGCGGACAGCATCAACCAAG	for RTqPCR	
BHLH34_fw	AATCCGGGTTGTGAATCAG	for RTqPCR	
BHLH34_rev	CTTCTCCGCCTTCAACAC	for RTqPCR	
BHLH115_fw	TGAATCAAGCAAGAGATGAA	for RTqPCR	
BHLH115_rev	CTGTTTCTCATCACGCAGC	for RTqPCR	
BTSL1_fw	CTCCCCAGTGAAGGCTCTTC	for RTqPCR	
BTSL1_rev	GACCTGCATATCTCCAAGCGA	for RTqPCR	
BTSL2_fw	GCTTGTATGTCGCGACTCAT	for RTqPCR	
BTSL2_rev	AGAGCCTTCACCGGAGAATT	for RTqPCR	
URI_fw	GGACTCCAACGAAGTTGC	for RTqPCR	
URI_rev	GTCTTCTCTGGCCTTTGC	for RTqPCR	
FER1_fw	TAAGCCACTACTCCCTCACG	for RTqPCR	
FER1_rev	TTGTTTGTGTCCACCGTAGC	for RTqPCR	
IMA1_fw	TGCTTCCACCGTGTATGTTG	for RTqPCR	
IMA1_rev	CAGGAGCATAATCATAGCCACTG	for RTqPCR	
mTurq2_fw	GTCCAAGCTGAGCAAAGACC	for RTqPCR	
mTurq2_rev	CTTGTACAGCTCGTCCATGC	for RTqPCR	
BHLH100_fw	GATGCATAGAGTAAAAGAGTCGCT	for RTqPCR	
BHLH100_rev	CCTCCCACCAATCAAACG	for RTqPCR	
BHLH11_fw	TCCATGCCTCTTCTTTAGC	for RTqPCR	
BHLH11_rev	GGAACTATCTTGAACAGCTTG	for RTqPCR	